# Model Reduction for the Kuramoto-Sakaguchi Model:

## analyzing the effect of non-entrained rogue oscillators

Wenqi Yue

Supervised by Georg Gottwald

A thesis submitted to fulfill requirements for the degree of
Doctor of Philosophy

School of Mathematics and Statistics
Faculty of Science
The University of Sydney

January 8, 2024

# Statement of Originality

This is to certify that to the best of my knowledge, the content of this thesis is my own work. This thesis has not been submitted for any degree or other purposes.

I certify that the intellectual content of this thesis is the product of my own work and that all the assistance received in preparing this thesis and sources have been acknowledged.

Wenqi Yue
January 8, 2024

# Authorship Statement

This thesis contains materials from the published work (Yue, Smith, Gottwald, *Phys. Rev. E* 101, 062213 (2020)). The materials from the work are presented in Section 2.3 and in Chapter 4.

Chapter 5 contains material that has been submitted for publication. A pre-print is available at arXiv:2310.20048 [nlin.AO].

For both works, the research direction was developed jointly. I contributed to the mathematical derivation, numerical investigation and implementation, and manuscript writing.

Wenqi Yue
January 8, 2024

As supervisor for the candidature upon which this thesis is based, I can confirm that the authorship attribution statements above are correct.

Georg Gottwald
January 8, 2024

## Acknowledgements

This has been a long and winding journey. I wish to express my gratitude to everyone who has been there along the way and made it possible.

First and foremost, I want to thank my supervisor, Georg Gottwald, for taking me on board, and for your guidance, help and encouragement throughout the years. It is your guidance, encouragement and enthusiasm that helped me proceed and move forward. You have been a great supervisor all along the way. Thank you for your patience, encouragement and support, especially during the last phases of this journey.

I want to thank Lauren Smith for jumping on board, and for the many helps, guidance and discussions.

Thank you to my friends and colleagues along the way, Caroline, Brent, Madeleine, Victor, Chunxi, Yingxin, Yuhuang, Zhuang, Shanta, Lijia and Andy, and many others, for the many chats and lunch-times, and for your encouragement. There have been several occasions that I have found myself stuck in emotionally undesirable places, and you have helped pull me out and move forward. I am very grateful that you have been there.

Thank you to the organizers of the Sydney Dynamics Group (SDG), for the many seminars and workshops that I attended. The experiences have made me feel that I am not alone and I am a part of a community.

Last, I want to thank my parents, for their love, support and encouragement throughout my life and during this journey.

# Abstract

The Kuramoto-Sakaguchi model is a paradigmatic model of coupled oscillator system which displays collective behaviour. This thesis is concerned with better understanding of the model through construction of lower-dimensional reduced models that are more tractable for analysis. The role of non-entrained rogue oscillators on the synchronized oscillators is highlighted. After reviewing traditional analysis via mean-field theory in the thermodynamic limit of infinitely many oscillators, we proceed to construct reduced models for finite-size systems, where we investigate on how the effects of rogue oscillators should be incorporated. We first describe the rogue oscillators' effect via averaging, leading to a closed deterministic system that involves the synchronized oscillators only. We perform model reduction analysis on the system via the collective coordinate framework. It is demonstrated that inclusion of the effect of rogue oscillators is crucial for obtaining an accurate description of the system. A new non-linear ansatz is introduced which significantly improves the accuracy of the reduced system, both for finite-size systems and in the thermodynamic limit. We then analyze the fluctuation of rogue oscillator's effect around their mean, by constructing stochastic process approximations. It is demonstrated that utilizing an Ornstein-Uhlenbeck process leads to stochastic reduced model that can capture the fluctuations exhibited in the full model. This thesis also adds to the mean-field theory analysis for Kuramoto-like model by performing mean-field analysis on the Kuramoto-Sakaguchi model with uniform intrinsic frequency distribution, which reviews that for a non-zero phase-offset parameter, the system exhibits an intricate transition to synchronization, with first-order transition to partial synchronization followed by a second-order transition to global synchronization.

# Contents

# Chapter 1

# Introduction

## 1.1 Background and Literature Review

### 1.1.1 Synchronization and the Kuramoto Model

Suppose there are two mechanical devices which, when left alone, display similar yet different dynamics. Now imagine imposing a coupling between them, e.g. wrapping a string around. How will this affect the devices' dynamics? We may postulate that it depends on the coupling's "strength": with no coupling, the devices perform their own dynamics; with a strong coupling, their dynamics become much closer to each other, thanks to the connecting string.

It turns out that such effects do indeed occur, in systems arising from many different backgrounds. A system consisting of distinct individual components often evolves to a synchronous state when a strong connection among the components is present. This phenomena of collective synchronization has attracted focus from many researches [62, 71], dating back at least to the 17th century when Huygens documented the observation that two pendulum clocks hanging on the same beam ended up swinging in a synchronous pattern. Collective synchronization has been ubiquitously observed in a vast range of fields and settings, from flashing of fireflies resting on the same tree [11], clapping of audience after a concert [50], to oscillating chemical reactions [34] and superconducting Josephson junctions [77].

To better understand the phenomena of collective synchronization, many mathematical models for coupled systems have been proposed, developed and analyzed. In recent years, a lot of focus has been on the paradigmatic Kuramoto model [36, 3, 72]. The model has a simple mathematical form, is tractable for analysis, yet is still complex enough to display a plethora of interesting, non-trivial dynamics. In particular it displays the transition from incoherence to increasing synchronization

as coupling between components strengthens, which is reminiscent to the emergence of collective synchronization in real-world systems. The model can be obtained from phase reduction analysis on systems of weakly coupled limit-cycle oscillators

In the Kuramoto model, each component compositing the system is modelled as a pure phase oscillator, whose dynamics is captured by a phase variable which represents relative position in terms of the component's periodic rhythm. When left to their own, each oscillator's phase evolves at a constant intrinsic frequency, which may be different for different oscillators. The intrinsic frequencies are often assumed to be drawn from a distribution. Interaction between two oscillators is represented through a coupling function, which has the form of a sinusoidal function of their phases' difference. The system is often assumed to be under an all-to-all coupling topology, in which each oscillator is coupled to every other oscillator in the same manner.

For a population of $N$ coupled phase oscillators, the Kuramoto model takes the form

$$\frac{d}{dt}\phi_i(t) = \omega_i + \frac{K}{N}\sum_{j=1}^{N} A_{ij}\sin(\phi_j(t) - \phi_i(t)), \qquad i = 1, 2 \ldots N. \tag{1.1}$$

Here $\phi_i(t)$ is the instantaneous phase of the $i$-th oscillator, which has intrinsic frequency $\omega_i$. The $\omega_i$s of different oscillators in a system are often assumed to be drawn from an intrinsic frequency distribution $g(\omega)$, which is often assumed to be a symmetric, uni-modal function. $K$ represents an overall coupling strength and $A_{ij}$ is an adjacency matrix depicting whether there is a connection between oscillators $i$ and $j$. The model is a set of $N$ non-linear ordinary differential equations (ODEs), one for each oscillator. We remark that originally the Kuramoto model only considered an all-to-all coupling topology, in which each oscillator is coupled to every other oscillator in the same manner, with $A_{ij} = 1$ for all $i, j$, and models with non-trivial adjacency matrix $A_{ij}$ are extension of the Kuramoto model with coupling under a complex network specified by $A_{ij}$. However by now the term Kuramoto model is used for systems (1.1) with arbitrary coupling network topology.

### 1.1.2 Order Parameter and Path to Synchronization

When analyzing the Kuramoto model and its extensions, a main focus is on the degree of alignment among the oscillators' phases, which is a representation of degree of synchronization among the components of a system. A common measure of alignment is through the mean-field

variables defined as the average of the oscillators' complex phases,

$$r(t)e^{\imath\psi(t)} = \frac{1}{N}\sum_{j=1}^{N} e^{\imath\phi_j(t)}, \tag{1.2}$$

with $\imath = \sqrt{-1}$ denoting the imaginary unit. Here $r(t)$ represents an order parameter measuring the degree of alignment. If all phases are perfectly aligned, $r = 1$, and as the phases become more and more spread out, $r$ decreases towards $r \approx 0$.

To better understand collective behaviour, investigations on Kuramoto-like models often focus on how $r$ varies as system parameters change. Regarding the overall coupling strength $K$, it is often the case that $r$ increases with $K$. In more detail, at low coupling strength $K$, oscillators tend to behave as if uncoupled to each other and rotate with their own intrinsic frequencies, and $r \approx 0$ for this *incoherence* state. After $K$ increases past a threshold $K = K_c$, a synchronized cluster of oscillators emerges, within which the oscillators' phases are entrained and evolve at a common frequency, and $r$ transitions to a non-zero value for this *partial synchronization* state. With $K$ increasing further, more and more oscillators become entrained to the cluster, and $r$ increases towards $r = 1$. This "path to synchronization" is very reminiscent to real-world coupled oscillatory systems, where collective rhythm emerges and encompasses larger and larger fraction of the system as connection/interaction between components strengthens. Resemblance to phase-transitions in statistical mechanics has also been pointed out. For generic symmetric uni-modal intrinsic frequency distributions $g(\omega)$, the transition is a smooth, second-order one: at $K = K_c$, a small synchronized cluster emerges, which grows in size as $K$ increases, and $r$ increases gradually from $r \approx 0$. For certain settings, the transition takes different form. For example, when $g(\omega)$ is a uniform distribution, the transition is an explosive, first-order one: at $K = K_c$, the system transitions directly from incoherence to global synchronization where all oscillators are entrained, and $r$ jumps from $r \approx 0$ to a non-zero value discontinuously [61]. Much focus of research has been put into the investigation and understanding of the path to synchronization in Kuramoto-like models.

### 1.1.3 The Kuramoto-Sakaguchi Model

The Kuramoto model (1.1) has received extensive analysis [72, 3, 54, 4, 25, 65]. Many generalizations of the model have been proposed and analyzed, from inclusion of external noise, non-zero momentum, to more general coupling function, systems coupled via complex networks, and nonlinear oscillators, and much more [3, 54, 4, 25, 65]. Additionally, it

has been applied in the modelling and analysis of a vast range of natural and engineered systems, from neurons [5], chemical oscillators [34] to the power grids [27, 24, 49, 51] and physical metronomes [59, 43].

One natural and common extension is the Kuramoto-Sakaguchi model [66], where the coupling function has an additional phase-offset parameter compared to a pure sine function. The model has the form

$$\frac{d}{dt}\phi_i(t) = \omega_i + \frac{K}{N}\sum_{j=1}^{N} A_{ij}\sin(\phi_j(t) - \phi_i(t) - \lambda), \qquad i = 1, 2 \dots N. \quad (1.3)$$

The phase-offset $\lambda$ is important for accurate modelling of many real-world systems [39]. It can serve as approximation for time-delayed coupling [18]. It often arises when constructing models for real-world systems such as power grids [24, 51] and physical metronomes [59, 43], and it occurs naturally when performing phase reductions on systems of weakly-coupled limit cycle oscillators [36].

With all-to-all coupling, $A_{ij} = 1$ for all $i, j$, if the intrinsic frequencies are symmetric about a centre, at $\omega = \bar{\omega}$, for the original Kuramoto model (1.1), which corresponds to $\lambda = 0$, the system dynamics will also possess that symmetry. Synchronized clusters, when formed, will be symmetric about $\omega = \bar{\omega}$, and will collectively rotate at that frequency. For the Kuramoto-Sakaguchi model (1.3) with a generic $\lambda \neq 0$, the symmetry of the intrinsic frequencies no longer carries over to the dynamics. Synchronized clusters will not be symmetric about $\omega = \bar{\omega}$, and will instead rotate at a collective frequency different to $\bar{\omega}$.

The Kuramoto-Sakaguchi model (1.3) exhibits a wider range of emergent dynamics. For certain classes of $g(\omega)$, the model has been demonstrated to display unusual pathway to synchronization, such as incoherence regaining stability with increasing coupling strength, and multistability between synchronized states and/or incoherence [52, 53]. Moreover, generalizations of the model, such as with non-local, non-global coupling structures, have been the showground for investigations on chimera states where a system simultaneously displays synchronous dynamics in some parts and incoherence in other parts, despite little difference in their intrinsic properties [37, 2, 1, 38, 42, 41] (for a review, see [58]). Chaotic dynamics have also been observed [9].

### 1.1.4 Analysis of the Kuramoto Model

In the following we restrict our analysis to the all-to-all coupling case, $A_{ij} = 1$ for all $i, j$. Despite its relatively simpler form, the Kuramoto model still posts great challenges for analysis, due to its non-linear, complex and high-dimensional nature. It is often desirable to obtain a reduced model description which is of lower dimension, more tractable yet

still captures the overall dynamics of the system well, since we are often more interested in descriptive properties of the whole system, such as the order parameter $r(t)$ (1.2), than behaviour of each individual oscillator.

Traditionally, analysis are performed by first passing through the thermodynamic limit of infinitely many oscillators, $N \to \infty$. In the limit, it is assumed that there is a continuum of oscillators with all possible intrinsic frequencies $\omega$, distributed according to $g(\omega)$. Moreover, at each $\omega$, there are infinitely many oscillators, depicted by a distribution density of their phases, $\rho(\phi, t; \omega)$. Instead of dynamics of $\phi_i(t)$ governed by a system of $N$ ODEs, one for each oscillator, the system can now be described by the time-evolution of $\rho(\phi, t; \omega)$, which is in turn governed by a partial differential equation (PDE) (actually they are partial integro-differential equations) derived from continuity condition [73, 72, 3].

Despite transforming from finite-dimensional ODEs to infinite dimensional PDEs, the Kuramoto model in the thermodynamic limit is much more tractable for analysis. In Kuramoto's classical analysis, self-consistency equations are obtained, which allows for the determination of $r$, among other macroscopic quantities, for the stationary state, at specified $K$ and for given $g(\omega)$ [36, 72, 3]. Some stability analysis results for the incoherent state in the PDE are derived in [73, 74, 17, 16, 6] (see also [72]). In the seminal work of Ott and Antonsen [55], the dynamics of $\rho(\phi, t; \omega)$ is shown to fall on a manifold of much reduced dimension under an ansatz for the form of $\rho$. This manifold is later shown to be attracting under a broad range of conditions [56, 57]. Along the manifold, dynamics of the system is much simpler, and, with a further condition that $g(\omega)$ is a rational function, can be expressed as a finite set of autonomous ODEs, which provides a much more approachable avenue for analysis. This allows for determination of both stationary states and the time-dependent dynamics around it.

### 1.1.5 Kuramoto Model at Finite Size

For the Kuramoto model of finite size $N$, it may not always be appropriate to directly carry over results from the corresponding thermodynamics limit. Descriptive statistics of the system, such as the order parameter $r$, may attain different values at finite $N$ compared to the thermodynamic limit, and the values may be $N$-dependent. Results obtained from the thermodynamic limit assume that the intrinsic frequencies $\omega$ are well-depicted by a density $g(\omega)$; for finite systems, this may not always be the case, and even for the case where the $\omega_i$s are drawn from a certain distribution $g(\omega)$, there could be strong sample-to-sample fluctuations depending on the particular set of $\omega_i$s drawn [32]. Moreover, it has been shown that in finite systems, the order parameter $r(t)$ displays persistent

temporal fluctuations [20, 19], whereas in thermodynamic limit it attains stable equilibrium values. In a sense, in the thermodynamic limit, influences of individual oscillators tend to smooth each other out through the averaging over distribution densities, whereas in finite systems, their individual influences retain, leading to pronounced finite-size effects.

Nonetheless, there is a strong interest in analyzing Kuramoto-like models of finite size. Studies of the models are often motivated as being a pathway towards understanding real-world coupled oscillatory systems, which consist of a finite number of components, for which finite Kuramoto models are more appropriate. Although it is generally the case that as the system size $N$ increases towards infinity, properties of finite Kuramoto models approach those of the corresponding thermodynamic limit provided that the limit is taken in a sensible way, it is still of great interest to investigate the manner in which the limit values are approached. In addition, for real-world systems, parameters of the components often do not follow a particular distribution, and instead are just a collection of certain values. For such systems, investigation may be better carried out by considering finite Kuramoto models where the intrinsic frequencies are just a collection of certain values. It can also be noted that although extensive analysis results have been obtained for the thermodynamic limit, direct simulations of the corresponding PDEs remain challenging, and the analysis results are often corroborated by comparing with simulations of Kuramoto models with large but finite size $N$.

Study on finite Kuramoto models commenced shortly after the model's conceptualization. For all-to-all coupling and uni-modal intrinsic frequency distribution, Daido [20, 19, 21, 22] conducted an extensive series of numerical and theoretical study on the scaling of the order parameter and its fluctuations in finite systems. It was demonstrated that $r(t)$ exhibits anomalously enhanced temporal fluctuations near the onset of partial synchronization, for $K \approx K_c$. Scaling forms for $r$ and its fluctuations were proposed based on theoretical arguments and verified with numerical simulations. Justifications for the scaling forms were also obtained via perturbation analysis. Further investigations were carried out by Hong et al. [32], where in addition, sample-to-sample fluctuations between systems with independent draws of intrinsic frequencies from the same distribution were analyzed. In Coletta et al. [15], a scaling law for the largest non-zero Lyapunov exponent of the system was also obtained.

Another approach for analyzing finite Kuramoto models is via more data-driven coarse-graining reduction [48, 64]. Based on judicious investigation of simulated dynamics, a set of coarse-grained variables are proposed, which are expected to be capable of capturing the system's overall dynamics. The coarse variables' dynamics are expected to be

closed within themselves, i.e. determined only through other coarse variables instead of all the phases, and their evolution can be efficiently analyzed with the aid of estimates obtained from fine-grained simulations of the full system.

More recently, in Snyder et al. [70], a coarse-grained model for finite system is proposed based on the autonomous ODEs for mean-field variables derived in Ott-Antonsen analysis [55] of the thermodynamic limit. Effects of finite system size are captured through both modified equation parameters and introduced additive white noise, leading to a stochastic differential equation (SDE) coarse-grained model. The modified equation parameters and diffusion coefficients of white noise are estimated via regression against simulation data through optimization. The coarse-grained SDE model captures the temporal fluctuations of the order parameter $r(t)$ and its scaling with finite system size $N$.

## 1.2 Collective Coordinate Analysis

Furthermore, model reduction analysis for coupled oscillator systems can also be performed via the collective coordinate framework [29]. Based on inspections of the system's dynamics, an ansatz is made that most components of the system follow a certain common shape profile, which is parameterized by a few parameters, which are the collective coordinates. Dynamics of the overall system is then approximated by that of the shape profile, which is captured by time-evolution of the collective coordinates. Intrinsic differences between the components are captured by the specific form of the shape profile. The ansatz is required to be optimal in the sense that its associated error should be orthogonal to the subspace spanned by the ansatz as collective coordinates vary. In a fashion similar to Galerkin methods, this determines the time-evolution of collective coordinates.

The collective coordinate framework originates in the study of solitary waves [67]. It has been applied to the Kuramoto model where it successfully describes both abrupt and gradual transition to synchronization, as well as time-dependent oscillator cluster dynamics, for systems with different $g(\omega)$ [29]. An advantage of the framework is that it is readily applicable to finite systems, for which it gives accurate estimates and captures finite-size effects [29]. For Kuramoto model with additive noise it captures the finite-size-scaled Brownian diffusion of synchronized cluster [30]. For a system with multi-modal $g(\omega)$, it captures the emergent chaotic cluster dynamics [68]. The framework has also been applied to derive reduced dynamics in Kuramoto model with arbitrary coupling network [31], and to derive optimal network topology [63] and coupling form [10] for synchronization. Recently it has been demonstrated that in the thermodynamic limit, the reduced equations obtained from collective

coordinate framework recover results from Ott-Antonsen analysis [69].

## 1.3 Accounting for the Effects of Rogue Oscillators

Our project aims to perform model reduction analysis for the Kuramoto-Sakaguchi model (1.3) that are applicable to finite systems. We found that for generic phase-offset $\lambda$ that is non-zero, capturing the effects of non-synchronized rogue oscillators in partial synchronization state is crucial to obtain accurate descriptions of the system. This is in contrast to the original Kuramoto model (1.1) where their effects can generally be ignored as they tend to cancel out due to symmetry of the system, which no longer pertains when $\lambda$ is non-zero.

In partial synchronization states, relative to the synchronized cluster, entrained oscillators are nearly stationary and fluctuate with small amplitudes, whereas non-entrained rogue oscillators rotate at non-zero frequencies, constantly overtaking the cluster. Utilizing this apparent time-scale separation between entrained and rogue oscillators, effective descriptions of the rogue oscillators can be obtained.

- In the first part of the project, effects of rogue oscillators are approximated by their averages over a density that is inversely proportional to their rotating velocities. Employing the averages, together with an improved ansatz, we perform model reduction analysis for the Kuramoto-Sakaguchi model via the collective coordinate framework [29, 69]. The resultant reduced equations both provide accurate descriptions for finite systems, and recover known analytical results in the thermodynamic limit. However, it does not capture the finite-size-scaled dynamical fluctuations exhibited in the system, such as those of $r(t)$.

- In the second part of the project, we construct a stochastic approximation for the effect of rogue oscillators. In a spirit similar to homogenization for systems with multiple time-scales [28, 60], we approximate their effects with Gaussian processes, the coefficients of which are estimated via fitting against data from direct simulation. Replacing rogue oscillators with the Gaussian process approximation, we arrive at a stochastic reduced model of the overall system, which is shown to be capable of capturing both the mean behaviour and the variance of fluctuations for the original system.

## 1.4 Main Contributions

We list the main original contributions of the thesis. The thesis makes contributions on three areas: Describing the role of rogue oscillators in Kuramoto-Sakaguchi models, in mean-field theory for the Kuramoto-Sakaguchi model and in improving the method of collective coordinates.

We provide a comprehensive treatment of the role of non-entrained rogue oscillators on the dynamics of the synchronized oscillators. We first establish the mean effect of the rogue oscillators on the synchronized cluster by averaging over the density of the rogue oscillators. This is akin to the law of large numbers and is shown to be valid for the case of infinitely many oscillators. To study finite size effects we quantify, akin to the central limit theorem, the fluctuations around the mean. This leads to a stochastic differential equation that involves only the synchronized oscillators. Interestingly and contrary to recent heuristic stochastic model reductions aimed at describing the fluctuations of the order parameter [70], the noise is not of a Brownian motion type but is instead a coloured Ornstein-Uhlenbeck noise.

We further add to the vast literature on mean-field theory of Kuramoto-like models and perform a mean-field analysis of the Kuramoto-Sakaguchi model for uniform intrinsic frequency distribution. Interestingly this reveals a transition to synchronization which is a hybrid between the explosive first-order phase transition of the Kuramoto model with $\lambda = 0$ for uniform intrinsic frequency distribution [61] and the smooth second-order phase transition for uni-modal intrinsic frequency distributions with partial synchronization: the transition is of first order for the order parameter; however at criticality the system exhibits partial synchronization.

The thesis contributes several improvements to the method of collective coordinates. We introduce a new ansatz function, the arcsine ansatz function, which significantly improves the method for all-to-all coupling topology. The ansatz introduced in this thesis has already been taken up to show that the method of collective coordinates converges to the Ott-Antonson ansatz in the thermodynamic limit while being superior for finite-size networks [69]. As a second improvement of the method of collective coordinates we show that for the Kuramoto-Sakaguchi model with $\lambda \neq 0$ the inclusion of effects of the rogue oscillators is crucial to obtain a good approximation of the full dynamics by the collective coordinates. This is achieved by the averaging techniques developed in this thesis.

## 1.5 Thesis Outline

This thesis is organized as follows. In Chapter 2 we provide results from numerical simulations to illustrate the collective behaviour of the Kuramoto-Sakaguchi model. In Chapter 3 we present an analysis of the Kuramoto-Sakaguchi model in the thermodynamic limit, which serves both as inspiration for ansatz function form for a collective coordinate analysis, and as a reference for comparison, for our model reduction analysis. In Chapter 4 we derive an expression for the average effect of the rogue oscillators on the synchronized oscillators, and we use this to modify the collective coordinate method with significant improvement over the standard collective coordinate reduction. This highlights the importance of including the dynamics of the rogue oscillators. In Chapter 5 we construct a stochastic approximation of the rogue oscillators with Gaussian processes, arriving at a stochastic reduced model for the synchronized oscillators. In Chapter 6 we conclude with a discussion and an outlook for future work.

# Chapter 2

# Dynamical Behaviour of The Kuramoto-Sakaguchi Model

In this chapter, after presenting the set-up for Kuramoto-Sakaguchi models to be investigated in this thesis, we illustrate the system's dynamical behaviour through results from direct numerical simulation, with a particular emphasis on the role of the rogue oscillators at different phase-offsets $\lambda$. We also introduce several quantities that are descriptive of the system's collective behaviour.

## 2.1 Set-up

In this thesis we focus on Kuramoto-Sakaguchi model with an all-to-all coupling network for $N$ phase oscillators

$$\frac{d}{dt}\phi_i(t) = \omega_i + \frac{K}{N}\sum_{j=1}^{N}\sin(\phi_j(t) - \phi_i(t) - \lambda), \quad i = 1, 2 \dots N. \tag{2.1}$$

$\phi_i(t)$ is the phase at time $t$ of the $i$-th oscillator, which has intrinsic frequency $\omega_i$. $K$ and $\lambda$ are the coupling strength and phase-offset parameters respectively. The $\omega_i$s are assumed to be drawn from a intrinsic frequency distribution $g(\omega)$. Comparing to (1.3), the coupling adjacency matrix $A_{ij}$ is set to $A_{ij} = 1\ \forall i, j$ representing all-to-all coupling, i.e. each oscillator is coupled to every other oscillator equally.

For a finite system with $N$ oscillators, we need to generate an ensemble of $N$ $\omega_i$s that constitutes a representative draw from the distribution $g(\omega)$. In our study we choose the $\omega_i$s deterministically in an equi-probability way: let $G(\omega) = \int_{-\infty}^{\omega} g(s)ds$ be the corresponding cumulative distribution of $g(\omega)$, and let $\{x_i\}_{i=1\dots N}$ be a set of $N$ points evenly spread along $[0, 1]$, we generate the $N$ $\omega_i$s as solutions to $G(\omega_i) = x_i$. We consider two sets of $\{x_i\}$: the end-points of $N + 1$ equal sub-intervals of

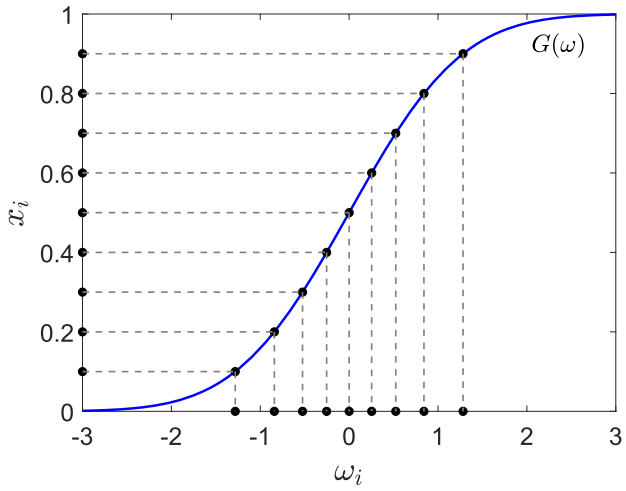


Figure 2.1: Illustration of the procedure for generating $N = 9$ intrinsic frequencies $\omega_i$s deterministically via the end-point rule (2.2), with $x_i$ being the end-points of 10 equal sub-intervals of $[0, 1]$. The solid curve is the cumulative density function (cdf) $G(\omega) = \int_{-\infty}^{\omega} g(s)ds$ of a Gaussian distribution $g(\omega)$ with mean 0 and variance 1.

$[0, 1]$ excluding 0 and 1:

$$x_i = \frac{i}{N+1}, \quad i = 1 \dots N, \tag{2.2}$$

and the mid-points of $N$ equal sub-intervals of $[0, 1]$,

$$x_i = \frac{1}{2N} + \frac{i-1}{N}, \quad i = 1 \dots N. \tag{2.3}$$

Generating the $\omega_i$s equi-probably eliminates the variation between different particular draws of $\omega_i$s from $g(\omega)$ which, although by itself a very interesting area for study [32], is not within the scope of this thesis. It also avoids that particular draws of $\omega_i$s lead to either large or small gaps in the frequencies, which imply local clustering [26]. Finite-size effects are still dynamically relevant as they determine the range of coupling strengths before new oscillators can be entrained, as will be discussed below and in later chapters. In Figure 2.1 we present an illustration of the procedure for generating $N = 9$ intrinsic frequencies $\omega_i$s deterministically via the end-point rule (2.2) for a Gaussian intrinsic frequency distribution $g(\omega)$ of mean 0 and variance 1.

For the intrinsic frequency distribution $g(\omega)$, we shall consider a Gaussian distribution with standard deviation $\sigma$,

$$g(\omega) = \frac{1}{\sqrt{2\pi\sigma^2}} e^{-\frac{\omega^2}{2\sigma^2}}, \tag{2.4}$$

a Lorentzian distribution with width $\Delta$,

$$g(\omega) = \frac{\Delta}{\pi} \frac{1}{\Delta^2 + \omega^2}, \tag{2.5}$$

and a uniform distribution with width $\gamma$,

$$g(\omega) = \mathcal{U}[-\gamma, \gamma] = \begin{cases} \frac{1}{2\gamma}, & -\gamma \leq \omega \leq \gamma \\ 0 & \text{otherwise} \end{cases}. \tag{2.6}$$

The first two are typical symmetric uni-modal frequency distributions that are widely studied. The last one is not uni-modal as it does not have a peak.

Note that the intrinsic frequencies can be set to have mean zero without loss of generality. If they have a non-zero mean, say $\bar{\omega}$, we can always shift to a frame that is rotating with a constant velocity $\bar{\omega}$, in which the phases are now $\phi_i(t) \to \phi_i'(t) = \phi_i(t) - \bar{\omega}t$. The system (2.1) will remain essentially the same except that the frequencies now become $\omega_i \to \omega_i' = \omega_i - \bar{\omega}$, which have mean zero.

The oscillators are arranged such that their intrinsic frequencies $\omega_i$ increase with their indices $i$, i.e. $i = 1$ corresponds to oscillator with the most negative $\omega_i$ and $i = N$ the most positive $\omega_i$.

Perhaps one of the most straight-forward approach of analyzing the Kuramoto-Sakaguchi model (2.1) is to directly simulate the system numerically.

After generating the intrinsic frequencies $\omega_i$ and setting the coupling parameters $K$ and $\lambda$, we directly simulate the system (2.1) numerically using a 4-th order Runge-Kutta (RK4) scheme with a time-step size $dt = 0.05$. Typically, we generate the initial phases $\phi_i(0)$ randomly as independent draws from a uniform distribution between $-\pi$ and $\pi$, simulate the system for sufficiently long time, and consider the first part of simulated trajectory, for $t \in [0, T_0]$, as transients. $T_0$ is chosen as a sufficiently large transient time. Computations of statistics such as time-averages are performed over a time range $t \in [T_0, T_0 + T]$ where $T$ is also large for better accuracy. Unless stated otherwise we choose $T_0 = T = 5 \times 10^4$ time units.

## 2.2 Dynamics at a Fixed System Setting

We expect the Kuramoto-Sakaguchi model (2.1) to exhibit synchronous behaviour at large coupling strengths $K$. In this section, focusing on dynamics at a system setting that leads to synchronous behaviour, we provide results of numerical simulations for (2.1) with a Gaussian invariant frequency distribution $g(\omega)$ (2.4) with $\sigma = 1$ at a coupling strength

$K = 3$ and phase-offset $\lambda = \pi/4$, at which the system displays partial synchronization. We consider $N = 159$ oscillators, with intrinsic frequencies generated equi-probably according to the end-point rule (2.2), corresponding to the end-points of 160 equi-probable sub-intervals of $[0, 1]$, excluding 0 and 1. Generating the intrinsic frequencies equi-probably via the end-point rule (2.2) allows for preserving some of the frequencies across different system sizes, for example, if we now generate $N = 319$ intrinsic frequencies according to (2.2), which correspond to the end-points of 320 equi-probable sub-intervals, all of the 159 intrinsic frequencies that were generated for the previous system size will remain among the $N = 319$ intrinsic frequencies. We remark that particular methods of generating the intrinsic frequencies $\omega_i$, either deterministically via the end-point method (2.2) or the mid-point method (2.3), or randomly as particular random draws from the intrinsic frequency distribution $g(\omega)$, all converge in the thermodynamic limit, $N \to \infty$.

To describe the collective behavior of the Kuramoto-Sakaguchi model, mean-field variables $r$ and $\psi$ are introduced such that

$$r(t)e^{\imath\psi(t)} = \frac{1}{N}\sum_{j=1}^{N} e^{\imath\phi_j(t)}, \tag{2.7}$$

with $\imath = \sqrt{-1}$ denoting the imaginary unit. The time average of the order parameter $r$,

$$\bar{r} = \lim_{T\to\infty} \frac{1}{T}\int_{T_0}^{T_0+T} r(t)dt \tag{2.8}$$

quantifies the degree of synchronization. Synchronized states correspond to $\bar{r} \approx 1$, whereas incoherent states correspond to $r \sim \mathcal{O}(1/\sqrt{N})$.

Figure 2.2 plots the evolution of $r(t)$ starting from a set of random initial phases $\phi_i(0)$. We observe that $r(t)$ quickly transitions from $r \sim \mathcal{O}(1/\sqrt{N})$ to values near $\bar{r} > 0$, and afterwards fluctuates around $\bar{r}$ persistently. The goal of this thesis is to understand and estimate both the average of the order parameter $r$ as well as its fluctuations.

Besides the order parameter $r(t)$, we also examine the dynamics of individual oscillators. Figure 2.3 shows the trajectories of phases $\phi_i(t)$ right after the transient $T_0$. We observe that a group of oscillators have their phases locked together, moving collectively at a common linear velocity. These are the entrained oscillators. Other oscillators are drifting with different speeds, and their trajectories appear smooth with certain periodic structure. These are the non-entrained rogue oscillators.

Figure 2.4(a) is a snapshot of the phases at a particular time after transient. The entrained oscillators have phases close to each other, which also display certain structure with respect to their indices $i$. The non-entrained rogue oscillators have phases spread out across $(-\pi, \pi]$.

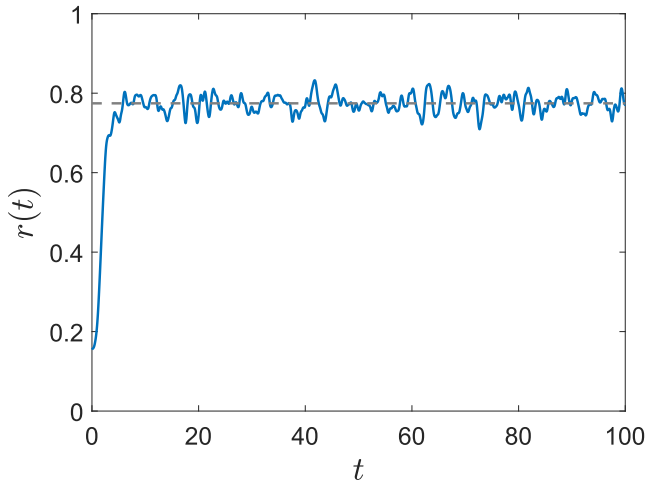


Figure 2.2: Time-series of the order parameter $r(t)$ for Kuramoto-Sakaguchi model (2.1) starting with random initial phases. The system has $N = 159$ oscillators from a Gaussian intrinsic frequency distribution (2.4) with $\sigma = 1$. The coupling strength and phase-offset are set at $K = 3$, $\lambda = \pi/4$. Dash line indicates the time average $\bar{r} = 0.7745$ calculated according to (2.8).

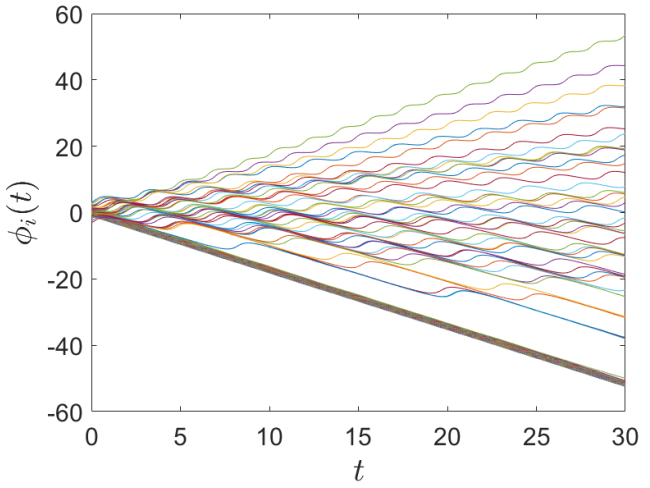


Figure 2.3: Trajectory of phases $\phi_i(t)$ from the Kuramoto-Sakaguchi model (2.1) with same setting as Figure 2.2. Here we show the trajectories right after the transient $T_0 = 5 \times 10^4$. The phases are shifted at the transient by integer multiples of $2\pi$ to be within $(\pi, \pi]$, but are unmodified afterwards.

The observations suggest the presence of a synchronized cluster. To identify more accurately which oscillators are within the cluster, we compute the effective frequencies,

$$\Omega_i = \left\langle \frac{d}{dt}\phi_i(t) \right\rangle_t ,$$

where $\langle a(t) \rangle_t$ denotes time average of a function $a(t)$ (computed in the same manner as (2.8)), and $\frac{d}{dt}\phi_i(t)$ is calculated as the right-hand-side of (2.1) at each time-step along the simulation trajectory.

Figure 2.4(b) plots the calculated $\Omega_i$s. Comparing with Figure 2.4(a), we observe that the entrained oscillators whose phases are close have effective frequencies that are very close to each other. We now determine the synchronized cluster $\mathcal{C}$ of entrained oscillators as the set of oscillators whose effective frequencies $\Omega_i$ are very close (numerically we check whether an oscillator's $\Omega_i$ are within $10^{-3}$ of that of its neighbouring oscillators). The remaining oscillators are determined as the set of non-synchronized, rogue oscillators $\mathcal{R}$. In the particular setting we identified the synchronized cluster $\mathcal{C}$ as oscillators with indices $1 \leq i \leq 116$ and the rogues $\mathcal{R}$ as those with $117 \leq i \leq 159 = N$. In Figure 2.4 different symbols are assigned to the synchronized and rogue oscillators according to this classification. For the parameters adopted here with $K = 3$ and $\lambda = \pi/4$, the rogue oscillators only appear at indices larger than the synchronized cluster $\mathcal{C}$. In general, however, for different parameters, rogue oscillators may appear at indices both above and below the cluster $\mathcal{C}$.

As oscillators are indexed by their intrinsic frequencies $\omega_i$, when synchronized clusters are formed, they tend to consist of oscillators with consecutive indices $i$. We denote the end indices of the cluster $i_{\min}$ and $i_{\max}$, and the corresponding intrinsic frequencies $\omega_{\min} := \omega_{i_{\min}}, \omega_{\max} := \omega_{i_{\max}}$. We estimate the common frequency of the cluster as the average of effective frequencies among synchronized oscillators,

$$\Omega = \frac{1}{N_c} \sum_{j \in \mathcal{C}} \Omega_j, \tag{2.9}$$

where $N_c = |\mathcal{C}| = i_{\max} - i_{\min} + 1$ denotes the size of the synchronized cluster. If we shift to a frame rotating at the common frequency $\Omega$, the synchronized oscillators will appear stationary.

## 2.3 Dynamics Across Different Parameter Settings

In this section, we investigate the effects of varying the coupling strength $K$ and the phase-offset $\lambda$ on the collective dynamics of the system. Here

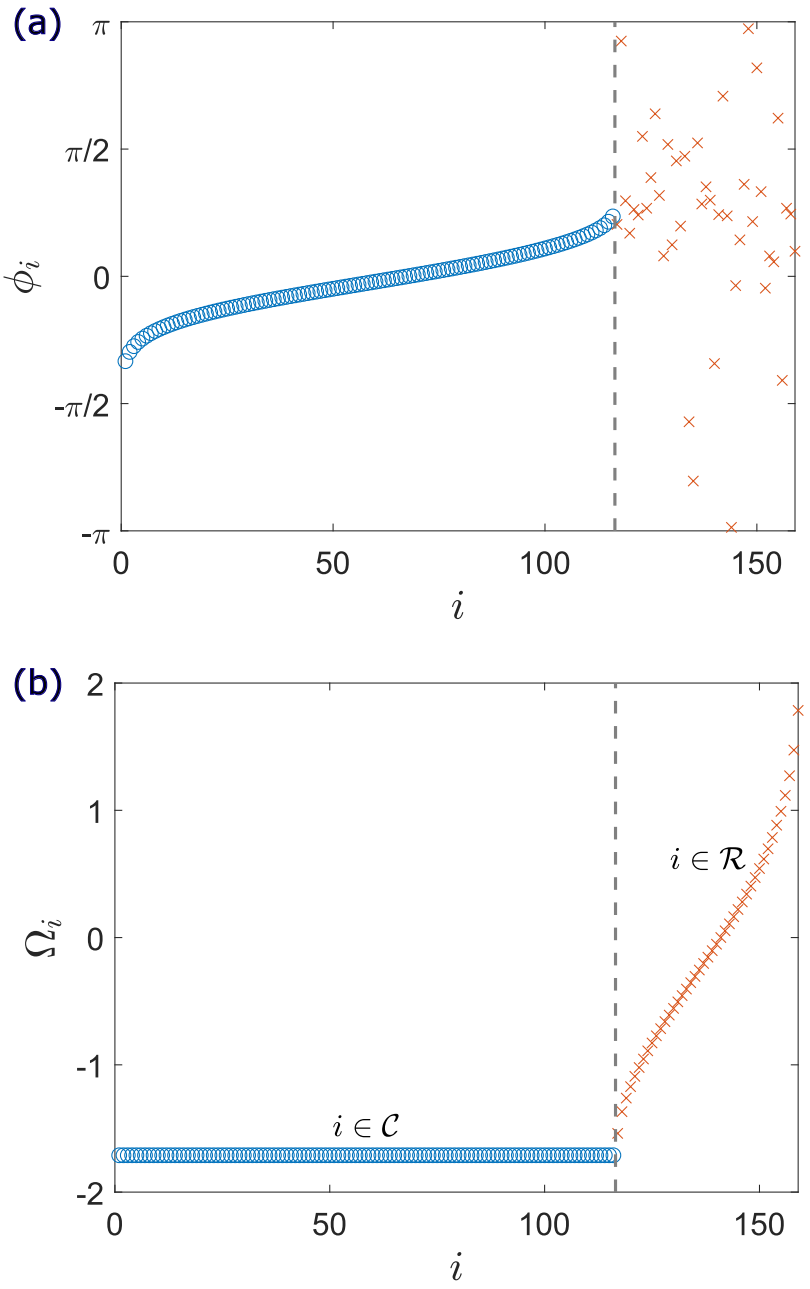


Figure 2.4: (a): Snapshot of phases $\phi_i$ at a particular time after transient. The phases are shifted by integer multiples of $2\pi$ to have values within $(-\pi, \pi]$. (b): The effective frequencies $\Omega_i$ of the oscillators. Parameter settings for both (a),(b) are the same as Figure 2.2. Blue circles and red crosses denote synchronized oscillators $i \in \mathcal{C}$ and rogue oscillators $i \in \mathcal{R}$ respectively. Dashed vertical line is a visual aid separating $\mathcal{C}$ and $\mathcal{R}$.

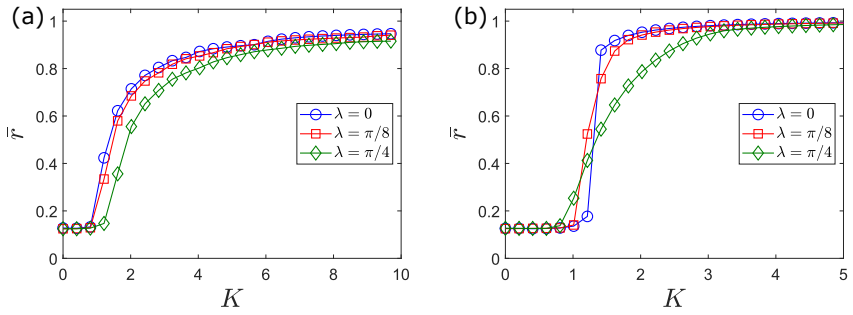


Figure 2.5: Order parameter $\bar{r}$ of the Kuramoto-Sakaguchi model (2.1) with $N = 50$ oscillators for different phase-offset parameters $\lambda$. (a) Lorentzian frequency distribution (2.5). (b) Uniform frequency distribution (2.6).

for the intrinsic frequency distribution $g(\omega)$ we consider a Lorentzian distribution (2.5) with $\Delta = 0.5$, and a uniform distribution (2.6) with $\gamma = 1$. We consider a system of $N = 50$ oscillators with intrinsic frequencies $\omega_i$ generated equi-probably according to the mid-point rule (2.3).

Focusing on the effect of $\lambda$ on the path to synchronization with increasing $K$, Figure 2.5 depicts the transition from incoherence with $\bar{r} \sim 1/\sqrt{N}$ to synchronization with $\bar{r} > 0$ upon increasing the coupling strength $K$ beyond a critical coupling strength $K_c$ for (a) the Lorentzian frequency distribution (2.5) and (b) the uniform frequency distribution (2.6). For a Lorentzian distribution, inclusion of the phase-offset $\lambda$ impedes synchronization, both lowering $\bar{r}$ for a given coupling strength $K$ as well as delaying the onset of synchronization to a higher value of $K$ for larger $\lambda > 0$. For a uniform distribution, increasing $\lambda$ similarly lowers $\bar{r}$ at large values of $K$. However, unlike for a Lorentzian distribution, the onset of partial synchronization around $K \approx 1$ occurs at lower values of $K$ as $\lambda$ increases. For $\lambda = 0$, it is well known that the transition for uniform $g(\omega)$ is an explosive first-order one from incoherence directly to global synchronization [61]. For $\lambda > 0$, we observe that the transition becomes smoother. For both distributions and for all phase-offsets $\lambda$, at lower coupling strengths $K$, the order parameter $\bar{r}$ tends to a value that is close to but not equal to 0 , of order $\mathcal{O}(1/\sqrt{N})$, which corresponds to $N$ randomly distributed phases $\phi_i$. This is an effect of finite system size and we expect the value to approach 0 as $N \to \infty$.

Next, we focus on the effect of $\lambda$ on the relative position of the synchronized cluster. In the original Kuramoto model with zero phase-offset $\lambda = 0$, synchronized clusters of size $N_c$ are always symmetric about $\omega = 0$ provided the intrinsic frequencies $\omega_i$ are symmetric about $\omega = 0$ (as is the case for equi-probable draws from a frequency distribution $g(\omega)$ that is symmetric about $\omega = 0$). In particular for $\lambda = 0$ we have $\omega_{\max} = -\omega_{\min}$

and as the coupling strength $K$ decreases, oscillators break off from the cluster in symmetric pairs as shown in Figure 2.6(a). In contrast, in the Kuramoto-Sakaguchi model with non-zero phase-offset $\lambda$, the synchronized cluster is not symmetric about $\omega = 0$ and oscillators break off from the cluster asymmetrically, as shown in Figure 2.6(b) for $\lambda = \pi/4$.

We proceed to examine the common frequency of the cluster, $\Omega$. For non-zero $\lambda$, the synchronized cluster rotates at a non-zero common frequency $\Omega$ in the rest frame, in contrast to the Kuramoto model at $\lambda = 0$ where the synchronized cluster is stationary. Figure 2.7 shows the cluster mean frequency $\Omega$ as a function of the coupling strength $K$ for different values of $\lambda$. We observe that at high coupling strength, $\Omega$ has a nearly linear dependence on $K$ with $\Omega \approx -K \sin\lambda$ for both a Lorentzian frequency distribution (2.5) and a uniform frequency distribution (2.6). For the Lorentzian distribution, the linear dependence extends over the whole range of coupling strengths. For the uniform distribution, $\Omega$ exhibits a non-linear dependency of $\Omega(K)$ close to the onset of partial synchronization.

In the following chapters we seek to capture the collective behaviour of the Kuramoto-Sakaguchi model with particular emphasis on the role of the non-entrained rogue oscillators.

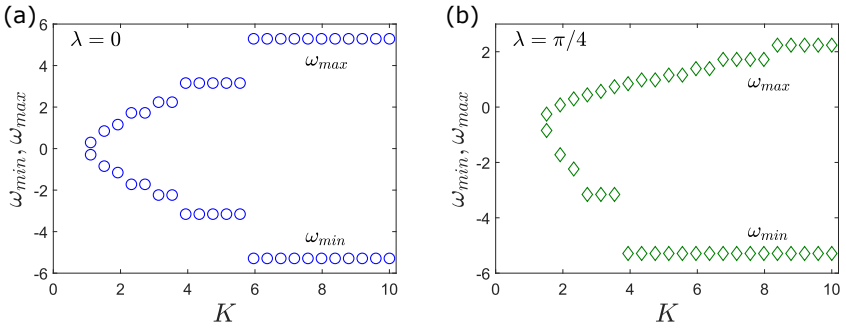


Figure 2.6: Minimum ($\omega_{\min}$) and maximum ($\omega_{\max}$) intrinsic frequencies of oscillators within the synchronized cluster at different coupling strengths $K$ for $N = 50$ oscillators. Intrinsic frequencies drawn from a Lorentzian distribution (2.5). (a) $\lambda = 0$, (b) $\lambda = \pi/4$.

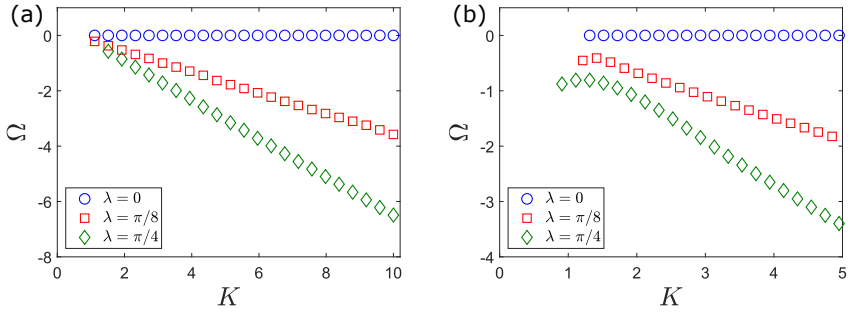


Figure 2.7: Mean frequency $\Omega$ of the synchronized cluster as a function of coupling strength $K$ for different phase-offset parameters $\lambda$ for the Kuramoto-Sakaguchi model (2.1) with $N = 50$ oscillators. (a) Lorentzian frequency distribution (2.5). (b) Uniform frequency distribution (2.6).

# Chapter 3

# The Thermodynamic Limit

Direct analysis of the finite-size Kuramoto-Sakaguchi model (1.3) is hard due to its high-dimensional, non-linear and complex nature. Analysis is often performed in the thermodynamic limit of infinitely many oscillators, $N \to \infty$, in which the system becomes more tractable. Furthermore, adopting an all-to-all coupling network allows for application of mean-field theory, leading to immensely reduced description of the collective behaviour of the system. Mean-field theory has been applied with great success to numerous systems of coupled oscillators arising from many different settings; see [8] for a recent review.

In this chapter, for the Kuramoto-Sakaguchi model (2.1) in the thermodynamic limit, we present the classical self-consistency analysis following Sakaguchi and Kuramoto [66], which leads to a description of collective behaviour in the equilibrium state. For the special case of a uniform intrinsic frequency distribution, we derive solutions from this approach, which reveal an intricate path to synchronization for non-zero phase-offset $\lambda > 0$, exhibiting an abrupt first-order transition to partial synchronization followed by gradual second-order transition to global synchronization, in contrast to the explosive direct transition from incoherence to global synchronization described by Pazó for $\lambda = 0$ [61]. We then review the more recent Ott-Antonsen analysis [55], which provides a description of the dynamical collective behaviour.

## 3.1 Classical Mean-Field Approach and Self-Consistency Analysis

The Kuramoto-Sakaguchi model (2.1) allows for a mean-field description in the thermodynamic limit, which reduces the dynamics to mean-field variables $r$ and $\Omega$. Here we follow the approach developed by Sakaguchi and Kuramoto [66] to find a self-consistency relation between $r$ and $\Omega$,

already introduced in Chapter 2. Focusing on settings where there is a synchronized cluster of oscillators, we shift to the frame rotating at the cluster mean frequency $\Omega$, and consider the phase variables $\theta_i(t) = \phi_i(t) - \Omega t$. Note that we assume $\Omega$ to be a constant that is yet to be determined. The Kuramoto-Sakaguchi model (2.1) is then written in terms of the $\theta_i$s as

$$\frac{d}{dt}\theta_i(t) = \omega_i - \Omega + \frac{K}{N}\sum_{j=1}^{N}\sin(\theta_j - \theta_i - \lambda), \tag{3.1}$$

We define the mean-field variables in the co-rotating frame as

$$r(t)e^{\imath\psi_0(t)} = \frac{1}{N}\sum_{j=1}^{N} e^{\imath\theta_j(t)}, \tag{3.2}$$

with $\imath = \sqrt{-1}$ denoting the imaginary unit. Comparing to the mean-field variables in the rest frame (2.7), $r(t)$ remains the same and $\psi_0(t)$ is related to $\psi(t)$ via $\psi_0(t) = \psi(t) - \Omega t$.

For systems with an all-to-all coupling topology, the mean-field variables (3.2) not only measure coherence and mean phase behaviour, but also allow for a simplification of the system. Indeed, substituting (3.2) into the system (3.1), we obtain the mean-field formulation of the Kuramoto-Sakaguchi model,

$$\frac{d}{dt}\theta_i(t) = \omega_i - \Omega + Kr\sin(\psi_0 - \theta_i - \lambda). \tag{3.3}$$

In this form, $\theta_i$ is coupled to the phases of the other oscillators only via the mean-field variables $r$, $\psi_0$ and $\Omega$. For later reference we define the right-hand side of (3.3) as

$$v(\theta_i;\omega_i) = \omega_i - \Omega + Kr\sin(\psi_0 - \theta_i - \lambda). \tag{3.4}$$

If we consider $r$, $\psi_0$ and $\Omega$ to be constants, then (3.3) is a 1-dimensional autonomous ODE for each $\theta_i$. It supports two kinds of solutions depending on the intrinsic frequency $\omega_i$:

- for oscillators with frequencies $|\omega_i - \Omega| \leq Kr$, (3.3) has a stationary solution

$$\theta_i = \theta_i^* = \psi_0 + \arcsin\left(\frac{\omega_i - \Omega}{Kr}\right) - \lambda. \tag{3.5}$$

  It has another stationary solution, $\theta_i = \psi_0 + \pi - \arcsin\left(\frac{\omega_i - \Omega}{Kr}\right) - \lambda$, which is unstable in the 1-dimensional ODE. These oscillators are stationary in the co-rotating frame, and partake in the collective rotation at frequency $\Omega$ in the rest frame. They are the synchronized oscillators entrained within the cluster, $i \in \mathcal{C}$.

- for oscillators with frequencies $|\omega_i - \Omega| > Kr$, (3.3) does not have a stationary solution. Its right-hand side remains the same sign for all $\theta_i \in (-\pi, \pi]$. $\theta_i(t)$ rotates in the same direction, governed by the Adler equation (3.3). Their dynamics are periodic and can be obtained analytically. These are the non-synchronized rogue oscillators, $i \in \mathcal{R}$.

We now pass through the thermodynamic limit of infinitely many oscillators, $N \to \infty$, in which it is assumed that there is a continuum of oscillators at each possible intrinsic frequency $\omega$, with relative number density given by the intrinsic frequency distribution $g(\omega)$. At each $\omega$, instead of the dynamics of individual oscillators $\theta_i(t)$, we focus on the instantaneous density function of oscillators with phase $\theta$ among all oscillators at the same $\omega$, $\rho(\theta, t; \omega)$. $\rho$ is normalized at each $\omega$,

$$\int_{-\pi}^{\pi} \rho(\theta, t; \omega) d\theta = 1 \quad \forall t, \omega. \tag{3.6}$$

The overall density over all intrinsic frequencies is then given as a product density as $\rho(\theta, t; \omega)g(\omega)$, which is normalized with

$$\int_{-\infty}^{\infty} \int_{-\pi}^{\pi} \rho(\theta, t; \omega) g(\omega) d\theta d\omega = \int_{-\infty}^{\infty} g(\omega) d\omega = 1 \quad \forall t.$$

The mean-field variables (3.2) are expressed in the thermodynamic limit as

$$r(t) e^{\imath \psi_0(t)} = \int_{-\infty}^{\infty} \int_{-\pi}^{\pi} e^{\imath \theta} \rho(\theta, t; \omega) g(\omega) d\theta d\omega. \tag{3.7}$$

The dynamics of the system is described by a continuity equation governing the density function $\rho(\theta, t; \omega)$. The continuity equation follows from the conservation of the number of oscillators at each intrinsic frequency $\omega$, i.e., each oscillator's intrinsic frequency $\omega$ is fixed and does not change over time. The continuity equation is

$$\frac{\partial}{\partial t} \rho = -\frac{\partial}{\partial \theta} (\rho v), \tag{3.8}$$

where $v = v(\theta, t; \omega)$ is given in (3.4), and its time dependence is only through the mean-field variables $r(t)$ and $\psi_0(t)$.

To seek stationary solutions of the continuity equation (3.8), we set $\frac{\partial}{\partial t} \rho = 0$, which leads to

$$\rho^*(\theta; \omega) v(\theta; \omega) = C(\omega),$$

where at each $\omega$, $C(\omega)$ is a constant independent of $\theta$. Note that for stationary states, $\rho(\theta, t; \omega)$ is constant in time, hence $r$, $\psi_0$ are constant in time through (3.7), and $v$ does not have time dependence.

As for the existence of the stationary solutions of (3.3), the form of stationary density $\rho^*(\theta;\omega)$ depends on the intrinsic frequency $\omega$ in the following way,

- for $|\omega-\Omega| \le Kr$, $v(\theta;\omega)$ attains zeros, and $\rho^*(\theta;\omega)$ is given by

$$\rho^*(\theta;\omega) = \delta\left(\theta - \left(\psi_0 + \arcsin\left(\frac{\omega_i-\Omega}{Kr}\right) - \lambda\right)\right). \tag{3.9}$$

  Comparing to (3.5), $\rho^*(\theta;\omega)$ is a delta function centered at the stable equilibrium. This corresponds to the synchronized oscillators.

- for $|\omega-\Omega| > Kr$, $v(\theta;\omega)$ does not have zeros, and

$$\rho^*(\theta;\omega) = \frac{C(\omega)}{|v(\theta;\omega)|} = \frac{C(\omega)}{|\omega-\Omega+Kr\sin(\psi_0-\theta-\lambda)|}. \tag{3.10}$$

  $C(\omega)$ are constants determined from the normalization condition (3.6). This corresponds to the non-synchronized rogue oscillators. Note that albeit individual oscillators at frequency $\omega$ rotate over time and are not stationary, their overall density $\rho^*(\theta;\omega)$ is constant in time.

Substituting the stationary densities for the entrained and for the non-entrained oscillators, (3.9) and (3.10), into the equation for the mean-field variables (3.7), we obtain

$$\begin{aligned} re^{\imath\lambda} = &\int_{|\omega-\Omega|\le Kr}\left(\sqrt{1-\frac{(\omega-\Omega)^2}{K^2r^2}} + \imath\frac{\omega-\Omega}{Kr}\right)g(\omega)d\omega \\ &+\imath\int_{|\omega-\Omega|>Kr}\left(\frac{\omega-\Omega}{Kr} - \frac{\omega-\Omega}{Kr}\sqrt{1-\frac{K^2r^2}{(\omega-\Omega)^2}}\right)g(\omega)d\omega. \end{aligned} \tag{3.11}$$

Separating real and imaginary parts of (3.11), we arrive at the following self-consistency relation for $r$ and $\Omega$,

$$r\cos\lambda = \int_{|\omega-\Omega|\le Kr}\sqrt{1-\frac{(\omega-\Omega)^2}{K^2r^2}}g(\omega)d\omega \tag{3.12}$$

$$\begin{aligned} r\sin\lambda = &\int_{|\omega-\Omega|\le Kr}\frac{\omega-\Omega}{Kr}g(\omega)d\omega \\ &+\int_{|\omega-\Omega|>Kr}\left(\frac{\omega-\Omega}{Kr} - \frac{\omega-\Omega}{Kr}\sqrt{1-\frac{K^2r^2}{(\omega-\Omega)^2}}\right)g(\omega)d\omega. \end{aligned} \tag{3.13}$$

Although they are complicated, in principle, for a specified intrinsic frequency distribution $g(\omega)$, the self-consistency equations (3.12)–(3.13) implicitly determine $r$ and $\Omega$ for a given coupling strength $K$ and phase-offset $\lambda$. This can be achieved numerically by standard root-finding algorithms, such as `fsolve` in MATLAB [44]. The evaluation of the integrals is also performed numerically.

*Remark* 1. For the Kuramoto model with $\lambda = 0$, the left-hand side of (3.13) is zero. If $g(\omega)$ is symmetric about $\omega = 0$, then (3.13) is satisfied for $\Omega = 0$ and (3.12) becomes

$$r = \int_{-Kr}^{Kr} \sqrt{1 - \frac{\omega^2}{K^2 r^2}} g(\omega) d\omega, \tag{3.14}$$

which is the classical self-consistency result for the Kuramoto model [36, 72, 3].

*Remark* 2. If the intrinsic frequency distribution $g(\omega)$ has finite support then for large enough $K$, the synchronized cluster $|\omega - \Omega| \leq Kr$ contains all the oscillators and if additionally $g(\omega)$ is symmetric about $\omega = 0$, (3.13) becomes

$$r \sin\lambda = \int_{-\infty}^{\infty} \frac{\omega - \Omega}{Kr} g(\omega) d\omega + 0 = -\frac{\Omega}{Kr}, \tag{3.15}$$

leading to $\Omega = -Kr^2 \sin\lambda$. For high $K$, $r \approx 1$ and $\Omega \approx -K \sin\lambda$, agreeing with the linear dependence observed in Figure 2.7.

### 3.1.1 The Case of Uniform Frequency Distribution $g(\omega)$

For some classes of intrinsic frequency distributions $g(\omega)$, the integrals in the self-consistency relations (3.12)–(3.13) can be computed explicitly, leading to a set of algebraic equations. Analysis of the system will be easier via analyzing the resulting algebraic equations that do not contain integrals. Numerical solution schemes are also easier to implement, as we now need to solve a set of algebraic equations, which is a standard problem with many established procedures, such as MATLAB's `fsolve` [44].

In this section we demonstrate this for a uniform intrinsic frequency distribution (2.6), which we recall here

$$g(\omega) = \mathcal{U}[-\gamma, \gamma] = \begin{cases} \frac{1}{2\gamma}, & -\gamma \leq \omega \leq \gamma \\ 0 & \text{otherwise.} \end{cases}$$

Despite its simplicity, to the best of our knowledge the mean-field limit has not been done before for the uniform distribution (2.6) for the Kuramoto-Sakaguchi model (2.1). In the following we show how the self-consistency relations (3.12)–(3.13) simplify to a set of algebraic equations.

For the classical Kuramoto model with no phase-offset, $\lambda = 0$, Pazó demonstrated in a seminal work [61] that a uniform $g(\omega)$ leads to an explosive first-order transition of the system from incoherence to synchronization. As $K$ increases across a critical coupling strength $K_c$, the order parameter $r$ jumps from $r \approx 0$ to a non-zero value $r > 0$ discontinuously, and the system transitions directly from incoherence to global synchronization where all oscillators are entrained within a synchronized cluster. In contrast, for a typical uni-modal $g(\omega)$, the Kuramoto model exhibits a smooth second-order transition: as $K$ increases past $K_c$, $r$ increases from $r \approx 0$ continuously, and the system transitions from incoherence to partial synchronization where the synchronized cluster gradually grows in size, starting off with few oscillators at $K$ slightly above $K_c$.

For the Kuramoto-Sakaguchi model with a generic $\lambda \neq 0$ under a uniform $g(\omega)$, we demonstrate, through investigating and numerically solving the self-consistency relations, that the transition from incoherence to synchronization is more intricate: as $K$ increases past a critical coupling strength $K_c$, $r$ still jumps from $r \approx 0$ to a non-zero value $r > 0$ discontinuously, however the system does not transition directly from incoherence to global synchronization. It instead transitions to a partial synchronization state where the synchronized cluster has a finite, non-zero size. As $K$ increases further, more oscillators become entrained to the cluster until $K$ passes $K = K_g$, at which all oscillators become entrained, corresponding to onset of global synchronization.

Evaluations of the integrals in (3.12)–(3.13) require determining the relative position of the bounds of synchronized cluster, $[\Omega - Kr, \Omega + Kr]$, which are also integration limits, compared to the bounds of $g(\omega)$'s support, $[-\gamma, \gamma]$. We consider different cases of their relative positions, which depend on the value of $K$. An illustration of the different cases is sketched in Figure 3.1.

*Case 1:* $\Omega - Kr < -\gamma < \gamma < \Omega + Kr$. For high enough coupling strength $K$, the synchronized cluster contains the entire support of $g(\omega)$, and the system is in the global synchronization state. There are no non-synchronized oscillators and from (3.13) we have

$$\Omega = -Kr^2 \sin\lambda. \tag{3.16}$$

Substituting into (3.12), using coordinate transformations $\eta = \frac{\omega - \Omega}{Kr}$ and

$\sin u = \eta$, we have

$$r\cos\lambda = \frac{Kr}{4\gamma}\left[\arcsin(\eta_2) - \arcsin(\eta_1) + \eta_2\sqrt{1-\eta_2^2} - \eta_1\sqrt{1-\eta_1^2}\right], \tag{3.17}$$

where

$$\eta_1 = -\frac{\gamma}{Kr} + r\sin\lambda, \qquad \eta_2 = \frac{\gamma}{Kr} + r\sin\lambda.$$

(3.17) is solved numerically to obtain $r$ at given value of $K$, $\lambda$. This solution is then substituted into (3.16) to obtain the corresponding value of $\Omega$.

*Case 2:* $\Omega - Kr < -\gamma < \gamma = \Omega + Kr$. For $\lambda > 0$, the cluster mean frequency at global synchronization, $\Omega = -Kr^2\sin\lambda$ is negative and is further away from the positive end of the support of $g(\omega)$, $\omega = \gamma$, than the negative end, $\omega = -\gamma$. As $K$ decreases, $\Omega + Kr$ reaches $+\gamma$ sooner than $\Omega - Kr$ reaches $-\gamma$. The critical case occurs when $\Omega + Kr = \gamma$, and comparing to Case 1 and Case 3, this corresponds to a transition from global synchronization to partial synchronization, at critical coupling strength $K = K_g$.

Substituting $\Omega + Kr = \gamma$ into (3.17) we have

$$\eta_2 = 1, \qquad \eta_1 = 2r\sin\lambda - 1$$

and

$$r\cos\lambda = \frac{1}{4(1-r\sin\lambda)}\Big[\frac{\pi}{2} - \arcsin(2r\sin\lambda - 1) - (2r\sin\lambda - 1)\sqrt{4r\sin\lambda(1-r\sin\lambda)}\Big].$$

This equation is solved numerically to obtain the value of $r$ at the onset of global synchronization, $r = r_g(\lambda)$. $r_g$ is substituted to find the corresponding value of $K_g(\lambda)$ and $\Omega_g(\lambda)$.

*Case 3*: $\Omega - Kr < -\gamma < \Omega + Kr < \gamma$. For lower values of $K$, the range of synchronized oscillators, $\Omega - Kr \le \omega \le \Omega + Kr$ does not cover the whole support of the frequency distribution $-\gamma \le \omega \le \gamma$, and the system is in a partial synchronization state. For $K$ slightly below $K_g$, the positive end of the support of $g(\omega)$ falls out of the synchronized range while the negative end remains within the synchronized range. This implies that the partial synchronization state is of the form that non-synchronized oscillators only occur at the positive end of $g(\omega)$, for $\Omega + Kr < \omega \le \gamma$, while all other oscillators up to the negative end of $g(\omega)$ remain synchronized.

For this case, the self-consistency relations (3.12)–(3.13) evaluate to

$$r\cos\lambda = \frac{Kr}{4\gamma}\left[\frac{\pi}{2} - \arcsin(\eta_1) - \eta_1\sqrt{1-\eta_1^2}\right] \tag{3.18}$$

$$r\sin\lambda = -\frac{\Omega}{Kr} + \frac{Kr}{4\gamma}\left[\ln\left(\eta_2 + \sqrt{\eta_2^2-1}\right) - \eta_2\sqrt{\eta_2^2-1}\right], \tag{3.19}$$

where

$$\eta_1 = \frac{-\gamma-\Omega}{Kr} \qquad \eta_2 = \frac{\gamma-\Omega}{Kr}.$$

The system of algebraic equations (3.18)–(3.19) is solved numerically to obtain $r$, $\Omega$ at given values of $K$, $\lambda$.

*Case 4:* $\Omega - Kr = -\gamma < \Omega + Kr < \gamma$. As the coupling strength $K$ further decreases, the negative end of the range of synchronized oscillators reaches the negative end of the support of $g(\omega)$, $\Omega - Kr = -\gamma$. Substituting into (3.18)–(3.19) $\eta_1 = -1$ and (3.18) becomes

$$r\cos\lambda = \frac{Kr\pi}{4\gamma}, \tag{3.20}$$

which has solution either $r = 0$ or $K = K_c$ where

$$K_c = \frac{4\gamma\cos\lambda}{\pi}.$$

The solution $r = 0$ corresponds to the incoherent state. For $K = K_c$, substituting we have

$$\frac{\Omega}{Kr} = 1 - \frac{\pi}{4r\cos\lambda}, \qquad \eta_2 = \frac{\pi}{2r\cos\lambda} - 1$$

and (3.19) becomes an equation for $r$ that is solved for the corresponding value of $r = r_c$. The corresponding value of $\Omega_c$ is obtained by substituting.

*Case 5.* $-\gamma < \Omega - Kr < \Omega + Kr < \gamma$. For lower values of $K$, $K < K_c$, the range of synchronized cluster $\Omega - Kr \le \omega \le \Omega + Kr$ falls completely within the support of the uniform frequency distribution, $-\gamma \le \omega \le \gamma$, and the system is in partial synchronization of the form that rogue oscillators appear at both ends of $g(\omega)$. Evaluating the self-consistency relation (3.12) then yields (3.20), which has solution either $r = 0$ or $K = K_c$. This corresponds to either incoherence, or partial synchronization that exists at one coupling strength $K = K_c$ only. It implies that there does not exist partial synchronization for coupling strength below

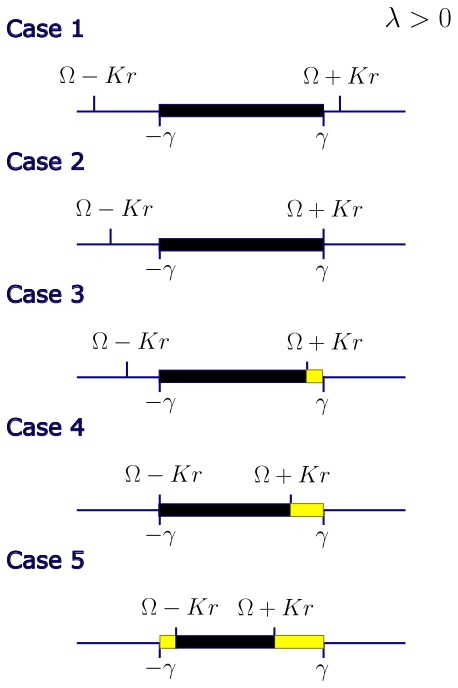


Figure 3.1: Illustration of the different cases of synchronization states corresponding to different coupling strength $K$ for the Kuramoto-Sakaguchi model (2.1) with a uniform intrinsic frequency distribution $g(\omega)$ (2.6) and a non-zero phase-offset $\lambda > 0$. For each diagram, upper ticks and labels correspond to possible location of the synchronized cluster obtained by the self-consistency analysis (3.12)–(3.13); lower ticks and labels correspond to the support of the uniform intrinsic frequency distribution $g(\omega)$, which stays at $[-\gamma, \gamma]$. Black solid lines and yellow solid lines indicate actual range of the synchronized oscillators and the non-synchronized rogue oscillators, respectively.

$K_c$ and there are no partial synchronization states of the form that rogue oscillators occur at both ends of $g(\omega)$. This agrees with numerical simulations: for uniform $g(\omega)$, for $0 < \lambda < \pi/2$, the partial synchronization states observed are always of the form that rogue oscillators occur at the positive end of $g(\omega)$ and all other oscillators up to the negative end of $g(\omega)$ are synchronized. Therefore, $K = K_c$ represents the transition from partial synchronization to incoherence.

We summarize the synchronization transition in the Kuramoto-Sakaguchi model (2.1) with uniform intrinsic frequency distribution $g(\omega)$ for $\lambda > 0$: at large $K$, all oscillators are synchronized; as $K$ decreases across $K = K_g$, oscillators at the positive end of $g(\omega)$ start to break off; more and

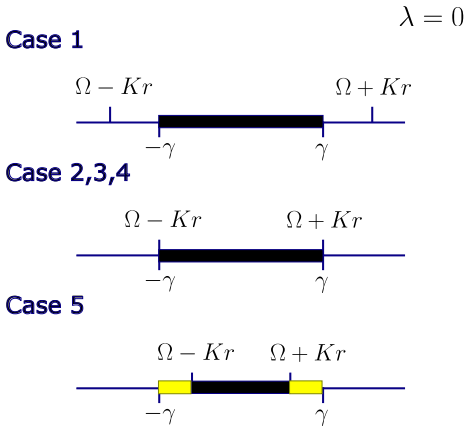


Figure 3.2: Illustration of the different synchronization states for the Kuramoto model with zero phase-offset $\lambda = 0$ and a uniform intrinsic frequency distribution $g(\omega)$. c.f. Figure 3.1.

more oscillators break off as $K$ decreases further until $K = K_c$, after which the synchronized cluster, which may still process a non-zero size, suddenly ceases to exist and the system transitions to incoherence, and remains for all $K < K_c$.

For $\lambda = 0$, in the global synchronization regime the cluster mean frequency is $\Omega = -Kr^2 \sin\lambda = 0$. The synchronized cluster, formed between $-Kr \leq \omega \leq Kr$ is symmetric about $\omega = 0$ and so is the support of $g(\omega)$. As $K$ decreases, the positive end of the synchronized cluster, $\omega = Kr$ reaches the positive end of the support of $g(\omega)$, $\omega = \gamma$ at the same time as do the negative ends $-Kr$ and $-\gamma$. Therefore for the previous analysis, Case 2 and Case 4 coincide and Case 3, which corresponds to partial synchronization state, does not exist. $K_g = K_c$ and the system is either in global synchronization state for $K \geq K_c$ or incoherent state for $K < K_c$.This is consistent with the result by Pazó [61]. Thus at $K = K_c$ the system experiences an explosive transition from incoherence to global synchronization. An illustration of the different synchronization states is provided in Figure 3.2.

Comparing to the synchronization transition for $\lambda = 0$, for systems with phase-offset $\lambda > 0$, at $K = K_c$, the onset of synchronization is still explosive, but instead of transitioning directly from incoherence to global synchronization, the system now transitions to partial synchronization with a synchronized cluster of a non-zero size. This cluster entrains oscillators up to the negative end of $g(\omega)$, while rogue oscillators are present at the positive end of $g(\omega)$. As $K$ increases from $K_c$ to $K_g$, the system exhibits an additional gradual transition to global synchronization, as

more and more oscillators become entrained to the cluster.

Figure 3.3 plots the numerical solutions of the self-consistency relations for the Kuramoto-Sakaguchi model with a uniform intrinsic frequency distribution $g(\omega)$ (2.6) with width $\gamma = 1$. The solution is corroborated with results from direct numerical simulation of the model with $N = 200$ oscillators generated equi-probably according to the mid-point rule (2.3). Shown are results for different coupling strengths $K$ and three values of phase-offsets, $\lambda = 0$ (left column), $\lambda = \pi/8$ (middle column) and $\lambda = \pi/4$ (right column). We display results of the order parameter $\bar{r}$ (top row), cluster mean-frequency $\Omega$ (middle row) and the location of synchronized cluster in terms of the smallest and largest intrinsic frequencies $\omega_{\min}, \omega_{\max}$ of oscillators within the synchronized cluster $\mathcal{C}$ (bottom row).

For $\lambda = 0$, we observe the explosive transition from incoherence to global synchronization at $K = K_c$, where a synchronized cluster containing all the oscillators emerges. For $\lambda = \pi/8$ we observe that at $K = K_c$, the system transitions to a partial synchronization state with a non-zero size of the synchronized cluster. The cluster gradually grows in size as $K$ increases until $K = K_g$ when all oscillators become entrained to the cluster. For $\lambda = \pi/4$, at $K_c$ the system still transitions to a partial synchronization state, but the cluster size is much smaller at $K_c$, and the transition at $K = K_c$ looks more similar to a smooth second-order transition.

We remark that at the partial synchronization states observed from direct numerical simulation for $\lambda = \pi/4$ and $\lambda = \pi/8$, the synchronized cluster always contain all oscillators up to the negative end of the support of the intrinsic frequency distribution $g(\omega)$, and rogue oscillators only appear near the positive end of $g(\omega)$, agreeing with results obtained from analyzing the self-consistency relation. (For $\lambda = \pi/4$, at $K = 0.9$ there appears to be a synchronized cluster that does not entrain all oscillators to the negative end of intrinsic frequencies. This is due to the strong fluctuations of the finite-size system near the onset of partial synchronization, and if one tightens the criteria when determining the synchronized cluster, this cluster of oscillators will not be considered as synchronized)

## 3.2 Ott-Antonsen ansatz

In Section 3.1, self-consistency relations were obtained for a generic intrinsic frequency distribution $g(\omega)$, allowing for determining the values of $r$ and $\Omega$ for the stationary state of the system. However, the argument and derivation rely on the condition of the system being in a stationary state, and the solutions obtained do not tell us much about the dynamical behaviours of the system.

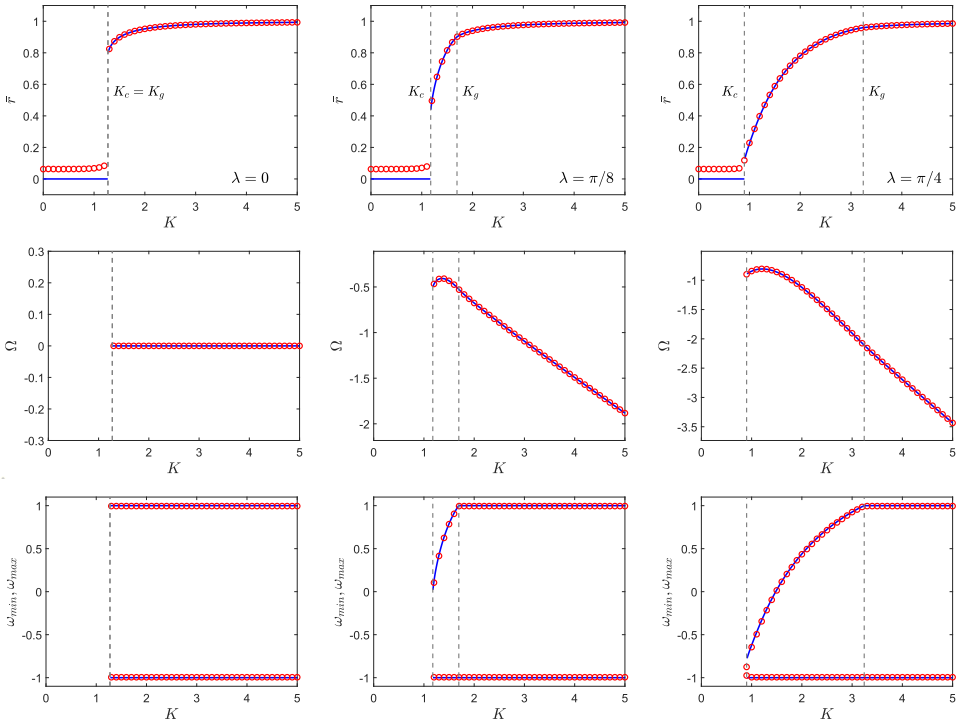


Figure 3.3: Collective behaviour of the Kuramoto-Sakaguchi model (2.1) with a uniform intrinsic frequency distribution (2.6) of width $\gamma = 1$. Shown are results obtained from numerical solution of the self-consistency relation (3.12)–(3.13) (blue solid line) and results from direct numerical simulation of the system with $N = 200$ oscillators of equi-probably generated intrinsic frequencies (red circles). Top row displays the result for the order parameter $\bar{r}$. Middle row displays the cluster mean-frequency $\Omega$. Bottom row displays location of synchronized cluster $\mathcal{C}$ in terms of the minimum and maximum intrinsic frequencies of oscillators within the cluster, $\omega_{\min}$, $\omega_{\max}$. Results are for phase-offset values $\lambda = 0$ (left column), $\lambda = \pi/8$, (middle column) and $\lambda = \pi/4$ (right column). Vertical lines indicate the coupling strengths corresponding to the onset of partial synchronization $K_c$, and onset of global synchronization $K_g$ obtained from the self-consistency relation.

Technically, the continuity equation (3.8) allows for determining the time evolution of the density $\rho(\theta, t; \omega)$, and hence the system's dynamical behaviour. However, directly solving this partial integro-differential equation is challenging.

The seminal work of Ott and Antonsen [55] demonstrated that under an ansatz for the form of $\rho(\theta, t; \omega)$, the dynamical equations become much simpler. The ansatz is in effect a restriction that $\rho$ lies on a lower-dimensional manifold, which has subsequently been shown to be attracting under broad conditions [56, 57]. Furthermore, for the case that $g(\omega)$ is Lorentzian, the equations can be further reduced, and the dynamics of the mean-field variables are described by a set of autonomous finite-dimensional ODEs.

The ansatz, which is referred to as the Ott-Antonsen (OA) ansatz, has since been extensively applied for analyzing the dynamics of a wide range of coupled oscillator system settings, from bi-modal distribution which exhibits standing wave solutions [40], system with external time-periodic driving [14] to systems consisting of sub-populations of oscillators with different inter- and intra- population coupling [1, 38, 9], in which the Ott-Antonsen ansatz provides great assistance in the analytical study of the emergent chimera states and chaotic dynamics.

Following [55, 38], we apply the Ott-Antonsen ansatz to the Kuramoto-Sakaguchi model (2.1) for a Lorentzian intrinsic frequency distribution $g(\omega)$ (2.5). The following derivation constitutes an application of the Ott-Antonsen ansatz to the Kuramoto-Sakaguchi model with a single population and a non-zero phase-offset, and is a sub-part of the analysis for more complicated systems, such as those in [38, 9].

Following on from Section 3.1, for the Kuramoto-Sakaguchi model in the thermodynamic limit, we consider the instantaneous density function of oscillators, $\rho(\theta, t; \omega)$. The phases $\theta$ are measured in a frame co-rotating with the synchronized cluster, at a constant frequency $\Omega$. Comparing with phases measured in the rest frame, $\phi$, there is a phase shift $\theta(t) = \phi(t) - \Omega t$ where $\Omega$ is a constant common frequency that is yet to be determined. Generally the Ott-Antonsen analysis concerns the density of phases in the rest frame, $\rho(\phi, t; \omega)$. We present here an analysis for the density of phases in a co-rotating frame, $\rho(\theta, t; \omega)$. The analysis is equivalent and gives the same result.

For ease of readability we recall from Section 3.1 that the density distribution $\rho(\theta, t; \omega)$ satisfies the continuity equation (3.8),

$$\frac{\partial}{\partial t}\rho = -\frac{\partial}{\partial \theta}\left(\rho v\right),$$

where

$$v(\theta, t; \omega) = \omega - \Omega + Kr\sin(\psi_0 - \theta - \lambda),$$

with the mean-field variables defined as in (3.7),

$$r(t)e^{\imath\psi_0(t)} = \int_{-\infty}^{\infty}\int_{-\pi}^{\pi} e^{\imath\theta}\rho(\theta,t;\omega)g(\omega)d\omega.$$

Since the phases $\theta$ are considered to be angles from $(-\pi,\pi]$, (i.e. angles that differ by integer multiples of $2\pi$ are identified as the same angle), the density function $\rho(\theta,t;\omega)$ should be $2\pi$-periodic in the phase argument $\theta$. Utilizing this, we can expand $\rho(\theta,t;\omega)$ as a Fourier series according to

$$\rho(\theta,t;\omega) = \frac{1}{2\pi}\left(1+\sum_{n=1}^{\infty} c_n(t;\omega)e^{\imath n\theta} + \overline{c}_n(t;\omega)e^{-\imath n\theta}\right). \tag{3.21}$$

Here and in the rest of this section, an overhead bar represents the complex conjugate. Substituting the Fourier expansion into the expression for the mean-field variables (3.7), we find that $r$ and $\psi_0$ now only depend on the first Fourier coefficient and we obtain

$$r(t)e^{\imath\psi_0(t)} = \int_{-\infty}^{\infty} \overline{c}_1(t;\omega)g(\omega)d\omega.$$

Substituting the Fourier expansion into the continuity equation (3.8), and comparing the coefficients of $e^{\imath n\theta}$ for each $n$, we arrive at an infinite set of equations for the $c_n(t;\omega)$s (each $n$ gives one equation).

The Ott-Antonsen (OA) ansatz assumes that the density $\rho(\theta,t;\omega)$ is in a form such that all the coefficients $c_n(t;\omega)$ are the consecutive powers of a function $\alpha(t;\omega)$, i.e.

$$c_n(t;\omega) = [\alpha(t;\omega)]^n \quad \forall n. \tag{3.22}$$

Substituting this ansatz into the infinite set of equations for $c_n(t;\omega)$, it turns out that all the equations from each power $e^{\imath n\theta}$ reduce to the exact same equation,

$$\dot{\alpha}(t;\omega) = -\imath(\omega-\Omega)\alpha - \frac{1}{2}\left(Ke^{-\imath\lambda}z\alpha^2 - Ke^{\imath\lambda}\overline{z}\right), \tag{3.23}$$

where

$$z(t) = r(t)e^{\imath\psi_0(t)} = \int_{-\infty}^{\infty}\overline{\alpha}(t;\omega)g(\omega)d\omega \tag{3.24}$$

is the complex mean-field variable. This is a striking result: as long as $\alpha(t;\omega)$ satisfies (3.23), the density function $\rho(\theta,t;\omega)$ with Fourier expansion coefficients given by the ansatz (3.22) will be a solution to the governing continuity equation (3.8). Thus, under the Ott-Antonsen ansatz for $\rho(\theta,t;\omega)$, the infinite dimensional partial integro-differential equation for the density $\rho(\theta,t;\omega)$ reduces to an infinite set of ODEs for $\alpha(t,\omega)$.

To proceed along the Ott-Antonsen analysis, further assumptions are made for $\alpha(t;\omega)$: it is assumed that $|\alpha(t;\omega)| \leq 1$ for all real $\omega$, and that $\alpha(t;\omega)$ can be analytically continued from real $\omega$ into the lower half complex $\omega$-plane, the continuation has no singularities, and $\alpha(t;\omega) \to 0$ as $\mathrm{Im}(\omega) \to -\infty$. It is demonstrated that if the conditions are satisfied for the initial $\alpha(0;\omega)$, it will be satisfied for $\alpha(t;\omega)$ at all finite time $0 < t < +\infty$ provided that $\alpha(t;\omega)$ is a solution to (3.23) [55].

Under these assumptions, for the case that the intrinsic frequency distribution $g(\omega)$ is Lorentzian (2.5), which we recall here as

$$g(\omega) = \frac{\Delta}{\pi}\frac{1}{\Delta^2+\omega^2} = \frac{1}{2\pi\imath}\left(\frac{1}{\omega-\imath\Delta} - \frac{1}{\omega+\imath\Delta}\right),$$

the dynamics can be simplified further. The integral for the complex order parameter (3.24) can now be performed via a contour integral, by enclosing with a semi-circle in the lower half $\omega$-plane. From the Residual Theorem, the value is given by the residual at $\omega = -\imath\Delta$,

$$z(t) = \int_{-\infty}^{\infty} \overline{\alpha}(t;\omega)g(\omega)d\omega = \overline{\alpha}(t;\omega = -\imath\Delta), \tag{3.25}$$

i.e. the order parameter $z(t)$ depends on the value of $\alpha(t;\omega)$ at a single point $\omega = -\imath\Delta$ only.

In (3.23), setting $\omega = -\imath\Delta$, utilizing (3.25), we arrive at an equation for $z(t)$ with

$$\dot{\overline{z}}(t) = (-\Delta + \imath\Omega)\overline{z} - \frac{1}{2}\left(Ke^{-\imath\lambda}z\overline{z}^2 - Ke^{\imath\lambda}\overline{z}\right).$$

Substituting $z(t) = r(t)e^{\imath\psi_0(t)}$, and after some re-arranging, we arrive at a set of two ODEs:

$$\dot{r} = -\frac{1}{2}Kr\cos\lambda\left(r^2 - 1 + \frac{2\Delta}{K\cos\lambda}\right) \tag{3.26}$$

$$r\dot{\psi}_0 = -\Omega r - \frac{1}{2}Kr\sin\lambda(r^2+1). \tag{3.27}$$

The equations are in skew product form: the dynamics of $r(t)$ depends on $r$ only and drives the dynamics of $\psi_0(t)$.

(3.26)–(3.27) constitute a set of 2 ODEs that specifies the dynamics of the mean-field variables $r(t)$, $\psi_0(t)$ explicitly. They are much simpler compared to the infinite-dimensional continuity equation (3.8). It should also be noted that under the Ott-Antonsen ansatz, the continuity equation reduces to (3.23), which is still an infinite-dimensional set of ODEs for $\alpha(t;\omega)$, one for each $\omega$ in the support of $g(\omega)$. It is only the dynamics of the mean-field variable $z(t) = r(t)e^{\imath\psi_0(t)}$ that reduces to a finite-dimensional set of ODEs.

The reduced ODEs (3.26)–(3.27) provide a much simpler avenue for analysis. Note that $r(t) = 0$ is always a solution. Focusing on the ODE for $r$, (3.26), for $0 \leq \lambda < \pi/2$, $r = 0$ is a stable equilibrium for $0 < K < K_c$, where

$$K_c = \frac{2\Delta}{\cos\lambda}. \tag{3.28}$$

For $K > K_c$, a set of equilibria $r = \pm r^*$, where

$$r^* = \sqrt{1 - \frac{2\Delta}{K\cos\lambda}}, \tag{3.29}$$

emerges via a supercritical pitchfork bifurcation at $K = K_c$. The solution $r = 0$ and $r = r^*$ correspond to incoherence and (partial) synchronization, respectively. $K = K_c$, at which the positive equilibrium $r = r^*$ emerges, corresponds to the onset of (partial) synchronization. For $K > K_c$ where $r = r^*$ exists, substituting $r = r^*$ into the equation for $\psi_0$, (3.27), we have

$$\dot{\psi_0} = -\Omega + \Delta\tan\lambda - K\sin\lambda = \text{const.}$$

This implies that in the partial synchronization state, the phase of a centre among all oscillators rotates at a constant rate. Currently we are in a reference frame assumed to be co-rotating with the synchronized cluster, at a constant frequency $\Omega$. In a frame of reference rotating at

$$\Omega = \Delta\tan\lambda - K\sin\lambda, \tag{3.30}$$

the cluster will be stationary with $\dot{\psi_0} = 0$. This also implies that in the rest frame, at partial synchronization, the synchronized cluster rotates at a constant frequency $\Omega$ given by (3.30).

Comparing to the self-consistency relations (3.12)–(3.13), the Ott-Antonsen analysis provides several additional results: the stability of incoherence $r = 0$ and partial synchronization state $r = r^*$ can now be obtained by analyzing the ODE (3.26). The analysis also provides the dynamics of $r(t)$, in addition to its equilibrium value.

# Chapter 4

# Average Effect of Rogue Oscillators and Their Incorporation Into Collective Coordinate Analysis

In this chapter we derive the average effect of rogue oscillators on the synchronized oscillators. This allows for a reduction of the full Kuramoto-Sakaguchi model to a closed system that involves the synchronized oscillators only.

We rewrite the Kuramoto-Sakaguchi model (2.1) by explicitly separating the interaction into those involving only the synchronized oscillators and those involving the rogue oscillators, and write

$$\frac{d}{dt}\theta_i(t) = \omega_i - \Omega + \frac{K}{N}\left[\sum_{j\in\mathcal{C}} \sin(\theta_j - \theta_i - \lambda) + \sum_{j\in\mathcal{R}} \sin(\theta_j - \theta_i - \lambda)\right]. \tag{4.1}$$

In this and in the following chapter we aim at expressing the interaction term involving the rogue oscillators as a function of the synchronized only, i.e.

$$\sum_{j\in\mathcal{R}} \sin(\theta_j - \theta_i - \lambda) = \mathcal{F}(\theta_i). \tag{4.2}$$

In this chapter we aim at finding $\mathcal{F}(\theta_i)$ as the mean of the interaction term. In Chapter 5 we then set out to describe the fluctuations around the mean.

After replacing the effects of rogue oscillators by their mean, in this chapter we apply the collective coordinate framework [29]. We derive thereby reduced dynamics for the synchronized oscillators, and show how

by incorporating the average effect of the rogue oscillators, the reduced dynamics approximate the dynamics of the full Kuramoto-Sakaguchi model well, in the case of finite-size systems.

## 4.1 The Average Effect of Rogue Oscillators

The following observation is crucial to construct an averaging procedure for the effect of the rogue oscillators. Rogue oscillators evolve at a time-scale much faster than that of the synchronized oscillators, which are nearly stationary in the co-rotating frame. This separation of time-scales suggest that a synchronized oscillator $\theta_i, i \in \mathcal{C}$ feels the effect of a rogue oscillator, $\theta_j, j \in \mathcal{R}$, as a time-average. Invoking Birkhoff's ergodic theorem the time-average can be approximated by averaging over the corresponding invariant density of the rogue oscillator's dynamics. For systems with an explicit time-scale separation, under the condition that the fast dynamics is ergodic with a unique invariant measure, in the limit of time-scale separation tending to infinity, Birkhoff's ergodic theorem applies, and the effects of the fast variables on the dynamics of the slow variables can be well-approximated by corresponding averages over the fast variables' invariant measure [28, 60]. Inspired by Birkhoff's ergodic theorem, identifying the synchronized oscillators $\theta_i, i \in \mathcal{C}$ and the rogue oscillators, $\theta_j, j \in \mathcal{R}$ as the fast and slow variables respectively, we may approximate the effect of the rogue oscillators on the synchronized oscillators via the time-average over the rogue oscillators' fast dynamics, which can in turn be approximated by averaging over the corresponding invariant density.

In the mean-field formulation (3.3), for rogue oscillators with $|\omega_i - \Omega| > Kr$, its velocity (3.4)

$$v_i(\theta_i; \omega_i) = \omega_i - \Omega + Kr \sin(\psi_0 - \theta_i - \lambda)$$

has no zeros and remains the same sign for all value of $\theta_i \in (-\pi, \pi]$. Here we are approximating the mean-field variables $r$, $\psi_0$ and $\Omega$ to be constants in time. Motivated by the fact that $dt/d\theta_i = 1/v_i(\theta_i)$ represents the time that the $i$-th oscillator's phase spend near an angle $\theta_i$, we argue that the invariant density $\rho_i(\theta_i)$ should be proportional to the inverse of its velocity, i.e.

$$\rho_i(\theta_i) = \frac{C_i}{|v_i(\theta_i)|} = \frac{C_i}{|\omega_i - \Omega + Kr \sin(\psi_0 - \theta_i - \lambda)|}, \tag{4.3}$$

where $C_i$ are normalization constants such that $\int_{-\pi}^{\pi} \rho_i(\theta_i) d\theta_i = 1$. Note that we already encountered this expression for the density of the non-entrained oscillators in Chapter 3 for the thermodynamic limit (c.f. (3.10)),

where it arises from the stationary solution of the continuity equation for the number density of infinitely many oscillators at the same intrinsic frequency $\omega$.

We provide numerical corroboration for the proposed invariant measure (4.3) in Figure 4.1, where we compare it with the empirical histogram of a rogue oscillator's phase from a long-time direct numerical simulations of the full Kuramoto-Sakaguchi model (2.1).

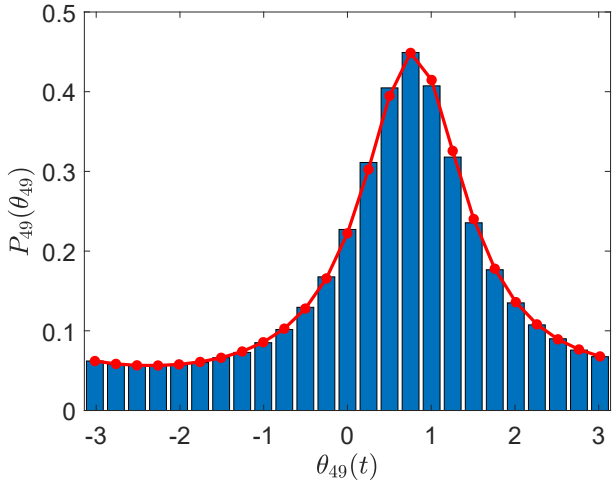


Figure 4.1: Normalized phase distribution of a single rogue oscillator $\theta_{49}$ obtained from numerical simulation of the full Kuramoto-Sakaguchi model (2.1) (histogram) and obtained from the ansatz (4.9) for the density function $P_i(\theta_i)$ (continuous curve). The Kuramoto-Sakaguchi model has $N = 50$ oscillators generated equi-probably according to the midpoint rule (2.3) from a Lorentzian frequency distribution (2.5) at $\Delta = 0.5$. The system has coupling strength $K = 10$ and phase-offset $\lambda = \pi/4$, at which a synchronized cluster forms for $2 \leq i \leq 47$. Phases from simulation $\phi_i(t)$ are shifted to obtain the corresponding phases $\theta_i(t)$ in the reference frame rotating with frequency $\Omega$. The values of $r$ and $\Omega$ in the proposed invariant density (4.3) are taken as their respective time-averages obtained from the simulation.

Then, writing the interaction term between rogue and synchronized oscillator (c.f. (4.1))

$$\begin{aligned}\sin(\theta_j - \theta_i - \lambda) &= \sin(\theta_j - \psi_0 + \lambda + \psi_0 - \theta_i - 2\lambda) \\ &= \sin(\theta_j - \psi_0 + \lambda)\cos(\psi_0 - \theta_i - 2\lambda) \\ &\quad + \cos(\theta_j - \psi_0 + \lambda)\sin(\psi_0 - \theta_i - 2\lambda),\end{aligned}$$

the average effect of rogue oscillators on a synchronized oscillator $\theta_i, i \in \mathcal{C}$

can be calculated via averaging over the invariant densities (4.3),

$$\begin{aligned}\sum_{j\in\mathcal{R}}\sin(\theta_j-\theta_i-\lambda) &\approx \sum_{j\in\mathcal{R}}\int_{-\pi}^{\pi}\sin(\theta_j-\theta_i-\lambda)\rho_j(\theta_j)d\theta_j\\ &=\sum_{j\in\mathcal{R}}\left[k_j\cos(\psi_0-\theta_i-2\lambda)+0\cdot\sin(\psi_0-\theta_i-2\lambda)\right]\\ &=\cos(\psi_0-\theta_i-2\lambda)\sum_{j\in\mathcal{R}}k_j,\end{aligned}$$

where

$$k_j=\frac{\omega_j-\Omega}{Kr}\left(1-\sqrt{1-\frac{K^2r^2}{(\omega_j-\Omega)^2}}\right). \tag{4.4}$$

In the governing equation for the synchronized oscillators (4.1), replacing the effects from rogue oscillators by their averages, we arrive at equations that involve the phases of synchronized oscillators only,

$$\frac{d}{dt}\theta_i(t)=\omega_i-\Omega+\frac{K}{N}\left(\sum_{j\in\mathcal{C}}\sin(\theta_j-\theta_i-\lambda)+\cos(\psi_0-\theta_i-2\lambda)\sum_{j\in\mathcal{R}}k_j\right), i\in\mathcal{C}. \tag{4.5}$$

Note that for the original Kuramoto model with $\lambda=0$ and with a symmetric frequency distribution with mean 0, for an ensemble of intrinsic frequencies $\omega_i$s that are exactly symmetric, where for each $i$ with $\omega_i=\hat{\omega}$, there is a $j$ with $\omega_j=-\hat{\omega}$, we have $\Omega=0$, which implies $\sum_{j\in\mathcal{R}}k_j=0$ as $k_j$s from opposite frequencies have opposite signs. This shows that the overall effect of rogue oscillators on synchronized oscillators cancels out in this case. Similarly, the rogue oscillators' overall effect on the mean-field variable $re^{\imath\psi}$ also cancels out due to symmetry for $\lambda=0$. This justifies that when constructing reduced models for the Kuramoto model with $\lambda=0$, the rogue oscillators can be ignored. For a general Kuramoto-Sakaguchi model with $\lambda\neq 0$, $\sum_{j\in\mathcal{R}}k_j\neq 0$ in general, and the effects of the rogue oscillators on the synchronized oscillators, as well as on the mean-field variable $re^{\imath\psi}$, do not cancel out.

We shall see in the numerical simulations presented in Section 4.3 that the inclusion of the rogue oscillators via the averaged effect on the synchronized cluster is crucial to obtain qualitative agreement between the reduced dynamics obtained from the collective coordinate framework and the full Kuramoto-Sakaguchi model. Ignoring the interaction term by setting $\sum_{j\in\mathcal{R}}k_j=0$ will be shown to only describe the collective behavior for large values of the coupling strength $K$ beyond the onset of global synchronization.

Next, we demonstrate the application of collective coordinate framework to derive reduced dynamics of the Kuramoto-Sakaguchi model,

where for the first time we incorporate the effect of the rogue oscillator.

## 4.2 Model Reduction via Collective Coordinate Framework

A model reduction method based on collective coordinates has recently been proposed and developed for finite-size Kuramoto models [29, 30, 31, 68, 69]. The approach is based on projecting the dynamics of the full model onto a judiciously chosen low-dimensional ansatz manifold to capture the collective dynamics of the system. The variables that are used to parameterize the ansatz manifold are the so-called collective coordinates.

For Kuramoto-like models, at high coupling strength, part of the oscillators form a single synchronized cluster, within which the phases stay close together. Thus a natural collective coordinate ansatz to propose is that the synchronized oscillators' phases can be well described by a certain shape profile. We make the ansatz that the synchronized cluster rotates at a constant frequency $\Omega$, and in a co-rotating frame, their phases are approximated by a shape profile

$$\theta_i(t) \approx \Theta_i(\alpha(t), \Omega), \quad i \in \mathcal{C}. \tag{4.6}$$

Here $\alpha(t)$ is a collective coordinate representing the spread of the phases. $\Omega$ is a collective parameter representing the common frequency of the cluster. Note that $\Omega$ does not have explicit time dependence. For now we assume that the synchronized cluster $\mathcal{C}$ is known *a priori*; we will discuss later how $\mathcal{C}$ can be determined via the collective coordinate approach.

We employ two ansatz functions for the shape profile $\Theta_i$, a linear function which approximates the phases at large coupling strength $K$, and a non-linear function which describes the exact stationary phase in the thermodynamic limit.

As presented in Section 3.1, in the co-rotating frame, from the mean-field formulation of the Kuramoto-Sakaguchi model (3.3), synchronized oscillators with $\frac{d}{dt}\theta_i(t) = 0$ have stable stationary solution (3.5) in terms of the mean-field variables given by

$$\theta_i^* = \psi_0 + \arcsin\left(\frac{\omega_i - \Omega}{Kr}\right) - \lambda.$$

Without loss of generality we assume $\psi_0 = 0$ from here on.

For high coupling strength $K$, expanding the stationary solution around $1/K \ll 1$ up to linear order suggests a shape profile of the form

$$\Theta_i = \frac{\omega_i - \Omega}{Kr} - \lambda. \tag{4.7}$$

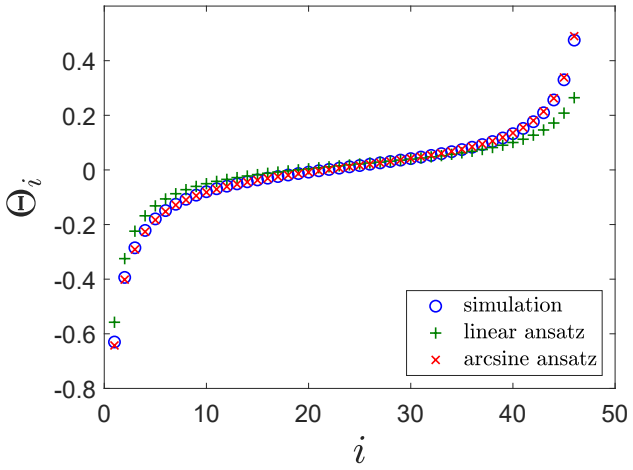


Figure 4.2: Stationary phases from the linear ansatz (4.7), the arcsine ansatz (4.8) and snapshot of the phases obtained from a simulation of the full Kuramoto-Sakaguchi model (2.1) with $N = 50$ oscillators. Parameters are the same as in Figure 4.1. The synchronized cluster forms for $2 \leq i \leq 47$. Each set of phases is shifted to have mean zero.

We coin this the *linear ansatz*.

Alternatively, using the full nonlinear solution, we arrive at

$$\Theta_i = \arcsin\left(\frac{\omega_i - \Omega}{Kr}\right) - \lambda. \tag{4.8}$$

We coin this the *arcsine ansatz*. Note that the arcsine ansatz is exact in the case of global synchronization.

For both ansatzes (4.7) and (4.8), we identify $\alpha(t) = r(t)$ as a time varying collective coordinate, and $\Omega$ as a collective parameter that does not have explicit time dependence. Note that $r(t)$ and $\Omega$ in the ansatz are now new variables that are different to the $r(t)$ and $\Omega$ defined for the original model.

Figure 4.2 compares the phases predicted by the linear ansatz (4.7) and the arcsine ansatz (4.8) with the phases obtained from simulations of the full Kuramoto-Sakaguchi model (2.1). The values of $r$ and $\Omega$ which appear in the ansatzes (4.7) and (4.8) are taken from time-averages from the numerical simulation. We will see below how to obtain their values from the collective coordinate approach. The arcsine ansatz produces phases which are barely distinguishable with the naked eye from those obtained from the simulations. The linear ansatz is also found to approximate the actual phases reasonably well.

In previous work on collective coordinates model reduction [29, 30, 31, 68, 69], non-entrained rogue oscillators $i \in \mathcal{R}$ and their effect on the

entrained oscillators, which are described by (4.6), were ignored. These works considered the standard Kuramoto model with $\lambda = 0$, where, as we argued before, the rogue oscillators' effect on the synchronized oscillators cancel out on average. Here we extend the collective coordinate framework to include the effect of non-entrained rogue oscillators, which will be shown in Section 4.3 to be crucial to accurately reproduce the collective dynamics of the Kuramoto-Sakaguchi model with $\lambda \neq 0$.

For the rogue oscillators $i \in \mathcal{R}$, we do not assume their phases to be well-described by a shape profile. Instead, as presented in Section 4.1, we treat their phases to be distributed according to their invariant density,

$$\theta_i \propto P_i(\theta_i), \quad i \in \mathcal{R}. \tag{4.9}$$

where $P_i(\theta_i)$ has the same function form as $\rho_i(\theta_i)$ specified in (4.3), but we now take the $r$ and $\Omega$ that appear in $P_i(\theta_i)$ (4.9) to be the collective variables in the ansatzes (4.7) and (4.8), rather than the mean-field variables defined for the original model. Again without loss of generality we set $\psi_0 = 0$. Effects of rogue oscillators, where present, are approximated by corresponding averages over the proposed invariant density (4.9).

We now derive the reduced system for the collective variables $r$ and $\Omega$. In the collective coordinate framework, the reduced dynamics for the collective coordinates are determined by requiring that the error associated with approximating the full system with the collective coordinate ansatz is minimal, in the sense that the error should be orthogonal to the subspace spanned by the ansatz as the collective coordinates vary, i.e., the error lies completely outside what can be captured by the ansatz. Note that one can view the method of collective coordinate as a Galerkin approximation.

The synchronized oscillators are governed in the co-rotating frame by (4.1) which, after replacing effects of rogue oscillators by averages through the invariant densities (4.9), becomes (4.5). We substitute the ansatz (4.6) into both left- and right-hand sides of the averaged Kuramoto-Sakaguchi equation (4.5). The left-hand side of (4.5) becomes

$$\text{LHS} = \frac{d}{dt}\Theta_i(r(t), \Omega) = \frac{\partial}{\partial r}\Theta_i(r(t), \Omega)\dot{r}.$$

Note that there are no terms involving $\dot{\Omega}$ as we assumed the collective parameter $\Omega$ to have no time dependence. The right-hand side of (4.5) becomes

$$\text{RHS} = \omega_i - \Omega + \frac{K}{N}\left[\sum_{j\in\mathcal{C}} \sin(\Theta_j - \Theta_i - \lambda) + \cos(\Theta_i + 2\lambda)\sum_{j\in\mathcal{R}} k_j\right].$$

The error associated with our ansatz is calculated as the difference between the two sides and reads

$$\mathcal{E}_i = \frac{\partial \Theta_i}{\partial r}\dot{r} - (\omega_i - \Omega) - \frac{K}{N}\left[\sum_{j\in\mathcal{C}} \sin(\Theta_j - \Theta_i - \lambda) + \cos(\Theta_i + 2\lambda)\sum_{j\in\mathcal{R}} k_j\right], \quad i \in \mathcal{C}. \tag{4.10}$$

The error is a vector with dimension equal to $|\mathcal{C}|$, the number of synchronized oscillators within the cluster $\mathcal{C}$.

The error (4.10) is required to be orthogonal to the subspace spanned by the ansatz (4.6) as the collective coordinates $r$ and $\Omega$ vary. The subspace is spanned by $\frac{\partial \Theta_i}{\partial r}$ and $\frac{\partial \Theta_i}{\partial \Omega}$, and the orthogonality condition is met when the projections of the error onto these two tangential directions are both zero. Thus we require

$$\sum_{i\in\mathcal{C}} \mathcal{E}_i \frac{\partial \Theta_i}{\partial r} = 0 \quad \text{and} \quad \sum_{i\in\mathcal{C}} \mathcal{E}_i \frac{\partial \Theta_i}{\partial \Omega} = 0. \tag{4.11}$$

This yields a 2-dimensional system of algebro-differential equations for the two collective coordinates $r$ and $\Omega$.

For both the linear ansatz (4.7) and the arcsine ansatz (4.8), the orthogonality condition (4.11) leads to a system of the form

$$\dot{r}\begin{pmatrix} H_r \\ H_\Omega \end{pmatrix} = \begin{pmatrix} F_r \\ F_\Omega \end{pmatrix} \tag{4.12}$$

where $H_{r,\Omega}, F_{r,\Omega}$ are (scalar) algebraic expressions involving $r$ and $\Omega$. The system (4.12) is equivalent to a set of one differential equation and one algebraic equation, of the form

$$\dot{r} = F_a(r, \Omega) \tag{4.13}$$

$$0 = F_b(r, \Omega), \tag{4.14}$$

where

$$F_a(r, \Omega) = F_r(r, \Omega)/H_r(r, \Omega)$$
$$F_b(r, \Omega) = H_\Omega F_r - H_r F_\Omega.$$

The simplification from (4.12) to (4.13)–(4.14) is valid provided the coefficient $H_r(r, \Omega)$ is non-zero, which, as shown in the following subsections for both the linear ansatz and the arcsine ansatz, holds for intrinsic frequencies $\omega_i$ that are not all identical, which is the situation considered in this thesis.

We remark that solving the algebraic equation (4.14) yields $\Omega = \Omega(r)$, which, upon substitution into (4.13), gives an explicit evolution equation for the order parameter

$$\dot{r} = F_a(r, \Omega(r)). \tag{4.15}$$

Note that $\Omega$ is given implicitly in (4.14), and has to be solved for numerically in practice.

For stationary states of the reduced system we set $\dot{r} = 0$, and (4.13)–(4.14) becomes a 2-dimensional systems of algebraic equations for $r$ and $\Omega$.

We now provide more explicit expressions of $H_{r,\Omega}$ and $F_{r,\Omega}$ for the two ansatzes in the two following subsections.

## Linear ansatz

For the linear ansatz (4.7) we evaluate

$$\frac{\partial \Theta_i}{\partial r} = -\frac{\omega_i - \Omega}{Kr^2}, \qquad \frac{\partial \Theta_i}{\partial \Omega} = -\frac{1}{Kr},$$

and (4.11) leads to the following system of two equations

$$\dot{r}\boldsymbol{H}_{\text{lin}} = \boldsymbol{F}_{\text{lin}}(r, \Omega), \tag{4.16}$$

where

$$\boldsymbol{H}_{\text{lin}} = \begin{pmatrix} \sum_{i\in\mathcal{C}} \frac{(\omega_i-\Omega)^2}{K^2r^4} \\ \sum_{i\in\mathcal{C}} \frac{\omega_i-\Omega}{K^2r^3} \end{pmatrix}$$

and

$$\boldsymbol{F}_{\text{lin}} = -\begin{pmatrix} \sum_{i\in\mathcal{C}} \frac{(\omega_i-\Omega)^2}{Kr^2} + \frac{K}{N}\sum_{i\in\mathcal{C}} \frac{\omega_i-\Omega}{Kr^2} h_i \\ \sum_{i\in\mathcal{C}} \frac{(\omega_i-\Omega)}{Kr} + \frac{K}{N}\sum_{i\in\mathcal{C}} \frac{1}{Kr} h_i \end{pmatrix},$$

with

$$h_i = \sum_{j\in C} \sin(\Theta_j - \Theta_i - \lambda) + \cos(\Theta_i + 2\lambda) \sum_{j\in\mathcal{R}} k_j,$$

where $k_j$ are as in (4.4).

Comparing (4.16) to (4.12), we identify $H_r = \sum_{i\in\mathcal{C}} \frac{(\omega_i-\Omega)^2}{K^2r^4}$, which is non-zero for intrinsic frequencies $\omega_i, i \in \mathcal{C}$ that are not all identical and equal to $\Omega$.

## Arcsine ansatz

Defining

$$s_i = \frac{\omega_i - \Omega}{Kr} \text{ and } c_i = \sqrt{1 - \frac{(\omega_i - \Omega)^2}{K^2r^2}},$$

we evaluate for the arcsine ansatz (4.8)

$$\frac{\partial \Theta_i}{\partial r} = -\frac{s_i}{r c_i}, \qquad \frac{\partial \Theta_i}{\partial \Omega} = -\frac{1}{K r c_i},$$

and (4.11) leads to the following system of two equations

$$\dot{r}\boldsymbol{H}_{\text{asin}} = \boldsymbol{F}_{\text{asin}}(r, \Omega), \tag{4.17}$$

where

$$\boldsymbol{H}_{\text{asin}} = \begin{pmatrix} \frac{1}{r^2} \sum_{i \in \mathcal{C}} \frac{s_i^2}{c_i^2} \\ \frac{1}{Kr^2} \sum_{i \in \mathcal{C}} \frac{s_i}{c_i^2} \end{pmatrix}$$

and

$$\boldsymbol{F}_{\text{asin}} = -G \begin{pmatrix} F_1 \\ F_2 \end{pmatrix}$$

with

$$\begin{aligned} G &= \begin{pmatrix} KC & KA \\ E & N_c \end{pmatrix} \\ F_1 &= 1 - \frac{1}{Nr}(A \sin\lambda + B \cos\lambda + D \sin\lambda) \\ F_2 &= \frac{1}{Nr}(A \cos\lambda - B \sin\lambda + D \cos\lambda), \end{aligned}$$

with

$$\begin{aligned} A &= \sum_{i \in \mathcal{C}} s_i, \;\; B = \sum_{i \in \mathcal{C}} c_i, \;\; C = \sum_{i \in \mathcal{C}} \frac{s_i^2}{c_i}, \\ D &= \sum_{i \in \mathcal{R}} k_i, \;\; E = \sum_{i \in \mathcal{C}} \frac{s_i}{c_i}. \end{aligned}$$

Comparing (4.17) to (4.12), we identify $H_r = \frac{1}{r^2} \sum_{i \in \mathcal{C}} \frac{s_i^2}{c_i^2}$, which again is non-zero provided the intrinsic frequencies $\omega_i, i \in \mathcal{C}$ are not all identical and equal to $\Omega$.

We are concerned with stationary solutions $\dot{r} = 0$, since stable stationary solutions correspond to synchronized states. For the arcsine ansatz with rogues included, setting $\dot{r} = 0$ in (4.17) results in

$$\mathbf{0} = \boldsymbol{F}_{\text{asin}}(r, \Omega).$$

This equation is satisfied if $F_1 = 0$, $F_2 = 0$, which is equivalent to

$$r\cos\lambda = \frac{1}{N}B,$$
$$r\sin\lambda = \frac{1}{N}\left(A + D\right),$$

or, when written out explicitly becomes

$$r\cos\lambda = \frac{1}{N}\sum_{j\in\mathcal{C}}\sqrt{1-\frac{(\omega_j-\Omega)^2}{K^2r^2}} \tag{4.18}$$

$$r\sin\lambda = \frac{1}{N}\left(\sum_{j\in\mathcal{C}}\frac{\omega_j-\Omega}{Kr} + \sum_{j\in\mathcal{R}}k_j\right). \tag{4.19}$$

In the thermodynamic limit $N \to \infty$ the collective coordinate approach recovers the mean-field self consistency equations (3.12)–(3.13). This correspondence with the mean-field theory is only achieved for the arcsine ansatz and when the rogue oscillators are taken into account.

In Section 4.3 we further show that the collective coordinate equations using the arcsine ansatz capture the collective dynamics of the full Kuramoto-Sakaguchi model with finitely many oscillators more accurately than when using the linear ansatz. However we remark that the linear ansatz (4.7), defined here for an all-to-all coupling network, can be extended to arbitrary network topologies, as carried out in [31], where for Kuramoto models with generic coupling networks, reduced dynamics are derived via the collective coordinate framework with the ansatz based on linearization of synchronized states at high coupling strength $K$. On the other hand, the (more accurate) arcsine ansatz (4.8), as developed here, is restricted to a globally connected all-to-all network.

## Identifying the Synchronized Cluster Within the Collective Coordinate Framework

At this stage, we have tacitly assumed that the cluster is known and we can separate the oscillators into those that synchronize $i \in \mathcal{C}$ and the non-entrained rogues $i \in \mathcal{R}$. To obtain the cluster via the collective coordinate method, we assume that if nodes can synchronize, they will do so. We therefore seek the maximal set of synchronized oscillators $\mathcal{C}$ such that the system of reduced algebro-differential equations (4.13)–(4.14) has a stable stationary solution. If stationary solutions cannot be found, we exclude nodes $i$ with maximal value of $|\Omega - \omega_i|$, check again for existence of stationary solutions, and, if needed, repeat this procedure until we arrive at a set $\mathcal{C}$ for which a stationary solution can be found. This criterion, however, is not sufficient to find the best approximation

for the synchronized cluster, as there may be a stationary solution of (4.13)–(4.14) which is linearly stable within the ansatz manifold $\Theta_i(r, \Omega)$, but is unstable in the full Kuramoto-Sakaguchi model (3.1), that is, the dynamics transverse to the ansatz manifold near the stationary solution is unstable. To account for this, we study the stability of the approximated phases $\Theta_i$ by substituting $\theta_i(t) = \Theta_i + \eta_i(t)$, where $\eta_i(t)$ represents small perturbations, into the full Kuramoto-Sakaguchi model (3.1). Expanding up to linear order of $\eta$ and assuming $\Theta_i$ satisfies the equation at lowest order, we arrive at a linear system of the form

$$\dot{\eta}_i = \sum_{j \in \mathcal{C}} L_{ij} \eta_j, \tag{4.20}$$

where

$$L_{ij} = \begin{cases} \cos(\Theta_j - \Theta_i - \lambda), & j \neq i \\ -\sum\limits_{l \in \mathcal{C}, l \neq i} \cos(\Theta_l - \Theta_i - \lambda) - \sin(\Theta_i + 2\lambda) \sum\limits_{l \in \mathcal{R}} k_l, & j = i \end{cases} \tag{4.21}$$

The matrix $L$ always has an eigenvector $(1, 1, \ldots, 1)$ with eigenvalue $\lambda_1 = 0$, corresponding to the system's invariance to a constant phase shift, if all oscillators partake in synchronisation. The presence of rogue oscillators leads to perturbations of this eigenvector and its associated eigenvalue. If all other eigenvectors have eigenvalues with negative real parts, we consider the phases $\Theta_i$ and the stationary solution $r$ and $\Omega$ to be stable in the full Kuramoto-Sakaguchi model. Note that this assumes that our collective coordinate ansatz and the stationary solutions $r$ and $\Omega$ are indeed a good approximation of the actual phases $\theta_i$. If $\Theta_i$ is not stable according to this definition, we again exclude the node with intrinsic frequency having maximal $|\Omega - \omega_i|$. This procedure is repeated until a stable stationary solution of the reduced equations (4.13)–(4.14) is found. At each step we check that there are no stable solutions possible for nearby clusters, displaced by up to 5 nodes.

In practice when sweeping through varying coupling strength $K$ we apply our analysis to systems at consecutive values of $K$ with small increments $\Delta K$, while keeping all other parameter settings the same. Starting from a large $K$, where synchronization is strong, after finding solutions $r$ and $\Omega$ of the reduced equations (4.13)–(4.14) at one value of $K$, we keep the solution as reference for the immediate lower $K$, which can provide some assistance. For instance, the value of $\Omega$ from previous $K$ can be a good indication of where the centre of the synchronized cluster should be at, which can assist us in determining which oscillators are to become rogues according to the value of $|\Omega - \omega_i|$.

### Extracting the Order Parameter from Collective Coordinate Framework

For a given ansatz function $\Theta$, i.e., the linear ansatz (4.7) or the arcsine ansatz (4.8), we can now determine the order parameter $\bar{r}$, the cluster mean frequency $\Omega$, the size of the synchronized cluster $\mathcal{C}$ and other properties of the collective behavior. When the effect of the rogue oscillators on the synchronized cluster is taken into account, the order parameter $r$ obtained as the stationary solution of the collective coordinate evolution equation (4.15) should satisfy

$$r = \left| \frac{1}{N} \left( \sum_{j \in \mathcal{C}} e^{i\Theta_j} + \sum_{j \in \mathcal{R}} \int_{-\pi}^{\pi} e^{i\theta_j} P_j(\theta_j) d\theta_j \right) \right|, \tag{4.22}$$

where $P_j(\theta_j)$ is the probability density function of the rogue oscillators (4.9). This equality, however, is only ensured for the arcsine ansatz and only if the rogue oscillators are included in the collective coordinate approach. For the arcsine ansatz (4.8) and the distributional ansatz for the rogue oscillators (4.9), splitting the real and imaginary parts of the sum within the absolute value readily yields (4.18)–(4.19), respectively. For the linear ansatz function the equality is only approximately satisfied up to $\mathcal{O}(1/K^2)$.

In the following section we demonstrate how each of the two ansatz functions (4.7) and (4.8) performs in reproducing the collective behavior of the full Kuramoto-Sakaguchi model, and, in particular, we show how the inclusion of the rogue oscillators is necessary to accurately capture the dynamics of the partially synchronized state near the onset of synchronization.

## 4.3 Numerical Results

In this section we illustrate the efficacy of the collective coordinate approach with the linear ansatz (4.7) and the arcsine ansatz (4.8) to approximate the collective behavior of the full Kuramoto-Sakaguchi model (2.1). We will cast particular emphasis on the inclusion or neglect of the effect of the rogue oscillators. Specifically, we present estimates for the order parameter $\bar{r}$ and the mean cluster frequency $\Omega$, as well as identification of the synchronized cluster $\mathcal{C}$ and the critical coupling strength for partial synchronization $K_c$ and for global synchronization $K_g$.

In the collective coordinate framework, the approximation for $\Omega$ is obtained directly from the stable stationary solution of the reduced equations (4.13)–(4.14), and the approximation for $\bar{r}$ is obtained by substituting the stable stationary solution into (4.22). We note that for the

arcsine ansatz with rogues included, $\bar{r}$ obtained via (4.22) coincides with the stationary solution of the order parameter of (4.13)–(4.14), i.e., it is self consistent, as discussed in the previous section. For the linear ansatz we found that using $r$ obtained via (4.22) yields a more accurate approximation of the order parameter than using the stationary solution directly. Note that in the cases where the rogue oscillators are ignored when finding the solution to (4.13)–(4.14), we still include the influence of rogues in (4.22). We find there is only a small difference between including or ignoring the rogue oscillators in (4.22) in these cases.

Real stationary solutions $r$ and $\Omega$ of the collective coordinate approximation (4.13)–(4.14) are found numerically using MATLAB's `fsolve` function [44]. The algebro-differential equations for the collective coordinates (4.13)–(4.14) typically have a pair of solutions, one stable and one unstable, corresponding to a saddle-node bifurcation, and care needs to be taken to select the correct stable solution. This is achieved by maintaining continuity when $K$ is varied. Furthermore, (4.13)–(4.14) contain square roots and arcsine functions and we need to check that their arguments are within the respective domain (otherwise `fsolve` seeks solutions in the complex domain).

A brief comment on the computational cost of the collective coordinate method compared to direct numerical simulation of the Kuramoto-Sakaguchi model. To estimate the order parameter using the collective coordinate method there are several steps involved. The root finding method to obtain the stationary solutions of the collective coordinates involves fast standard root finding routines such as `fsolve` in MATLAB [44]. When cycling through different values of the coupling strength the stationary solutions of a previous value of the coupling strength can be used as initial condition for the adjacent coupling strength to facilitate the root finding. In the case that no stationary solution can be found, we check whether a stationary solution exists for synchronized clusters shifted up to 5 frequencies in each direction. The stability of stationary solutions that are found is then tested by employing standard eigenvalue routines for the Jacobian. The computational cost has to be set against the computational complexity associated with the temporal evolution of the full Kuramoto-Sakaguchi model. Since the Kuramoto-Sakaguchi model does not evolve into stationary states due to the effect of the rogue oscillators, the length of the simulation may be very large to ensure convergence of the averaged order parameter. This is especially the case close to the bifurcation from incoherence to partial synchronization when the number of rogue oscillators is large, which can be prohibitive.

### 4.3.1 Order Parameter $\bar{r}$

Figure 4.3 shows the order parameter $\bar{r}$ for a phase-offset $\lambda = \pi/4$. We show results obtained from the collective coordinate approach, where $\bar{r}$ is defined via (4.22), using both the linear ansatz (4.7) and the arcsine ansatz (4.8), and both with and without the inclusion of the rogue oscillators. This is compared with the order parameter obtained from a numerical simulation of the full Kuramoto-Sakaguchi model (2.1). We show results for a Lorentzian intrinsic frequency distribution (2.5) with $\Delta = 0.5$ (Figure 4.3(a)) and for a uniform intrinsic frequency distribution (2.6) with $\gamma = 1$. (Fig. 4.3(b)). The intrinsic frequencies $\omega_i$ are drawn equi-probably according to the mid-point rule (2.3) for $N = 50$ oscillators. Vertical dashed lines indicate the onset of partial synchronization, for which a synchronized cluster emerges, at $K = K_c$, and the onset of global synchronization, for which all oscillators become synchronized, at $K = K_g$.

It is seen that including the rogue oscillators is crucial in obtaining a correspondence between the results of the full Kuramoto-Sakaguchi model (2.1) and of our model reduction, for both frequency distributions and for both types of ansatz. The effect the rogue of oscillators is particularly striking for the arcsine ansatz; including the rogues leads to a very small error in the estimate of the order parameter for all values of the coupling strength $K$, whereas without the rogue oscillators no stationary solutions can be found for $K \lesssim 4$ for the Lorentzian distribution and for $K \lesssim 2.5$ for the uniform distribution, completely missing the critical coupling strengths for the onset of partial synchronization at $K_c \approx 1.45$ and $K_c \approx 0.95$, for the respective intrinsic frequency distributions. Similarly, the inclusion of rogue oscillators markedly improves the estimate of the order parameter for the linear ansatz.

To quantify the accuracy of the collective coordinate approaches, we compute the error in their estimates of $\bar{r}$, when the rogue oscillators are included, compared to $\bar{r}$ obtained from a simulation of the full Kuramoto-Sakaguchi model (2.1). We also compute the order parameter $\bar{r}$ in the thermodynamic limit $N \to \infty$. For Lorentzian frequency distributions this was calculated via the Ott-Antonsen ansatz as in Section 3.2 which yields (3.29). For uniform frequency distribution this was calculated via the self-consistency relation as in Section 3.1.1. The errors are plotted in Figure 4.5(a,b) for the Lorentzian and the uniform frequency distribution, respectively. The error is lowest for the arcsine ansatz which is designed for finite networks. For the uniform frequency distribution, the error of the arcsine ansatz is of the order of the numerical round-off error when the system is in global synchronization with $K > K_g \approx 3.2$; this is because for global synchronization the arcsine ansatz (4.8) is exact. For the Lorentzian frequency distribution $K_g \approx 53.7$ which is not in the range

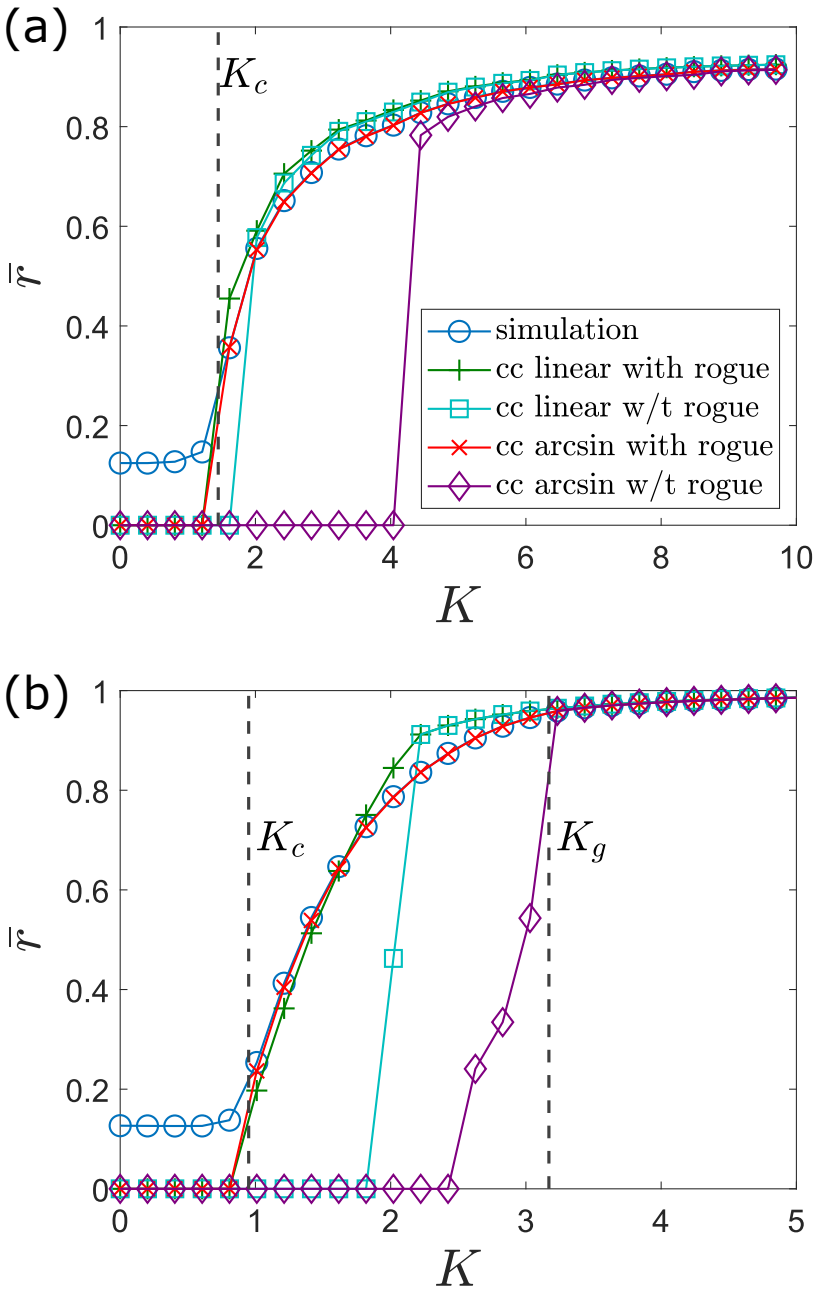


Figure 4.3: Order parameter $\bar{r}$ for the Kuramoto-Sakaguchi model (2.1) with $\lambda = \pi/4$ and $N = 50$ oscillators. Shown are estimates obtained using the collective coordinate approach (labelled cc) with a linear ansatz (4.7) and an arcsine ansatz (4.8), both with and without including the effect of rogue oscillators, as well as obtained from a numerical simulation of the full Kuramoto-Sakaguchi model (2.1). (a): Lorentzian distribution (2.5) with $\Delta = 0.5$. (b): uniform distribution (2.6) with $\gamma = 1$. Dotted vertical lines denote the onset of partial synchronization at $K = K_c$ and of global synchronization, at $K = K_g$.

shown in Figure 4.3. The mean-field solution is generally more accurate than the collective coordinate solution using the linear ansatz. The sharp drops of the error of the mean-field limit for the Lorentzian frequency distribution stem from the estimate of $\bar{r}(K)$ crossing the curve of the order parameter of the full Kuramoto-Sakaguchi model near $K \approx 7.5$ for the mean-field limit.

### 4.3.2 Cluster Mean Frequency $\Omega$

Figure 4.4 shows the cluster mean frequency $\Omega$. In the collective coordinate approach $\Omega$ is estimated directly with the stationary solution of the reduced system (4.13)–(4.14). Here we show results from both the linear ansatz (4.7) and the arcsine ansatz (4.8), both including the effect of rogue oscillators, and compare with the cluster mean frequency obtained from numerical simulation of the full system. It is seen that both ansatzes approximates $\Omega$ quite accurately. In particular, the non-monotonic dependence of $\Omega$ on $K$ for the uniform distribution near the onset of partial synchronization as observed in Figure 2.7(b) is well captured.

Figure 4.5(c,d) shows the error in estimating the cluster mean frequency $\Omega$ for a phase-offset $\lambda = \pi/4$ (c.f. Figure 2.7 for $\Omega(K)$ for the full Kuramoto-Sakaguchi model). We further show the error from the Ott-Antonsen analysis (3.30) for Lorentzian $g(\omega)$ and from the self-consistency analysis (as in Section 3.1.1) for uniform $g(\omega)$. Again, the collective coordinate approach using the arcsine ansatz achieves the smallest error, and since the ansatz is exact for globally synchronized oscillators the error is negligible for $K > K_g$.

Not surprisingly, the behavior of the error for $\Omega$ echos the behavior of the error for the order parameter. As for the order parameter $\bar{r}$, including the effect of the rogue oscillators is crucial to accurately estimate the cluster mean frequency of the actual Kuramoto-Sakaguchi model (2.1) for the whole range of coupling strengths. When the effect of the rogue oscillators is included, the cluster mean frequency $\Omega(K)$ is very well approximated by the collective coordinate approach, for both the linear and the arcsine ansatz. Again, the collective coordinate approach using the linear ansatz exhibits the largest errors, except for dips when the curves $\Omega(K)$ obtained from the collective coordinates crosses the curve of the full Kuramoto-Sakaguchi model.

### 4.3.3 Synchronized Cluster $\mathcal{C}$

Figure 4.6 shows the minimal and maximal intrinsic frequencies $\omega_{\min}$ and $\omega_{\max}$, respectively, such that all oscillators with intrinsic frequencies $\omega_{\min} \leq \omega_i \leq \omega_{\max}$ partake in synchronized dynamics. The rogue

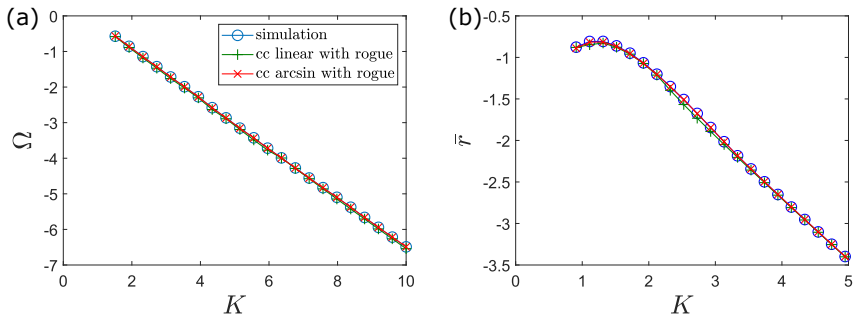


Figure 4.4: Cluster mean frequency $\Omega$ for the Kuramoto-Sakaguchi model (2.1) with $\lambda = \pi/4$ and $N = 50$ oscillators. Shown are estimates obtained using the collective coordinate approach (labelled cc) with a linear ansatz (4.7) and an arcsine ansatz (4.8), both including the effect of rogue oscillators, as well as obtained from a numerical simulation of the full Kuramoto-Sakaguchi model (2.1). (a): Lorentzian distribution (2.5) with $\Delta = 0.5$. (b): uniform distribution (2.6) with $\gamma = 1$.

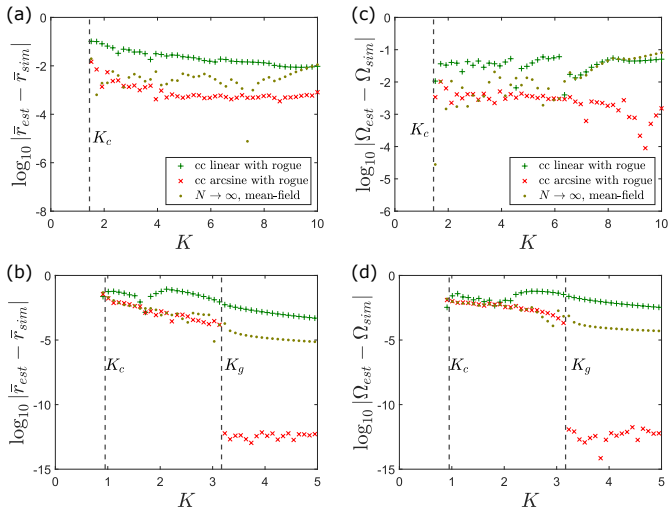


Figure 4.5: Error in estimates of the order parameter $\bar{r}$ (a,b) and of the cluster mean frequency $\Omega$ (c,d) for the various collective coordinate approaches (labelled cc) shown in Figure 4.3. Top row: Lorentzian distribution (2.5); shown is also results in the thermodynamic limit from Ott-Antonsen analysis (3.29)–(3.30) for comparison. Bottom row: uniform distribution (2.6); shown is also results in the thermodynamic limit from the self-consistency relation as in Section 3.1.1. Dotted vertical lines denote the onset of partial synchronization at $K = K_c$ and of global synchronization, at $K = K_g$.

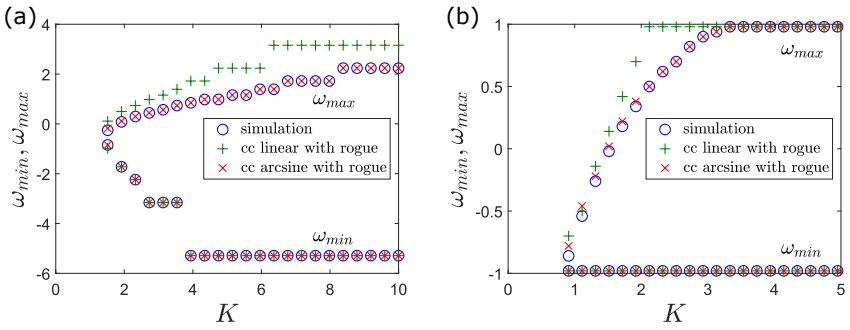


Figure 4.6: Minimal and maximal intrinsic frequencies $(\omega_{\min}, \omega_{\max})$ of the synchronized cluster $\mathcal{C}$ for a phase-offset $\lambda = \pi/4$. We show results obtained from the collective coordinate approach (labelled cc) using the linear ansatz (4.7) and the arcsine ansatz (4.8), both including the effect of rogue oscillators, and obtained from a numerical simulation of the full Kuramoto-Sakaguchi model (2.1) with $N = 50$ oscillators. (a) Lorentzian frequency distribution (2.5). (b) Uniform frequency distribution (2.6).

oscillators, by definition, are those with intrinsic frequencies outside this range (i.e., with intrinsic frequencies $\omega_i < \omega_{\min}$ or $\omega_i > \omega_{\max}$). We show results of the synchronized cluster obtained from numerical simulation of the full Kuramoto-Sakaguchi model (2.1), as well as results from the collective coordinate approach using the linear ansatz (4.7) and the arcsine ansatz (4.8), both with the inclusion of the rogue oscillators. We recall that, for the collective coordinate approach, the synchronized cluster $\mathcal{C}$ is defined as the largest set of oscillators for which the reduced equations (4.13)–(4.14) have a stationary solution that is stable in the full Kuramoto-Sakaguchi model (3.1). It is seen that the arcsine ansatz captures the synchronized cluster very well, with small discrepancies occurring only close to the onset of partial synchronization at $K_c$. The linear ansatz tends to overpredict the size of the synchronized cluster.

### 4.3.4 Critical Coupling Strengths $K_c$ and $K_g$

We estimate the critical coupling strength $K_c = K_c(\lambda)$ corresponding to the onset of partial synchronization as the smallest value of $K$ such that the order parameter $\bar{r}$ exceeds a threshold value $\bar{r} > 0.2$, where $\bar{r}(K)$ is sampled in increments $\Delta K = 0.01$. We obtain $K_c(\lambda)$ in this way for the full Kuramoto-Sakaguchi model (2.1) and for the collective coordinate approach with the arcsine ansatz and rogues included (4.13)–(4.14). The critical coupling strength $K_g$ corresponding to the onset of global synchronization is obtained such that all of the oscillators synchronize. For the collective coordinate approach, $K_g$ is defined as the lowest value of $K$ such that a stationary solution of the reduced equations (4.13)–

(4.14) exists for $\mathcal{C}$ consisting of all $N$ oscillators, and is stable in the full Kuramoto-Sakaguchi model (3.1).

In Figure 4.7 we compare the critical coupling strength $K_c$ and $K_g$ as a function of the phase-offset parameter $\lambda$ estimated from numerical simulations of the full Kuramoto-Sakaguchi model (2.1), and from the collective coordinate approach (using the arcsine-ansatz including the rogue oscillators) for the Lorentzian and the uniform frequency distribution. For both frequency distributions the collective coordinate approach captures the onset of partial and of global synchronization remarkably well. For the Lorentzian frequency distribution we also show results of the mean-field analysis for partial synchronization which captures the onset very well even for the finite network with only $N = 50$ oscillators. The onset of global synchronization can be approximated using the mean-field analysis relation $\Omega = -Kr^2 \sin\lambda$ (c.f. (3.15)). Approximating $r \approx 1$ and that the last oscillator to be entrained at the onset of global synchronization is $\omega_N$, we approximate $K_g = \omega_{50}/(1 - \sin\lambda)$. This approximation also captures the onset of global synchronization very well. For the uniform frequency distribution we also show the critical coupling strengths $K_c$ and $K_g$ obtained from solutions of the self-consistency relation (3.12)–(3.13) as described in Section 3.1.1, which captures the onset of partial and global synchronization reasonably well.

## 4.4 Discussion and Outlook

In this chapter we investigated the effect of rogue oscillators on synchronized oscillators via averaging the rogue oscillators' fast dynamics over the corresponding invariant density. Inspired by Birkhoff's ergodic theorem, we approximated the invariant density to be proportional to the inverse of the rogue oscillators' velocities, $\rho_i(\theta_i) \propto 1/|v_i(\theta_i)|$. This was then incorporated into the derivation of reduced dynamics via the collective coordinate framework that also accounts for the effect of rogue oscillators. We proposed two ansatz functions for the phases of synchronized oscillators, a linear ansatz based on linearizing around $1/K$ for large $K$, and a fully nonlinear arcsine ansatz. We presented results from numerical implementations of the reduced dynamics for both ansatzes and demonstrated their capabilities in capturing the collective behaviour of finite-size systems by comparing with results from direct numerical simulations of the original system. This was performed for quantities including the order parameter $\bar{r}$, cluster mean frequency $\Omega$, location of the synchronized cluster, and the critical coupling strengths $K_c$ and $K_g$ corresponding to the onset of partial and global synchronization. The results were also compared with results from the corresponding thermodynamic limit. The reduced dynamics from both the linear and arcsine

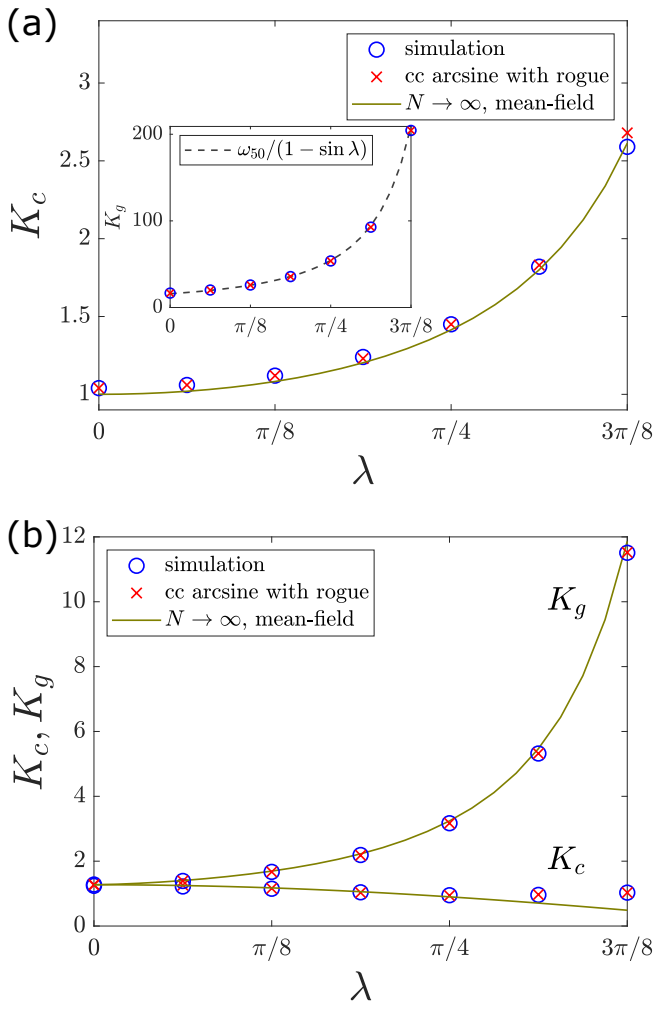


Figure 4.7: Critical coupling strengths $K_c$ and $K_g$ obtained from a numerical simulation of the full Kuramoto-Sakaguchi model (2.1) with $N = 50$ oscillators, and obtained from the collective coordinate approach (labelled cc) using the arcsine ansatz (4.8) including the effect of rogue oscillators. For the Lorentzian frequency distribution, for the onset of global synchronization we also show the estimate $K_g = \omega_{50}/(1 - \sin\lambda)$ borrowed from a mean-field analysis. For the onset of partial synchronization we also show results from the Ott-Antonsen ansatz. For the uniform frequency distribution, for the onset of partial and global synchronization we also shows the results from solving the self-consistency relation (3.12)–(3.13) as described in Section 3.1.1. (a) Lorentzian frequency distribution (2.5). (b) Uniform frequency distribution (2.6).

ansatz produced results with good accuracy. The arcsine ansatz tends to produce results that are more accurate than the linear ansatz. We also demonstrated that reduced dynamics from the arcsine ansatz has the property of converging to the mean-field theory in the thermodynamic limit of infinitely many oscillators, while being more accurate than the corresponding results from the mean-field theory for finite-size systems. We highlighted the importance of incorporating the effects of the rogue oscillators in the derivation of reduced dynamics, by presenting results from reduced dynamics where the effect of rogue oscillators were ignored, which were shown to deviate from the actual dynamics, for both the linear and arcsine ansatzes.

While the arcsine ansatz produces results of higher accuracy than the linear ansatz and has the property of converging to results from the mean-field theory in the thermodynamic limit, we remark that here the arcsine ansatz is only developed for the case of all-to-all coupling topology, $A_{ij} = 1 \ \forall i, j$. The linear ansatz can be readily extended to systems with arbitrary coupling network $A_{ij}$, as carried out in [31], where for Kuramoto model on complex network,

$$\frac{d}{dt}\phi_i(t) = \omega_i + \frac{K}{N}\sum_{j=1}^{N} A_{ij}\sin(\phi_j(t) - \phi_i(t)), \quad i = 1, 2 \dots N,$$

for high coupling strengths $K$, one may approximate the stationary state to have the form that all oscillators are synchronized, with their phases staying very close to one another. Linearizing the coupling function by approximating that the phases are close, one obtains a linear equation of the stationary, synchronized phases

$$0 \approx \omega_i + \frac{K}{N}\sum_{j=1}^{N} A_{ij}(\phi_j^* - \phi_i^*) = \omega_i - \frac{K}{N}\sum_{j=1}^{N} L_{ij}\phi_j^*, \tag{4.23}$$

where

$$L = D - A$$

is the graph Laplacian of the adjacency matrix $A$, and $D = \mathrm{diag}([d_1, d_2, \dots d_N])$ is the degree matrix with $d_i = \sum_{k=1}^{N} A_{ik}$ the degree of node $i$ in the network. ($A$ is taken to be symmetric, $A_{ji} = A_{ij} \ \forall i, j$, representing that $\phi_j$ is coupled to $\phi_i$ in the same way that $\phi_i$ is coupled to $\phi_j$ ). An approximate solution for the stationary phases $\phi_i^*$ is then given via the Moore-Penrose pseudo-inverse of the graph Laplacian, $L^+$, as

$$\phi_i^* \approx \hat{\phi}_i = \frac{N}{K}\sum_{j=1}^{N} \left(L^+\right)_{ij} \omega_j. \tag{4.24}$$

(The graph Laplacian $L$ is not invertible as the vector $(1, 1 \dots 1)^\mathsf{T}$ is an eigenvector with eigenvalue 0.)

A collective coordinate ansatz can thus be formulated as

$$\Phi_i(t) = \alpha(t)\hat{\phi}_i \tag{4.25}$$

with $\alpha(t)$ being a time-dependent collective coordinate, and $\hat{\phi}_i$ as specified in (4.24). Reduced dynamics of the system is then obtained via requiring that the error associated with the ansatz (4.25) is minimal, in the same way as carried out in the collective coordinate framework (c.f. (4.11)). We remark that the ansatz (4.25) contains information of both the individual oscillators' properties and the coupling structure of the system, through the linearized phases $\hat{\phi}_i$s, via the intrinsic frequencies $\omega_i$s and the graph Laplacian $L$, respectively.

This approach has been further extended to describe systems where most, but not all oscillators partake in the synchronized cluster, as well as systems where oscillators organize into several synchronized clusters, for which oscillators within each cluster are well synchronized while the clusters exhibit non-trivial inter-cluster dynamics [31].

The derivation of the reduced dynamics via the collective coordinate framework with the arcsine ansatz, as presented in this chapter, was heavily inspired by the mean-field theory results, such as the stationary solution for phases of the synchronized oscillators (3.5) and the stationary density for phases of the non-synchronized rogue oscillators (3.10), which are pertinent to systems under an all-to-all coupling topology. It is an intriguing avenue to investigate whether the arcsine ansatz can also be extended to systems under complex coupling networks, especially given that it produces results with higher accuracy than the linear ansatz for systems under all-to-all coupling network.

In this chapter, the numerical results were demonstrated mainly focusing on the stationary solution of the reduced equations (4.12) from the collective coordinate framework. The convergence property was also demonstrated for the stationary state. It is an interesting problem to further investigate the dynamical properties of (4.12), such as the rate at which the system returns to its equilibrium from small perturbations, which could give an indication of how fast the equilibrium state is approached in the original coupled oscillator system in the Kuramoto model (2.1). One challenge that we foresee may occur is that in the derivation of the reduced equations from the collective coordinate framework, the location of the synchronized oscillators $\mathcal{C}$ is determined in a way which depends on the current value of the collective coordinate $r(t)$ (and also on the collective parameter $\Omega$). If we are to simulate the dynamics of $r(t)$ over time from (4.12), as $r(t)$ varies, the location of the synchronized

cluster $\mathcal{C}$ may vary, which may affect the form of the reduced equations (4.12).

Given the massive reduction in dimension of the reduced equations (4.12) compared to the original Kuramoto-Sakaguchi model (2.1), as well as its relative accuracy, one may further employ the reduced equations to investigate the properties of the original system, especially in the setting of finite-system sizes, where other theoretical approaches, such as an analysis via the mean-field theory, may not be as applicable. One such area of interest may be on the scaling laws between varies quantities, such as how the critical coupling strength corresponding to onset of synchronization, $K_c$, scales with system size $N$, or how the order parameter $r$ scales with the coupling strength $K$ [19, 32].

Another interesting avenue is to apply the framework to describe systems where the oscillators' intrinsic frequencies $\omega_i$s are just a collection of certain specified values, which may not have been drawn from an underlying distribution $g(\omega)$. These cases may be more relevant to analyzing coupled oscillatory systems arising from real-world setting, such as an ensemble of a few coupled mechanical oscillators, where the dynamical properties of the oscillatory components can be measured, but they may not represent a draw from a predefined distribution. For such systems, analysis via mean-field theory of the thermodynamic limit may not be as applicable due to the lack of, or deviation from, a predefined frequency distribution $g(\omega)$. For the collective coordinate framework, the specification of ansatz function and subsequent derivation of the corresponding reduced dynamics do not require a predefined distribution and apply for an arbitrary ensemble of intrinsic frequencies $\omega_i$s. For instance, the linear ansatz (4.7) and the arcsine ansatz (4.8) both only require specification of the frequencies $\omega_i$s and do not require knowing the underlying distribution $g(\omega)$. Hence, the collective coordinate framework has the potential of providing a valuable tool for investigating coupled oscillatory systems where the components' parameters are just a collection of specified values. This has already been carried out in [69] for the Kuramoto model with a finite ensemble of randomly drawn intrinsic frequencies $\omega_i$s, where it was demonstrated that collective coordinate framework with arcsine ansatz yields reduced dynamics that is of much higher accuracy compared to results from the thermodynamic limit, and captured the pronounced finite-size effects very well, including a non-monotonic dependence of the second derivative of the order parameter $r$ with respect to the coupling strength $K$ along the path to synchronization.

For the Kuramoto-Sakaguchi model with all-to-all coupling (2.1) we demonstrated that reduced dynamics derived via the collective coordi-

nate framework with arcsine ansatz produces accurate results for finite-size systems and converges to analytical results in the thermodynamic limit. Inspired by this, one may wonder whether this framework can be extended to systems with more complex settings.

An intriguing avenue is for coupled oscillator systems that exhibit chimera states, for example the setup in [1, 38], where the oscillators are organized in two populations, the coupling topology is still all-to-all, but there are now two different coupling strengths, an intra-population strength for coupling between oscillators within the same population, and an inter-population coupling strength for coupling between oscillators that are from different populations. Parameters of the system can be set such that the two populations possess identical setup to each other, and the system remains the same when we exchange the two populations. The intriguing discovery of chimera state is that for certain initial conditions, the system evolves to a state where the two populations exhibit drastically different dynamics, for instance one becomes synchronized while the other remains incoherent. Analysis on the system have been traditionally performed in the thermodynamic limit, where the Ott-Antonsen ansatz reduces the original system to a (low-dimensional) set of ODEs, and the chimera states are identified with certain particular solutions of the ODEs [1, 38, 58]. After reduction to ODEs, a multitude of available techniques can be applied to study the chimera states' properties, such as their stability and bifurcation structure. Study for finite-size systems exhibiting chimera states have been conducted for the case of identical intrinsic frequencies, for which a model reduction technique known as the Watanabe-Strogatz ansatz applies [75, 76, 9]. For finite systems with non-identical oscillators, the particular sets of intrinsic frequencies may affect the properties of the exhibited chimera states. In many systems studied, chimera states seem to manifest at system settings where the coupling function contains a non-zero phase-offset $\lambda$. Given the applicability of the collective coordinate framework in deriving reduced dynamics for the Kuramoto-Sakaguchi model with an all-to-all coupling network and non-zero phase-offsets $\lambda$ (2.1), and given the similarity of the aforementioned coupled oscillator system exhibiting chimera states [1, 38] to the all-to-all Kuramoto-Sakaguchi model, one may wonder if we could apply the collective coordinate framework to derive reduced dynamics for the systems that exhibit chimera states, especially for the case of finite ensembles of non-identical oscillators.

One important step in applying the collective coordinate framework to coupled oscillator systems with more complex settings is to formulate for the case where oscillators are organized into several populations. Such systems may exhibit richer dynamics, including where the different populations evolving to different dynamical states, as in the case of chimera

states, or where the oscillators organize into several synchronized clusters, with oscillators within each cluster staying synchronized while the clusters themselves display non-trivial inter-cluster dynamics, including standing waves and chaos, as observed for the setting where the intrinsic frequency distribution $g(\omega)$ is a multi-modal function, i.e. with several distinct peaks [40, 68].

In previous works [29, 31, 68], for applying the collective coordinate framework with the linear ansatz to systems exhibiting multiple clusters, in addition to the shape profiles for oscillators within each synchronized cluster, the ansatz also included additional collective coordinates representing the phase positions for each cluster. Oscillators within the same cluster share the same phase position collective coordinate, while each cluster contains a different one. In the corresponding derived reduced dynamics, evolution of the shape profile collective coordinates capture the synchronization dynamics for oscillators within each cluster, while evolution of the phase position collective coordinates capture the inter-cluster dynamics for each cluster.

Previous application of the collective coordinate framework for depicting multi-cluster dynamics has been carried out for the Kuramoto model with zero phase-offset, $\lambda = 0$, using linear ansatzes. An attractive extension is the application of the framework for systems with a non-zero phase-offset $\lambda \neq 0$ displaying intriguing dynamical behaviour including chimera states. The extension may entail development of ansatzs to capture the more complicated dynamics.

The Kuramoto model has been a paradigmatic model for coupled oscillatory systems. Over the years, a plethora of extensions have been developed and investigated, such as models where second-order time derivative of the phases are also depicted, and models with different forms of coupling function and structure [3]. Moreover, a large number of other mathematical models have been developed which describe dynamics of coupled oscillatory systems, including models where oscillators are described by a phase and an amplitude, both of which are coupled to other oscillators [46, 47, 45], as well as various models describing networks of coupled neurons [5, 8]. The models possess varying degrees of resemblance to the paradigmatic Kuramoto model. It is an interesting avenue to investigate the extend to which the collective coordinate framework can be applied for deriving reduced dynamics for the various models.

# Chapter 5

# Fluctuations Around the Average Effect of the Rogue Oscillators

In Chapter 4 we were able to describe the average effect of the rogue oscillators on the synchronized cluster and gave explicit expressions for the interaction terms involving the rogue oscillators. This allowed us to find a closed deterministic system of equations for the synchronized oscillators, which allowed for the estimation of the onset of synchronization and the determination of the average behaviour of the order parameter.

Whereas the previous chapter captured the averaged effect of the rogue oscillators on the synchronized oscillators, in this chapter we set out to quantitatively describe the fluctuations around this average behaviour and capture the effective stochastic dynamics of the synchronized phase oscillators and the order parameter. We show how the thermodynamic limit is approached for increasing number of oscillators. In particular, we will derive a closed set of equations for the finite number of synchronized oscillators where the effect of the non-entrained rogue oscillators is modelled by coloured noise, the variance of which decreases as the number of oscillators increases. This implies, as we will show, a stochastic differential equation (SDE) for the order parameter. SDEs driven by Brownian motion for the order parameter were recently postulated and determined using a data-driven approach [70]. We show here that the SDEs driven by coloured noise provide better approximations.

## 5.1 Numerical results for finite $N$

We now present results of numerical simulations of the Kuramoto-Sakaguchi model (2.1), illustrating finite-size effects. We follow the same simulation procedure as described in Chapter 2. In the following we fix the phase-

offset parameter to $\lambda = \pi/4$ and consider a Gaussian distribution (2.4) of the intrinsic frequencies with mean 0 and variance 1. To avoid sampling effects we consider again intrinsic frequencies $\omega_i$s that are drawn deterministically via equi-probable intervals, according to (2.2). For each intrinsic frequency distribution $g(\omega)$ and population size, we generate the corresponding set of intrinsic frequencies $\omega_i$s once and show results for this single realization. When reporting $N$ in the legends of the figures, it refers to the number of chosen intervals. Unless specified otherwise we set the coupling strength $K = 3$.

The effect of the non-collective behaviour of the rogue oscillators induces a seemingly stochastic behaviour of the order parameter $r(t)$ as was shown in Figure 2.2 in Chapter 2. It was seen that after an initial transient the order parameter exhibits persistent fluctuations around a mean value with a constant variance of $4.16 \times 10^{-4}$. The size of the fluctuations is $N$ dependent and we expect that for $N \to \infty$, the variance of the fluctuations approaches zero, in accordance with the law of large number result obtained in Chapter 4.

To investigate the effect of finite system size, we simulated the system at increasing system size $N = \{40, 80, 160, 320, 640, 1280, 2560\}$ with other settings kept the same. Figure 5.1(a) shows the distribution of $r(t)$ for varying system size. As $N$ increases, the distribution of $r(t)$ becomes, as expected, narrower with decreasing variance and its mean value approaches a fixed value $\bar{r}_\infty = 0.766$, as shown in Figures 5.1(b)-(c). We find that $\bar{r} - r_\infty \sim N^{-0.859}$. The variance of $r(t)$ decreases towards 0 as $N$ increases with $\mathrm{Var}(r) \sim N^{-0.976}$. The scaling of the variance suggests an underlying Central Limit Theorem which would imply a scaling of the variance with $1/N$. For a system with Lorentzian intrinsic frequency distribution $g(\omega)$ (2.5) with mean 0 and width $\Delta = 1$, at the parameter setting of $K = 3$, $\lambda = 4$, we observed similar scaling with the system size $N$, with the scaling law $\bar{r} - r_\infty \sim N^{-1.031}$, $\mathrm{Var}(r) \sim N^{-0.963}$. We expect similar characteristics for systems with generic uni-modal intrinsic frequency distribution $g(\omega)$.

Figure 5.2 shows the transition from incoherence to synchronization for increasing coupling strength $K$ for fixed number of oscillators $N = 160$, which we already encountered in previous chapters. In Figure 5.2(a) we show the order parameter $\bar{r}$ with the second-order phase transition for Gaussian intrinsic frequencies from incoherence with $\bar{r} \sim \mathcal{O}(1/\sqrt{N})$ to partial synchronization at $K_c = 1.93$, after which the synchronized cluster continues to grow in size until all oscillators become synchronized at $K_g = 8.34$. In Figure 5.2(b) we further show the variance of the order parameter as a function of the coupling strength. The almost constant variance for small coupling strength around $\mathrm{Var}(r) = 1.35 \times 10^{-3}$ corresponds to the almost random distribution of the $N$ uncoupled

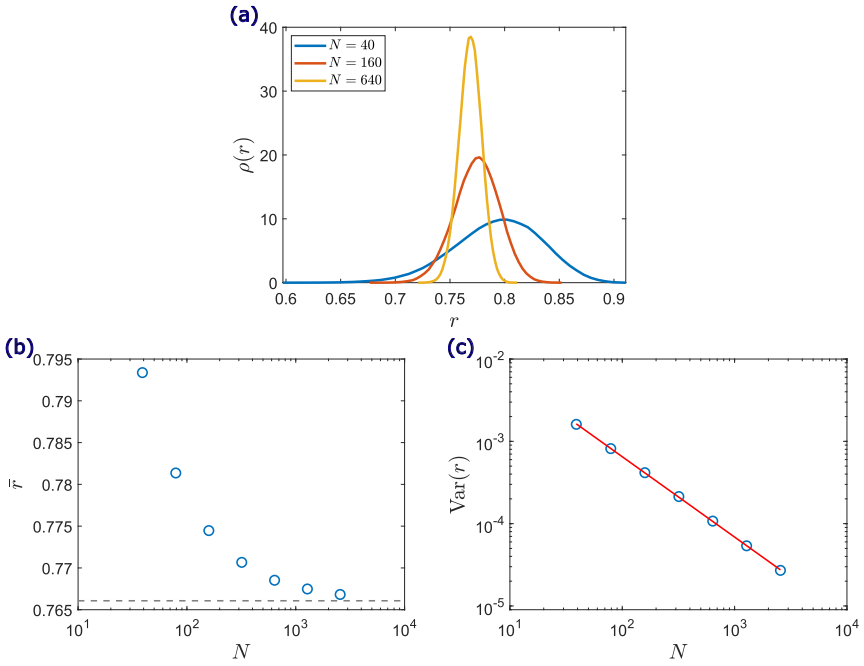


Figure 5.1: (a): Empirical distribution of the order parameter $r(t)$ obtained from a single simulation of the Kuramoto-Sakaguchi model (2.1) at different system sizes $N$. (b): Mean value of $r(t)$ for different $N$. The dashed line indicates the value at the corresponding thermodynamic limit, $\bar{r}_\infty$, obtained from numerically solving the self-consistency relations (3.12)–(3.13). (c): Variance of $r(t)$ for different $N$. The red line represents the best-fit suggesting a scaling law of $N^{-0.976}$. Results are for a coupling strength $K = 3$ and phase-offset $\lambda = \pi/4$, with a Gaussian intrinsic frequency distribution $g(\omega)$ of mean 0 and variance 1.

oscillators. The variance exhibits a singularity at $K = K_c$ and approaches zero for $K \geq K_g$. The singular behaviour of the variance is a well-studied phenomenon and known under the name of anomalous enhancement of fluctuations [20, 19, 21, 22, 32]. Figure 5.2(c) shows the cardinalities of the synchronized cluster $\mathcal{C}$ and the set of rogue oscillators $\mathcal{R}$, $N_c = |\mathcal{C}|$ and $N_r = |\mathcal{R}|$, with $N_c + N_r = N$. For $K < K_c$ all oscillators are rogue whereas for $K > K_g$ all oscillators are synchronized. The synchronized cluster grows steadily for increasing $K_c < K < K_g$.

## 5.2 Stochastic model reduction

The numerical results presented in Section 5.1 suggest that the non-entrained rogue oscillators exert a stochastic forcing on the synchronized cluster. To develop a stochastic approximation of the Kuramoto-

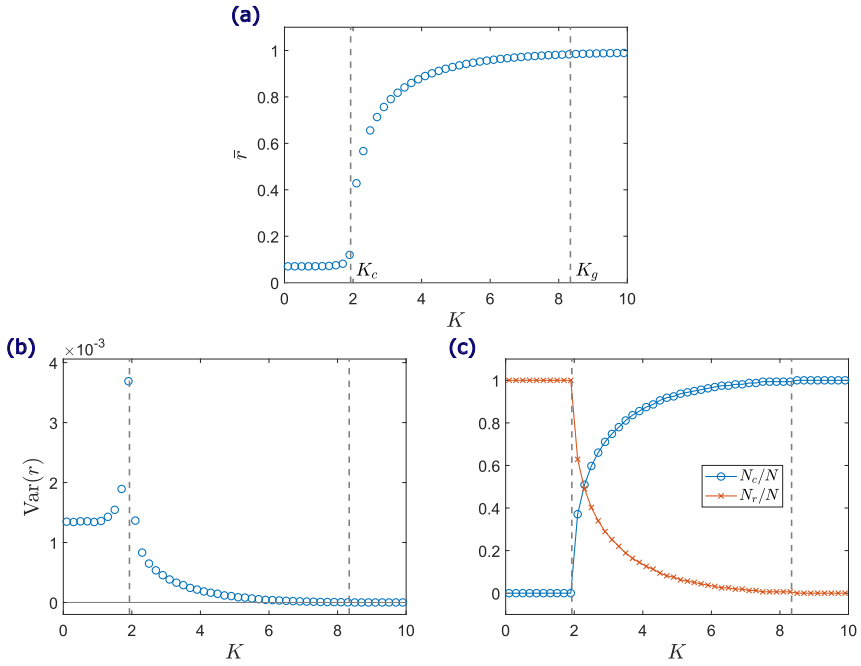


Figure 5.2: Transition from incoherence to synchronization of the Kuramoto-Sakaguchi model (2.1) with increasing coupling strength $K$ with $N = 160$ for a Gaussian intrinsic frequency distribution $g(\omega)$ with mean zero and variance 1. (a): Order parameter $\bar{r}$. (b): Variance of the order parameter, quantifying the size of fluctuations. (c): Number of entrained oscillators $N_c$, (circles, online blue) and number of non-entrained rogue oscillators $N_r$ (crosses, online red). Shown are relative numbers. The vertical lines mark the onset of partial synchronization at $K_c = 1.93$ and the onset of global synchronization at $K_g = 8.34$.

Sakaguchi model we hence aim to establish a closed evolution equation for the phases of the synchronized oscillators in which the driving force exerted by the rogue oscillators is approximated as a stochastic process. The challenge is how to describe this stochastic process. As in Chapter 4, we begin by separating the coupling terms which only involve the synchronized oscillators and those which contain the rogue oscillators, and write the Kuramoto-Sakaguchi model (2.1) for $i \in \mathcal{C}$ as

$$\dot{\theta}_i = \omega_i - \Omega + \frac{K}{N}\left(\sum_{j\in\mathcal{C}} \sin(\theta_j - \theta_i - \lambda) + \sum_{j\in\mathcal{R}} \sin(\theta_j - \theta_i - \lambda)\right).$$

The sum over the rogue oscillators can be written as

$$\begin{aligned}\frac{1}{N}\sum_{j\in\mathcal{R}} \sin(\theta_j - \theta_i - \lambda) &= \frac{1}{N}\sum_{j\in\mathcal{R}} \sin(\theta_j - \psi_c + \lambda + \psi_c - \theta_i - 2\lambda) \\ &= \cos(\psi_c - \theta_i - 2\lambda)\, S(t) + \sin(\psi_c - \theta_i - 2\lambda)\, C(t),\end{aligned}$$

where we define

$$S(t) = \frac{1}{N}\sum_{j\in\mathcal{R}} \sin(\theta_j - \psi_c + \lambda) = \frac{N_r}{N} r_r \sin(\psi_r - \psi_c + \lambda), \tag{5.1}$$

$$C(t) = \frac{1}{N}\sum_{j\in\mathcal{R}} \cos(\theta_j - \psi_c + \lambda) = \frac{N_r}{N} r_r \cos(\psi_r - \psi_c + \lambda), \tag{5.2}$$

after introducing the mean-field variables pertaining to oscillators within the synchronized cluster $\mathcal{C}$ and the rogue oscillators $\mathcal{R}$, respectively,

$$r_c e^{\imath\psi_c} = \frac{1}{N_c}\sum_{j\in\mathcal{C}} e^{\imath\theta_j}, \qquad r_r e^{\imath\psi_r} = \frac{1}{N_r}\sum_{j\in\mathcal{R}} e^{\imath\theta_j}.$$

The overall influence of the rogue oscillators on a synchronized oscillator $\theta_i$ is now captured by $S(t)$ and $C(t)$, while the remaining terms are expressed entirely in terms of the synchronized oscillators. Note that $S(t)$ and $C(t)$ are the same for each synchronized oscillator $\theta_i, i \in \mathcal{C}$. We arrive at

$$\begin{aligned}\dot{\theta}_i = \omega_i - \Omega + \frac{K}{N}\sum_{j\in\mathcal{C}} \sin(\theta_j - \theta_i - \lambda) \\ + K\cos(\psi_c - \theta_i - 2\lambda)\, S(t) + K\sin(\psi_c - \theta_i - 2\lambda)\, C(t).\end{aligned} \tag{5.3}$$

Recalling from Chapter 4, we can determine the average of the drivers $S(t)$ and $C(t)$ via averaging over the invariant densities of the rogue oscillators (4.3). Averaging (5.1) yields

$$\begin{aligned}\langle S\rangle_t &\approx \frac{1}{N}\sum_{j\in\mathcal{R}} \int_{-\pi}^{\pi} \sin(\theta_j - \psi_c - \lambda)\rho_j(\theta_j) d\theta_j \\ &= \frac{1}{N}\cos(\psi_0 - \psi_c)\sum_{j\in\mathcal{R}} k_j,\end{aligned} \tag{5.4}$$

where $k_j$s are the same as in (4.4),

$$k_j = \frac{\omega_j - \Omega}{Kr}\left(1 - \sqrt{1 - \frac{K^2 r^2}{(\omega_j - \Omega)^2}}\right),$$

and $\psi_0$ denotes the overall phase of all oscillators in the frame of reference rotating with the synchronized cluster at mean frequency $\Omega$. Similarly, averaging (5.2) yields

$$\langle C\rangle_t \approx -\frac{1}{N}\sin(\psi_0 - \psi_c)\sum_{j\in\mathcal{R}} k_j. \tag{5.5}$$

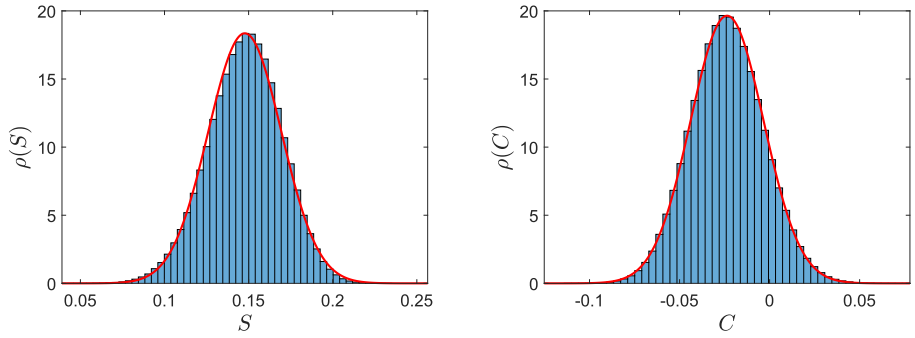


Figure 5.3: Empirical histogram of $S(t)$ and $C(t)$ obtained from a single trajectory of the Kuramoto-Sakaguchi model (2.1) with $N = 160$. The continuous curve indicates the corresponding Gaussian best fit.

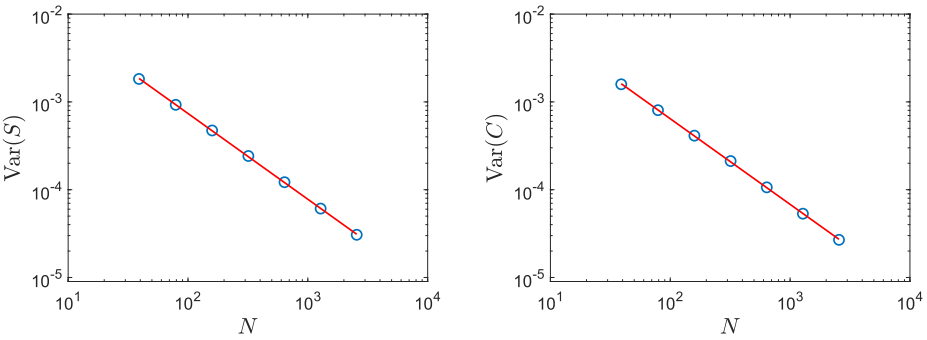


Figure 5.4: Scaling of the variance of $S$ and $C$ with varying system size $N$. The continuous lines are linear best fits indicating a scaling with $N^{-0.977}$ for $S$ and $N^{-0.975}$ for $C$.

Figure 5.3 shows the empirical histogram of $S$ and $C$ for $N = 160$ at $K = 3$ obtained from a single long simulation of the Kuramoto-Sakaguchi model (2.1). The means are well approximated by the averaging procedure described above (c.f. (5.4) and (5.5)). However, $S(t)$ and $C(t)$ experience significant fluctuations. It is clearly seen that the distribution of the fluctuations is Gaussian. In Figure 5.4 we show that the variance of $S$ and of $C$ scales approximately as $1/N$.

Hence, approximately, as $N$ varies, $S(t)$ and $C(t)$ both have means that do not scale with $N$ and have variances that scale as $1/N$. This suggests that the scaled mean-subtracted variables

$$\begin{aligned} \xi_t &= \sqrt{N}\,(S(t) - \langle S\rangle_t) \\ \zeta_t &= \sqrt{N}\,(C(t) - \langle C\rangle_t) \end{aligned} \tag{5.6}$$

can be approximated by Gaussian processes that do not scale with $N$,

and are defined entirely in terms of their mean and covariance functions

$$R_{ab}(\tau) = \mathrm{cov}\left(a(t), b(t+\tau)\right), \tag{5.7}$$

for $a$ and $b$ being either $\xi$ or $\zeta$. The covariance is taken over time $t$. Indeed, Figure 5.5 shows that correlations decay in time with increasing system size $N$, and the auto-covariance function (5.7) of the scaled variables converge as $N$ increases. This allows us to approximate $Z = (\xi_t, \zeta_t)^\mathsf{T}$ as a two-dimensional Ornstein-Uhlenbeck (OU) process with

$$dZ = (-\Gamma Z + \Upsilon Z)\, dt + \Sigma\, dB_t \tag{5.8}$$

with two-dimensional Brownian motion $B_t = (W_1, W_2)^\mathsf{T}$ and diagonal matrix $\Gamma = \gamma \mathrm{I}$ and skew-symmetric rotation matrix $\Upsilon$ with entries $\upsilon_{12} = -\upsilon_{21} = \upsilon$ and $\upsilon_{11} = \upsilon_{22} = 0$ and a symmetric diffusion matrix $\Sigma$ with entries $\sigma_{ij}$ with $i, j = 1, 2$. The parameters of the OU process are determined such that its mean is zero and its covariance function

$$R^{(\mathrm{OU})}(\tau) = \langle e^{-(\Gamma-\Upsilon)\tau} Z_0 Z_0^\mathsf{T} \rangle_{\mathrm{OU}}, \tag{5.9}$$

where $Z_0$ is drawn from the stationary distribution of the OU process and $\langle - \rangle_{\mathrm{OU}}$ denotes an average over this distribution, matches the observed covariance function $R^{(\mathrm{KS})}(\tau)$ (5.7) of $Z = (\xi_t, \zeta_t)^\mathsf{T}$ associated with the full deterministic Kuramoto-Sakaguchi model. We perform a nonlinear least-square optimization minimizing the objective function

$$E(\gamma, \upsilon, \Sigma) = \sum_{a,b} \Bigg( \int_{\tau_{\min}}^{\tau_{\max}} ||R_{ab}^{(\mathrm{KS})}(\tau) - R_{ab}^{(\mathrm{OU})}(\tau)||^2 d\tau + \beta ||R_{ab}^{(\mathrm{KS})}(0) - R_{ab}^{(\mathrm{OU})}(0)||^2 \Bigg),$$

where the sum goes over all entries of the covariance matrix, and $\tau_{\min}$, $\tau_{\max}$ specify the range of data to be fitted, here chosen as $\tau_{\min} = 0.5, \tau_{\max} = 2.5$. We choose $\beta = 1,000$ to enforce that the variances of $S$ and $C$, which correspond to the covariance function evaluated at $\tau = 0$, are reproduced. Figure 5.6 shows the four entries of the covariance matrix of $Z = (\xi_t, \zeta_t)^\mathsf{T}$ together with the best fit of an OU process. The fit is significantly better for small times $\tau$. We remark that the Kuramoto-Sakaguchi model is deterministic and hence the derivatives of the covariance functions $R_{\xi\xi}^{(\mathrm{KS})}(\tau)$ and $R_{\zeta\zeta}^{(\mathrm{KS})}(\tau)$ are zero at $\tau = 0$ [23]. This feature cannot be reproduced by the stochastic OU process which supports covariance functions that are non-differentiable at $\tau = 0$. In the fitting procedure, we choose a $\tau_{\min}$ that is larger than 0.

The effective stochastic dynamics of $S(t)$ and $C(t)$ are generated by the weak chaoticity of the non-entrained rogue oscillators [13, 68]. We

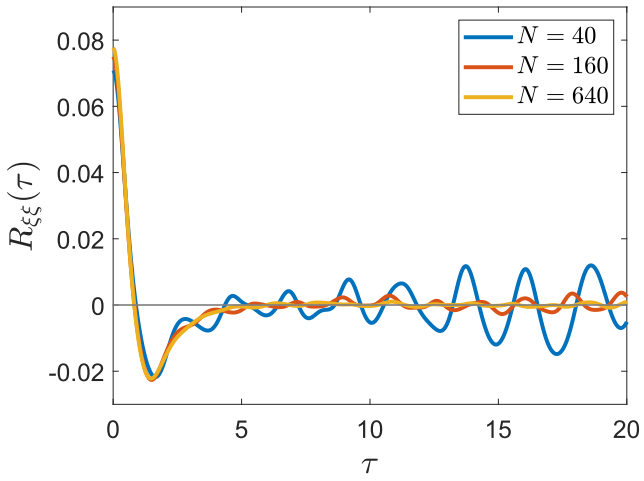


Figure 5.5: Entry $R_{\xi\xi}(\tau)$ of the covariance function of $Z = (\xi(t), \zeta(t))^{\mathsf{T}}$ obtained from a single trajectory of the Kuramoto-Sakaguchi model (2.1) for different system sizes $N$.

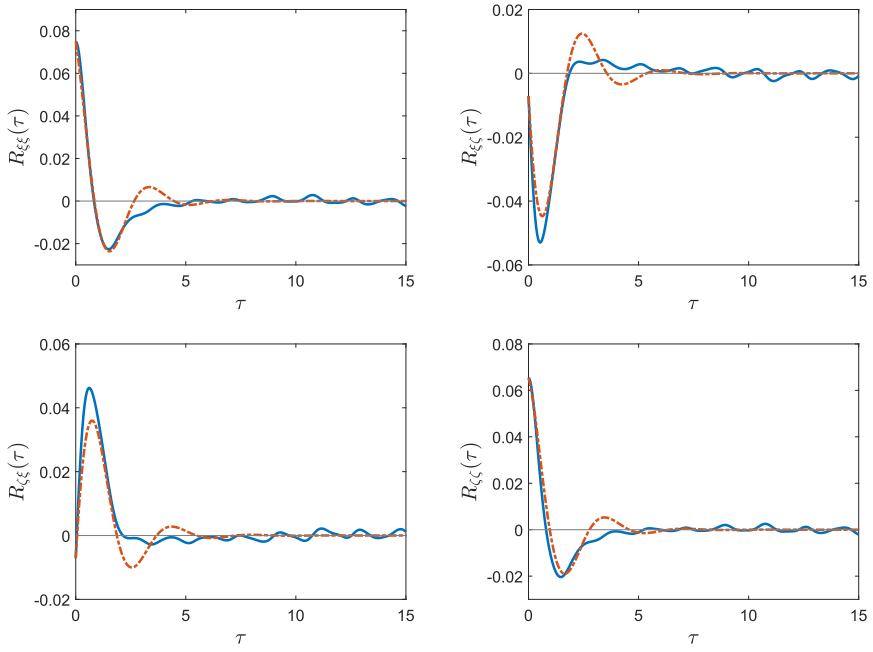


Figure 5.6: Covariance function of $\xi(t)$ and $\zeta(t)$ for $N = 160$ (solid, online blue), together with the covariance function of a corresponding fitted two-dimensional Ornstein-Uhlenbeck process (dot-dashed line, online red).

show in Figure 5.7 typical trajectories of rogue oscillators. The dynamics of the weakly chaotic rogue oscillators is characterized by a nearly periodic motion (indeed under the assumption of constant mean-field

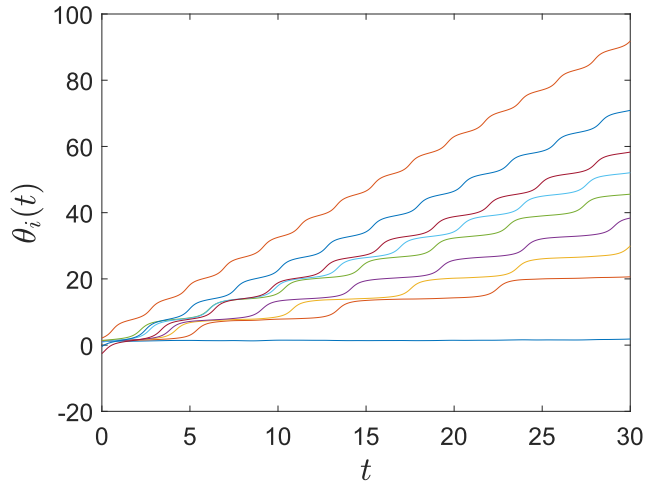


Figure 5.7: Typical trajectories of rogue oscillators obtained from a single simulation of the Kuramoto-Sakaguchi model (2.1) for $N = 160$, including the rogue oscillators with the native frequency closest to that of an entrained oscillator (online blue) and the rogue oscillator with the largest intrinsic frequency (online red).

variables $r$ and $\psi_0$ the dynamics of each rogue oscillator is approximately governed by an Adler equation, (c.f. (3.3)). Note that the rogue oscillators closest to the synchronized cluster evolve slowly, almost aligned with the synchronized cluster, for long periods interrupted by fast slips. The interaction terms (5.1) and (5.2) hence constitute sums of nearly periodic functions of time with random initial phases. It is well known that a sum of many trigonometric functions with uncorrelated random initial conditions approximates a Gaussian processes [33, 28]. Hence the mechanism for the deterministic generation of diffusive behaviour is less a matter of the time-scale separation between faster chaotic rogue oscillators and slower synchronized oscillators, but more related to a weak coupling of the synchronized oscillators to many uncorrelated rogue oscillators.

## 5.3 Numerical Verification of the Stochastic Reduced Model

We now show that the fluctuations of the order parameter as observed in Figure 2.2 can be captured by the closed stochastic evolution equation for the entrained oscillators $\theta_i$ with $i \in \mathcal{C}$, established in the previous

section which we summarize here as

$$\begin{aligned} d\theta_i = \Bigg[ & \omega_i - \Omega + \frac{K}{N} \sum_{j \in \mathcal{C}} \sin(\theta_j - \theta_i - \lambda) \\ & + K \cos(\psi_c - \theta_i - 2\lambda) \left( \langle S \rangle_t + \frac{1}{\sqrt{N}} \xi_t \right) \\ & + K \sin(\psi_c - \theta_i - 2\lambda) \left( \langle C \rangle_t + \frac{1}{\sqrt{N}} \zeta_t \right) \Bigg] dt, \end{aligned} \tag{5.10}$$

where $\xi_t$ and $\zeta_t$ are components of a 2-d OU process governed by

$$\begin{pmatrix} d\xi_t \\ d\zeta_t \end{pmatrix} = \begin{pmatrix} -\gamma & \upsilon \\ -\upsilon & -\gamma \end{pmatrix} \begin{pmatrix} \xi_t \\ \zeta_t \end{pmatrix} dt + \begin{pmatrix} \sigma_{11} & \sigma_{12} \\ \sigma_{21} & \sigma_{22} \end{pmatrix} \begin{pmatrix} dW_1 \\ dW_2 \end{pmatrix}. \tag{5.11}$$

The SDE (5.10)–(5.11) is simulated numerically with an Euler-Maruyama scheme with time-step $dt = 0.01$.

From a simulation of the SDE, we can readily compute the mean-field variables $r_c e^{\imath \psi_c}$ along a trajectory.

Further, we can establish expressions for the full order parameter $r$ associated to the stochastic reduced system (5.10)–(5.11). The full order parameter $r$ can be expressed as

$$r e^{\imath \psi_0} = \frac{N_c}{N} r_c e^{\imath \psi_c} + \frac{N_r}{N} r_r e^{\imath \psi_r}. \tag{5.12}$$

Using the definitions for $S$ and $C$ (5.1)–(5.2) which imply

$$(C + \imath S) e^{-\imath \lambda} = \frac{N_r}{N} r_r \, e^{\imath(\psi_r - \psi_c)},$$

we can express (5.12) in terms of the complex Ornstein-Uhlenbeck variable $Z_t = \zeta_t + \imath \, \xi_t$ as

$$r(t) = \left| \frac{N_c}{N} r_c(t) + (\langle C \rangle + \imath \, \langle S \rangle) e^{-\imath \lambda} + \frac{1}{\sqrt{N}} Z_t e^{-\imath \lambda} \right| \tag{5.13}$$

utilizing the definition (5.6).

Note that (5.13) is only an approximation for $r(t)$ as we require $r(t) \leq 1$ for all times $t$. The variances of the perturbing Ornstein-Uhlenbeck process $Z_t/\sqrt{N}$ is much larger than those associated with the synchronized cluster, which we numerically verify as $\mathrm{Var}(r_c) \approx 1.41 \times 10^{-5}$ and $\mathrm{Var}(r_r) \approx 6.5 \times 10^{-3}$. This suggests that in the equation (5.13) for the order parameter $r(t)$ the stochasticity of $r_c$, as established above, can be neglected and we can approximate $r_c \approx \bar{r}_c = \text{const}$ and write

$$r(t) = \left| \frac{N_c}{N} \bar{r}_c + (\langle C \rangle + \imath \, \langle S \rangle) e^{-\imath \lambda} + \frac{1}{\sqrt{N}} Z_t e^{-\imath \lambda} \right|. \tag{5.14}$$

Figure 5.8 shows the empirical histograms of the total order parameter $r$ for all oscillators when simulated using the full Kuramoto-Sakaguchi model (2.1) with $N = 160$ oscillators and when estimated by the reduced stochastic system (5.10)–(5.11) using the approximation (5.13) for its associated order parameter. We further show the histogram of $r_c$ the order parameter pertaining to synchronized oscillators. It is seen that our stochastic reduction captures the observed fluctuations very well. We remark that the histograms for $r$ are not distinguishable by eye if the order parameter $r$ is calculated by an actual time trajectory of $r_c(t)$, (i.e. via (5.13)) or by its constant mean $\bar{r}_c$ (i.e. via (5.14)).

Noting that the stochastic perturbations are small we can approximate further and write

$$r(t) = \bar{\rho}_c + \frac{1}{\sqrt{N}} \mathrm{Re}\left[\frac{|\bar{\rho}_c|}{\bar{\rho}_c} Z_t e^{-\imath\lambda}\right], \tag{5.15}$$

where $\bar{\rho}_c = \frac{N_c}{N}\bar{r}_c + (\langle C\rangle + \imath\,\langle S\rangle)e^{\imath\lambda}$. This is equivalent to the following evolution equation for the order parameter

$$dr = \frac{1}{\sqrt{N}} \mathrm{Re}\left[\frac{|\bar{\rho}_c|}{\bar{\rho}_c} e^{-\imath\lambda} dZ_t\right] \tag{5.16}$$

with

$$r(0) = \bar{\rho}_c, \qquad Z_0 = 0. \tag{5.17}$$

We remark that long-time solutions of (5.16)–(5.17) generate empirical histograms indistinguishable by eye from those presented in Figure 5.8. Note that here the order parameter is driven by coloured noise. This is in contrast to Snyder et al. [70] who postulated Brownian motion as the driving noise. In Figure 5.9 we show the time evolution of the order parameter $r_c(t)$ from the full Kuramoto-Sakaguchi model (cf. Figure 2.2) and from our reduced SDE driven by integrated OU noise, (5.10)–(5.11). The qualitative smooth character of the fluctuations is reproduced by our stochastic system.

To further probe the ability of the reduced stochastic model (5.10)–(5.11) to capture the collective dynamics of the synchronized oscillators we show results for the fluctuations of the oscillators around the mean phase of the synchronized cluster, $\theta_i - \psi_c$ for $i \in \mathcal{C}$. These fluctuations are Gaussian for all entrained oscillators. In Figure 5.10 we compare the histogram of $\theta_i - \psi_c$ for several synchronized oscillators obtained from the reduced stochastic system with the histograms from direct numerical simulation of the full Kuramoto-Sakaguchi model (2.1). We observe that the reduced stochastic model captures the fluctuations of the synchronized phases well, except for oscillators with large indices $i$ which are on

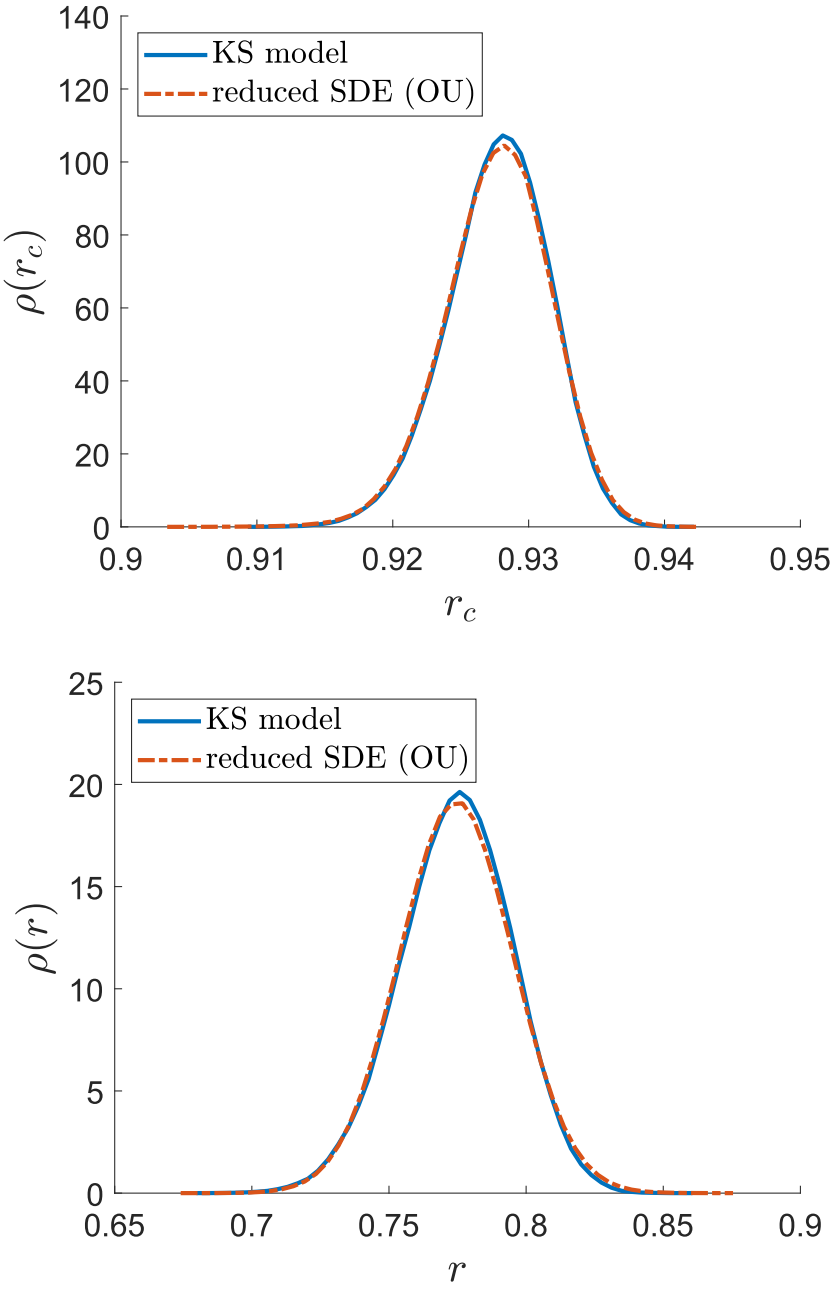


Figure 5.8: Comparison of the empirical histograms for $r_c$ (top) and $r$ (bottom) obtained from a single trajectory of the Kuramoto-Sakaguchi model (2.1) for $N = 160$ and from a simulation of the reduced stochastic model (5.10) driven by an OU process, with $r$ estimated via (5.13). All other parameters are the same as in Figure 5.1.

the edge of the synchronized cluster. In Figure 5.11 we show the mean and the variance of $\theta_i - \psi_c$, $i \in \mathcal{C}$ estimated from a long simulation of

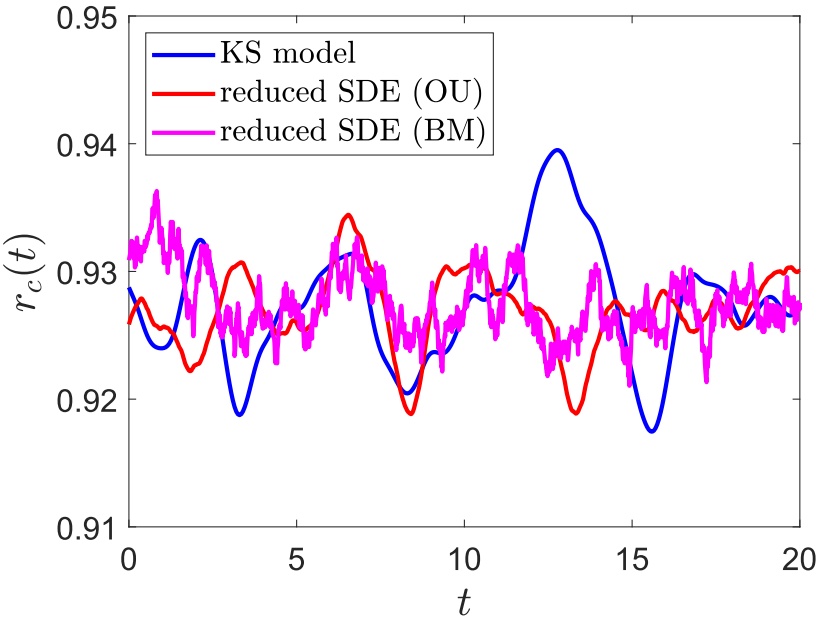


Figure 5.9: Temporal evolution of the order parameter $r_c(t)$. Shown are results obtained from the full Kuramoto-Sakaguchi model (2.1) (online blue), the reduced stochastic model (5.10)–(5.11) (online red) and from a Brownian motion approximation (5.29) (online magenta).

the full Kuramoto-Sakaguchi model (2.1) and from the reduced stochastic model (5.10)–(5.11). It is seen that the mean is very well recovered by the reduced stochastic model. The variance is very well captured for oscillators with lower indices $i$, i.e. those that are not too close to the rogues.

For the current parameter setting, in the full Kuramoto-Sakaguchi model, the first rogue oscillator is at $i = 117$. The oscillator with index $i = 116$, i.e. the oscillator on the edge of the synchronized cluster, is fully entrained. However, for the approximate stochastic model (5.10)–(5.11) the oscillator with index $i = 116$ experiences rare fast random slips between long periods of entrainment, of the order of $1,000$ time units on average. In comparison, the rogue oscillator with index $i = 117$, i.e. the one closest to the synchronized cluster, exhibits jumps that are about 40 time units apart. The rare and fast slips do not affect the mean which is still close to the mean corresponding to the Kuramoto-Sakaguchi model, but the variance is much higher with a value of 0.012. Its variance is omitted in the plot for variance in Figure 5.11).

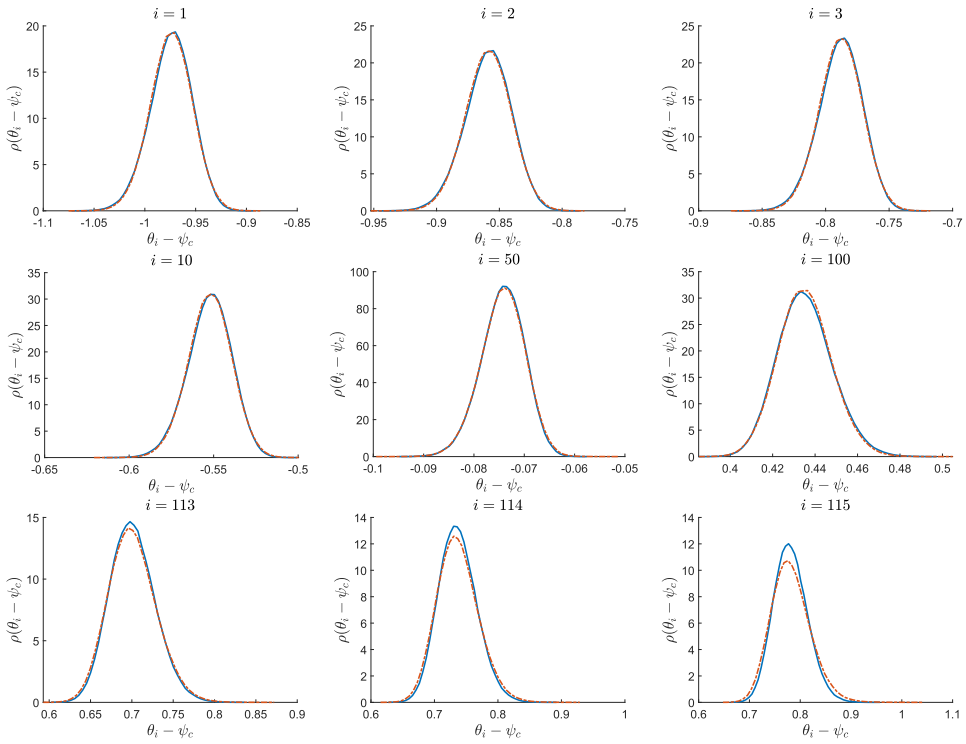


Figure 5.10: Histogram of the phases of several synchronized oscillators. Shown are histograms from direct simulation of the Kuramoto-Sakaguchi model (2.1) (blue continuous line), and from simulation of the reduced stochastic system driven by OU process (5.10)–(5.11) (red dot-dashed line)

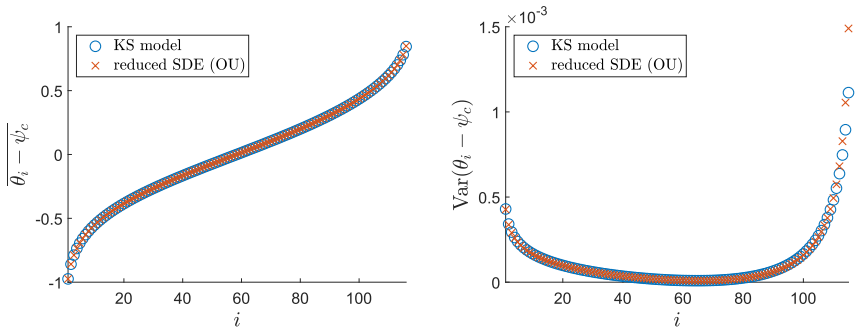


Figure 5.11: Mean (left) and variance (right) of the fluctuations of the synchronized oscillators around their mean phase, $\theta_i - \psi_c$ $i \in \mathcal{C}$. Shown are results for the full Kuramoto-Sakaguchi model (2.1) for $N = 160$, and for the reduced stochastic model (5.10)–(5.11).

## 5.4 Approximation by Brownian motion: Homogenization results

A valid question is if one may model the effect of the rogue oscillators by Brownian motion instead of the more complex Ornstein-Uhlenbeck equation and describe the effective dynamics of the synchronized oscillators by a single system of SDEs [70]?

In order to derive such a reduced SDE driven by Brownian motion we employ the method of homogenization. In particular, we treat the fluctuations, described by the Ornstein-Uhlenbeck process (5.11), as a fast process compared to the slow dynamics of the synchronized oscillators, described by (5.10). Stochastic homogenization theory allows to derive an effective SDE for the slow variables, where effects from the fast variables are accounted for as drift and diffusion terms (see, for example, [28, 60]).

We consider slow-fast system

$$\dot{x} = a(x) + \epsilon^{-1} b(x) v(y) \tag{5.18}$$

$$dy = \epsilon^{-2} g(y) dt + \epsilon^{-1} \sigma(y) dB, \tag{5.19}$$

for slow variables $x \in \mathcal{X} = \mathbb{R}^d$ and fast variables $y \in \mathcal{Y} = \mathbb{R}^q$. $B$ is $q$ dimensional Brownian motion. $0 < \epsilon \ll 1$ is a small parameter representing the separation of time-scale between the slow and fast systems. Note that our system (5.10)–(5.11) falls into this class of systems. The functions

$$a : \mathbb{R}^d \to \mathbb{R}^d, \quad b : \mathbb{R}^d \to \mathbb{R}^{d \times m}, \quad v : \mathbb{R}^q \to \mathbb{R}^m, g : \mathbb{R}^q \to \mathbb{R}^q \quad \sigma : \mathbb{R}^q \to \mathbb{R}^{q \times q}$$

and the drift and diffusion terms in the fast dynamics allow for a unique stationary density of the fast variables $\rho_\infty(y)$, which constitutes the ergodicity assumption on the fast dynamics of $y$. Additionally, we assume a centering condition $\int v(y)\, \rho_\infty(y) dy = 0$.

Averaging and homogenization theory establishes that for large time-scale separation, $\epsilon \to \infty$, dynamics of the slow variables $x$ can be well-approximated by a closed one which involves $x$ only, with effects of the fast variables $y$ accounted for as modifications of drift and diffusion terms. This can be established via the correspondence between the SDE of the slow-fast system and the corresponding backward Kolmogorov equation describing evolution of an observable function on the system. Alternatively, for the derivation one can also consider the dual, forward Kolmogorov equation, which is also known as the Fokker-Planck equation, describing the evolution of a density of the system. (See, for example, [28, 60].)

For the derivation, one first obtains the backward Kolmogorov equation corresponding to the SDE of the slow-fast system, substitutes in

a perturbation expansion in $\epsilon$ for the solution and matches terms with the same order of $\epsilon$. The first few orders give a backward Kolmogorov equation which in turn corresponds to an SDE that involves the slow variable $x$ only, with effects of the fast variable $y$ presenting as drift and diffusion terms, the coefficients of which are obtained as certain averaged quantities over the fast dynamics' unique stationary density $\rho_\infty(y)$. For more details we refer the reader to, for example, [28, 60]. In the following we present a brief recount of the derivation.

For the slow-fast system (5.18)–(5.19), the corresponding backward Kolmogorov equation is

$$\frac{\partial}{\partial t}u(x,y,t) = \left(\frac{1}{\epsilon^2}\mathcal{L}_0 + \frac{1}{\epsilon}\mathcal{L}_1 + \mathcal{L}_2\right)u(x,y,t) \tag{5.20}$$

where the generators are given by

$$\begin{aligned}
\mathcal{L}_0 &= g(y)\cdot\nabla_y u + \frac{1}{2}\sigma(y)\sigma^\mathsf{T}(y) : \nabla_y\nabla_y u \\
\mathcal{L}_1 &= b(x)v(y)\cdot\nabla_x u \\
\mathcal{L}_2 &= a(x)\cdot\nabla_x u.
\end{aligned}$$

Substituting a perturbation expansion

$$u = u_0 + \epsilon u_1 + \epsilon^2 u_2 \cdots$$

into the backward Kolmogorov equation (5.20) and matching terms of the same order of $\epsilon$, we have

$$0 = \mathcal{L}_0 u_0 \tag{5.21}$$

$$0 = \mathcal{L}_0 u_1 + \mathcal{L}_1 u_0 \tag{5.22}$$

$$\frac{\partial}{\partial t}u_0 = \mathcal{L}_0 u_2 + \mathcal{L}_1 u_1 + \mathcal{L}_2 u_0 \tag{5.23}$$

The first equation (5.21) implies that $u_0(x,y,t)$ is independent of $y$, $u_0(x,y,t) = u_0(x,t)$, which corresponds to the assumed ergodicity of the underlying dynamics of the fast variables $y$ (i.e. expectation values are constant and do not depend on the initial condition). The second equation (5.22) gives a solution that can be expressed formally as $u_1 = -\mathcal{L}_0^{-1}\mathcal{L}_1 u_0$. The third equation (5.23) can be re-written in the form

$$\mathcal{L}_0 u_2 = \frac{\partial}{\partial t}u_0 - \mathcal{L}_1 u_1 - \mathcal{L}_2 u_0.$$

By Fredholm's alternative, solvability condition of $u_2$ requires that the right-hand-side is orthogonal to the null-space of the adjoint of $\mathcal{L}_0$. By

the ergodicity assumption on the dynamics of the fast variable $y$, the null-space is one-dimensional and spanned by the unique stationary density $\rho_\infty(y)$, thus the solvability condition requires that the right-hand-side averages to 0 over $\rho_\infty(y)$,

$$\int_{\mathcal{Y}} \left( \frac{\partial}{\partial t} u_0 - \mathcal{L}_1 u_1 - \mathcal{L}_2 u_0 \right) \rho_\infty(y) dy = 0.$$

Since $u_0$ is independent of $y$, its average over $\rho_\infty(y)$ is the same as itself, $\int_{\mathcal{Y}} u_0 \rho_\infty(y) dy = u_0$. We thus arrive at a PDE for $u_0$, of the form

$$\frac{\partial}{\partial t} u_0(x,t) = - \left\langle \mathcal{L}_1 \mathcal{L}_0^{-1} \mathcal{L}_1 \right\rangle_y u_0 + \left\langle \mathcal{L}_2 \right\rangle_y u_0 \tag{5.24}$$

where $\langle \cdot \rangle_y$ denotes averaging with respect to the stationary density $\rho_\infty(y)$.

The right-hand-side of (5.24) only involves the first and second derivatives of $u_0(x,t)$ with respect to the slow variables $x$, while effects of the fast variables $y$ present as coefficients of the first and second order derivatives, with values specified as certain averages over the stationary density $\rho_\infty(y)$. The PDE (5.24) can in turn be considered as a backward Kolmogorov equation corresponding to an SDE involving the slow variables only.

The corresponding SDE has the form

$$dX = \tilde{a}(X)\, dt + b(X) \circ dW, \tag{5.25}$$

where $W$ is $d$-dimensional Brownian motion, the stochastic integral $b(X) \circ dW$ has the Stratonovich interpretation, and $\tilde{a}$ is a modified drift term incorporating eventual corrections to the Stratonovich integral. Homogenization establishes that the Brownian motion $W$ has covariance matrix $\Sigma$ and the modified drift term is given by

$$\tilde{a}(X) = a(X) + \tfrac{1}{2} \sum_{\alpha,\beta,\gamma=1}^{d} E^{\gamma\beta} \partial_\alpha b^\beta(X) b^{\alpha\gamma}(X). \tag{5.26}$$

Here, $Z^{ij}$ denotes the $(i,j)$'th entry of a matrix $Z$ and $b^\beta$ denotes the $\beta$'th column of $b$. The symmetric and positive-definite covariance matrix $\Sigma$ is given by a Green-Kubo formula

$$\Sigma = \int_0^\infty \int_\Lambda \left\{ v \otimes v_t + v_t \otimes v \right\} d\mu\, dt, \tag{5.27}$$

where $u \otimes v = u v^\mathsf{T} \in \mathbb{R}^{d \times d}$ for $u, v \in \mathbb{R}^d$ and $v_t = v(y,t) = v(y(t); y(0) = y)$. The integral $d\mu$ is taken over the stationary density of the fast variable

$y$ generated by the fast dynamical process. The Lévy area $E$ is given by the skew-symmetric matrix

$$E = \int_0^\infty \int_\Lambda \left\{ v \otimes v_t - v_t \otimes v \right\} d\mu \, dt. \tag{5.28}$$

Homogenization theory further establishes that indeed solution of the slow-variable $x$ in the slow-fast system (5.18)–(5.19) converges weakly to the solution $X$ of the effective SDE (5.25) in the limit of infinite time-scale separation, $\epsilon \to 0$.

In the previous and current chapter, we have constructed reduced models for the Kuramoto-Sakaguchi model (2.1) utilizing the fact that synchronized oscillators appear nearly stationary in a co-rotating frame while rogue oscillators continue to rotate with non-zero frequencies, and can thus be considered to be evolving on a time scale much faster than that of the synchronized oscillators. In particular, the reduced SDE (5.10)–(5.11) were derived by approximating effects of the fast rogue oscillators on synchronized oscillators with a stochastic Ornstein-Uhlenbeck process. In (5.10)–(5.11) we can further consider the stochastic variables $\xi_t, \zeta_t$ to be evolving at a time scale much faster than that of the synchronized oscillators, $\theta_i$, $i \in \mathcal{C}$, and apply homogenization theory to arrive at a reduced dynamics that involves only the synchronized oscillators $\theta_i$, with effects of the stochastic variables $\xi_t, \zeta_t$ being presented as drift and diffusion terms.

Comparing the reduced SDE (5.10)–(5.11) with the slow-fast system (5.18)–(5.19), we identify the synchronized oscillators $\theta_i$, $i \in \mathcal{C}$ as the slow variable $x$, and the stochastic variables $\xi_t, \zeta_t$ as the fast variable $y$. We identify

$$\begin{aligned} b_i(\theta_i) &= K/\sqrt{N} \Big( \cos(\psi_c - \theta_i - 2\lambda), \sin(\psi_c - \theta_i - 2\lambda) \Big) \in \mathbb{R}^{1\times 2} \\ v_i &= (\xi_t, \zeta_t)^{\mathsf{T}} \in \mathbb{R}^{2\times 1} \end{aligned}$$

and $a_i(\theta_i)$ is the remaining terms in (5.10).

We compute

$$\Sigma = 2 \int_0^\infty \begin{pmatrix} R_{\xi\xi}^{(\mathrm{OU})}(t) & 0 \\ 0 & R_{\zeta\zeta}^{(\mathrm{OU})}(t) \end{pmatrix} dt,$$

where we approximated $R_{\xi\zeta}^{(\mathrm{OU})}(t) = -R_{\zeta\xi}^{(\mathrm{OU})}(t)$, and

$$E = 2 \int_0^\infty \begin{pmatrix} 0 & R_{\xi\zeta}^{(\mathrm{OU})}(t) \\ -R_{\xi\zeta}^{(\mathrm{OU})}(t) & 0 \end{pmatrix} dt.$$

It turns out that the Stratonovich correction

$$h_i = \frac{1}{2}\sum_{j=1}^{d}\sum_{k=1}^{2}\Sigma_{kk}\frac{\partial b_{ik}}{\partial\theta_j}(\theta_i)b_{jk}(\theta_j) = 0$$

vanishes if we neglect derivatives of the mean phase $\psi_c$ with respect to $\theta_i$ and assume $\Sigma_{11} = \Sigma_{22}$ consistent with the numerical observations (cf. Figure 5.6). The drift correction associated with the Lévy area is calculated as $\delta\Omega := (K^2/2N)E^{12}/2 = (K^2/N)\int_0^\infty R^{(\mathrm{OU})}_{\xi\zeta}(t)dt$. Note that this correction is a constant for all oscillators $i$, and hence only constitutes a correction to the global mean frequency $\Omega$. Also note that in the thermodynamic limit the Lévy area correction vanishes as expected.

Hence, following the procedure of homogenization, for the SDE system (5.10)–(5.11), under the assumption that the OU process is fast, we arrive at a homogenized SDE for the synchronized oscillators:

$$\begin{aligned} d\theta_i = \Big[&\omega_i - \tilde{\Omega} + \frac{K}{N}\sum_{j\in\mathcal{C}}\sin(\theta_j - \theta_i - \lambda) \\ &+ K\cos(\psi_c - \theta_i - 2\lambda)\,\langle S\rangle_t + K\sin(\psi_c - \theta_i - 2\lambda)\,\langle C\rangle_t\Big]dt \\ &+ \frac{K}{\sqrt{N}}\Big(\cos(\psi_c - \theta_i - 2\lambda),\ \sin(\psi_c - \theta_i - 2\lambda)\Big)dW, \end{aligned} \tag{5.29}$$

where $dW = (dW_1, dW_2)^\mathsf{T}$ is two-dimensional Brownian motion with covariance matrix $\Sigma$ and $\tilde{\Omega} = \Omega - \delta\Omega$.

Figure 5.12 shows that the overall statistics of the order parameter $r_c$ is reasonably well described by the homogenized reduction (5.29), albeit to a lesser degree than with our stochastic reduced system (5.10)–(5.11). We remark that for the homogenized reduction (5.29) we are not able to define a meaningful expression for the overall order parameter $r$ in the manner of (5.13), as $\xi_t, \zeta_t$ are now described by Brownian motion, which is non-stationary, and $Z_t = \zeta_t + \imath\,\xi_t$ does not attain a constant variance. Albeit the relatively good recovery of the statistical properties of the order parameter $r_c$ by the homogenized system (5.29), Figure 5.9 shows that its actual temporal evolution exhibits unrealistically non-smooth fluctuations, compared to $r_c$ obtained from the SDE driven by the smoother OU process, (5.10)–(5.11).

It is worthwhile to mention that the mean-square-displacement of $S(t)$ and $C(t)$, i.e.

$$M_S(t) = \lim_{T\to\infty}\frac{1}{T}\int_0^T (S(s+t) - S(s))^2 ds,$$

and $M_C(t)$ for $C(t)$, do not scale linearly as would be expected for Brownian motion, but instead quickly saturate, in agreement with a stationary OU process, as shown in Figure 5.13.

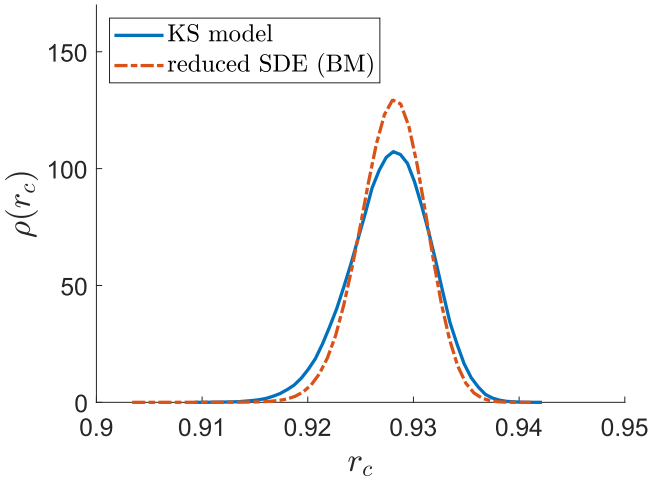


Figure 5.12: Comparison of the empirical histograms for $r_c$ obtained from a single trajectory of the Kuramoto-Sakaguchi model (2.1) for $N = 160$ and from the homogenized reduced stochastic model driven by Brownian motion, (5.29).

These results agree with our earlier observation that the emerging stochastic behaviour of synchronized oscillators is not caused by a time-scale separation between slow synchronized cluster and the assumed fast rogue oscillators with larger intrinsic frequencies. We had already seen in Figure 5.7 that the dynamics of the rogue oscillators contains extended slow periods of near alignment with the synchronized cluster. Instead our work shows that the stochasticity emerges as a weak coupling effect of a large number of uncorrelated rogue oscillators.

## 5.5 Discussion & Outlook

In this Chapter we analyzed the stochastic fluctuations exhibited in finite-size deterministic Kuramoto-Sakaguchi model (2.1) and constructed stochastic reduced systems. In particular we focused on the fluctuations around their mean of the effect of rogue oscillators on synchronized oscillators. After investigating the full Kuramoto-Sakaguchi model via numerical simulation, we set out to construct stochastic approximations for the rogue oscillators' effects, motivated by trigonometric approximations of Gaussian process. A 2-d Ornstein-Uhlenbeck process was taken as the approximate model, with coefficients obtained via optimization on comparison between the approximate model and the actual dynamics from numerical simulation. After replacing the effect of rogue oscillators with the OU approximate model, we arrived at reduced SDE of the full system.

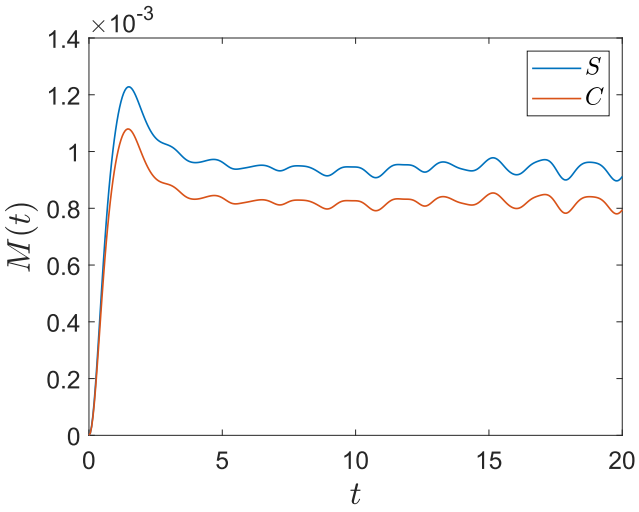


Figure 5.13: Mean-square-displacement $M(t)$ of $S(t)$ and $C(t)$ from a single trajectory of the Kuramoto-Sakaguchi model (2.1) for $N = 160$. All other parameters are the same as in Figure 5.1

The reduced SDE only involves the synchronized oscillators, and is shown to be capable of reproducing the full system's dynamics to a certain degree, including the fluctuations of both the overall order parameters and phases of individual synchronized oscillators. We further constructed a homogenization approximation utilizing the separation of time-scale between the slow synchronized oscillators and the fast rogue oscillators. In the model resulting from homogenization, effects of rogue oscillators are accounted for as Brownian motions. However, in this model, the reproduced time-evolution of order parameter $r_c$ displays non-smooth trajectories, in contrast to the original full model (2.1) where the trajectories of $r_c$ are smooth. The reduced model with rogue oscillators approximated by OU process, on the other hand, produces trajectories of $r_c$ that are smoother, agreeing qualitatively with the full model. Further, the model with OU captures statistics of the full model more accurately than the model from homogenization with Brownian motion.

In this chapter, the results for constructing stochastic reduced models were obtained for one particular setting of intrinsic frequency distribution $g(\omega)$, coupling strength $K$ and phase-offset $\lambda$. One could extend the analysis to different system settings, and investigate how the fitted OU process varies with parameters such as $K$ and $\lambda$. In particular, it would be interesting to investigate whether the stochastic reduction can capture the anomalous enhancement of the order parameter near the onset of partial synchronization [20, 19, 21, 22, 32].

The construction of the stochastic reduced models in this chapter

constitutes a dimension reduction as effects of all the rogue oscillators are captured with low-dimension Gaussian processes. The reduced SDE now only involves the synchronized oscillators, and is of lower dimension compared to the original full system. A further dimension reduction may be achieved by obtaining a lower-dimensional description of the synchronized oscillators in the reduced SDE, which appears quite plausible given that the synchronized oscillators exhibit very similar dynamics (c.f. Figure 5.11). One possible candidate is to again apply the collective coordinate framework [29, 30], to the stochastic reduced system (5.10)–(5.11. In previous work [30], the collective coordinate framework has already been applied to Kuramoto model with external white noise driving force, where it leads to reduced dynamics that capture the dynamics of the full system quite well, including the fluctuations of the synchronized cluster that is pertinent to finite-size system.

In this chapter, the OU process for approximating the effects of the rogue oscillators were constructed by fitting against numerical simulation results of the full system. In particular, the OU process's parameters were obtained via optimization of the error between the OU process and statistics of the full system from simulation. One may further probe whether stochastic approximations for the fast rogue oscillators can be obtained in a more analytical way. For instance, one may proceed via homogenization theory utilizing the apparent time-scale separation between the synchronized oscillators and the rogue oscillators. Further, as already pointed out in previous sections, the effective stochastic behaviour of the overall effects of the rogue oscillators appears to be more related to the weak coupling effect of many uncorrelated rogue oscillators. The weakly chaotic dynamics of the rogue oscillators appear nearly periodic (c.f. Figure 5.7), and the overall effect of rogue oscillators on the synchronized cluster can be captured via a sum of trigonometric functions of the phases of the rogue oscillators, as in (5.1)–(5.2). It has been established that the sum of a large number of trigonometric functions with distributed frequencies can approximate a Gaussian process [33, 35, 28] (known as the trigonometric approximation of Gaussian process). It would thus be interesting to examine whether this can be applied to derive a more analytical construction of the stochastic approximation of the overall effects of the rogue oscillators (5.1)–(5.2), from system parameters and statistics such as the order parameter $r$ and the set of intrinsic frequencies $\omega_i$s.

# Chapter 6

# Summary and Outlook

This thesis provided a comprehensive treatment of the effect of non-entrained rogue oscillators on the collective behaviour of the synchronized oscillators. We first established an average effect in the spirit of a law of large numbers in Chapter 4 and then determined the fluctuations around that mean effect akin to the central limit theorem in Chapter 5.

After an introduction and review of literature in Chapter 1 we presented numerical simulation results for the finite-size Kuramoto-Sakaguchi model (2.1) in Chapter 2. Chapter 3 reviewed traditional analysis of the model in the thermodynamic limit of infinitely many oscillators. We also presented the results from a self-consistency analysis on the system with a uniform intrinsic frequency, as well as the application of the Ott-Antonsen ansatz on the Kuramoto-Sakaguchi model with a non-zero phase-offset.

In Chapter 4 we derived an analytical expression for the mean effect of the rogue oscillators. We showed that the rogue oscillators significantly affect the behaviour of the synchronized oscillators. We have, furthermore, derived reduced dynamics of the Kuramoto-Sakaguchi model through the collective coordinate framework. We have extended the collective coordinate approach by including the effect of non-entrained rogue oscillators, and have shown that the inclusion of these rogue oscillators is essential to accurately describe the collective dynamics of the Kuramoto-Sakaguchi model. We have compared two ansatz functions, a linear ansatz function obtained as a linearization around $1/K$, and a nonlinear arcsine ansatz, motivated by mean-field analysis.

We find that the arcsine ansatz with the effect of the rogues included provides a remarkably good approximation of the collective dynamics of finite Kuramoto-Sakaguchi systems, quantified by the order parameter, the cluster mean frequency, the identification of the cluster as well as the critical coupling strengths for partial and for global synchronization, and

we find that the arcsine ansatz is far superior to the linear ansatz which had so far been used as an ansatz for collective coordinates [29, 30, 31, 68]. This constitutes another novel contribution of this thesis. However, the arcsine ansatz is limited to networks with an all-to-all coupling topology, whereas the linear ansatz can be applied to any complex network [31]. We have also shown that for finite networks the arcsine ansatz is far superior to classical self-consistency equations, which assume $N \to \infty$. Moreover, in the thermodynamic limit of infinitely many oscillators, we have shown that the arcsine ansatz recovers well-known results obtained by mean-field analysis.

Taken the issue of computational cost aside achieved by the reduction from $N$ oscillators to 2 collective coordinates, the advantage of the model reduction presented here is that a reduced dynamical description allows a more detailed analysis of the macroscopic dynamics; in particular, to establish and quantitatively capture dominant effects such as the influence of the mean-field of the non-entrained rogue oscillators on the synchronized macroscopic behavior.

Chapter 5 established a study of the fluctuations around the mean effect of the rogue oscillators. We presented results from numerical simulations which suggest that the fluctuations can be approximated by a Gaussian process with a stationary density and fluctuations which decay as $1/\sqrt{N}$. Hence for fluctuations to have a significant effect one needs the number of rogue oscillators to sufficiently large to allow for a central limit theorem and sufficiently small to have a non-negligible variance. Gaussian processes are determined entirely by their mean and their covariance function. For task at hand the mean was established in Chapter 4, and the covariance function was numerically estimated. This allowed us to replace the interaction term involving the rogue oscillators by an Ornstein Uhlenbeck process, and to formulate a closed equation for the entrained oscillators only, which are driven by a complex Ornstein-Uhlenbeck process. The reduced system of stochastic differential equations showed remarkable capability to reproduce the statistical behaviour of the entrained oscillators such as the probability density function of the order parameter. It is pertinent to mention that the order parameter is driven by coloured Ornstein-Uhlenbekc noise and not, as previously claimed on heuristic grounds, by Brownian motion. We showed that Brownian motion will lead to far rougher time evolution of the order parameter than the actual Kuramoto-Sakaguchi equation.

In addition this thesis contributed to the analysis of the Kuramoto-Sakaguchi equation in the thermodynamic limit, and we established an analytical treatment of the thermodynamic limit for an assumed uniform

distribution of intrinsic frequencies in Chapter 3.

Here we have considered the Kuramoto-Sakaguchi model with an all-to-all coupling and a phase-offset parameter that is common to all oscillators. Generalization of the model, such as a system consisting of two populations of oscillators with different inter- and intra-population coupling strengths and phase-offsets, have been shown to display intriguing dynamics such as chimera states and chaos [1, 38, 41, 7, 7, 9, 12]. The success of the collective coordinate approach in the one-population Kuramoto-Sakaguchi model suggests that it will also be able to capture the complex collective dynamics of those more general models. Furthermore, the methods developed in [31, 68] allow to study local frequency clusters, caused by finite size sampling effects in the natural frequencies, and their mutual interaction in phase-frustrated systems.

Further, it is now possible to employ the collective coordinate framework for stochastic Kuramoto models established in [30] to the reduced stochastic equation for the entrained synchronized oscillators derived in Chapter 5.

Comparing to the traditional analysis of Kuramoto-like models, we feel that the analysis method and framework presented in Chapter 4 and Chapter 5 have the advantage of being applicable to systems with finite, non-identical ensembles of oscillators. Thus the method may have particular advantage in analyzing coupled oscillatory systems arising from real-world systems, such as mechanical oscillators [59, 43], power grids [24, 51] and neuron networks [5], where the components may not have come from a predefined distribution. The presented framework has the capability of accurately approximating the statistics of finite-size systems, as well as capturing the fluctuations exhibited by the systems. These may be an advantage for analyzing real-world systems which may exhibit such finite-size effects. We remark that in most cases, the presented framework leads to approximate reduced systems for the full model, whereas many previous analysis do give analytical results that are exact, for example in the thermodynamic limit of infinitely many oscillators, or for systems with identical oscillators.

# Bibliography


[1] Daniel M. Abrams, Rennie Mirollo, Steven H. Strogatz, and Daniel A. Wiley. Solvable model for chimera states of coupled oscillators. *Phys. Rev. Lett.*, 101:084103, 2008.

[2] Daniel M. Abrams and Steven H. Strogatz. Chimera states for coupled oscillators. *Phys. Rev. Lett.*, 93:174102, 2004.

[3] Juan A. Acebrón, L. L. Bonilla, Conrad J. Pérez Vicente, Félix Ritort, and Renato Spigler. The Kuramoto model: A simple paradigm for synchronization phenomena. *Rev. Mod. Phys.*, 77:137, 2005.

[4] Alex Arenas, Albert Díaz-Guilera, Jürgen Kurths, Yamir Moreno, and Changsong Zhou. Synchronization in complex networks. *Phys. Rep.*, 469:93, 2008.

[5] P. Ashwin, S. Coombes, and R. Nicks. Mathematical frameworks for oscillatory network dynamics in neuroscience. *J. Math. Neurosci.*, 6:2, 2016.

[6] Neil J Balmforth and Roberto Sassi. A shocking display of synchrony. *Physica D*, 143:21, 2000.

[7] Christian Bick and Peter Ashwin. Chaotic weak chimeras and their persistence in coupled populations of phase oscillators. *Nonlinearity*, 29:1468, 2016.

[8] Christian Bick, Marc Goodfellow, Carlo R. Laing, and Erik A. Martens. Understanding the dynamics of biological and neural oscillator networks through exact mean-field reductions: a review. *J. Math. Neurosc.*, 10:9, 2020.

[9] Christian Bick, Mark J. Panaggio, and Erik A. Martens. Chaos in Kuramoto oscillator networks. *Chaos*, 28:071102, 2018.

[10] Markus Brede and Alexander C. Kalloniatis. Frustration tuning and perfect phase synchronization in the Kuramoto-Sakaguchi model. *Phys. Rev. E*, 93:062315, 2016.

[11] John Buck. Synchronous rhythmic flashing of fireflies. II. *Quart. Rev. Biol.*, 63:265, 1988.

[12] Oleksandr Burylko, Erik A. Martens, and Christian Bick. Symmetry breaking yields chimeras in two small populations of Kuramoto-type oscillators. *Chaos*, 32:093109, 2022.

[13] Mallory Carlu, Francesco Ginelli, and Antonio Politi. Origin and scaling of chaos in weakly coupled phase oscillators. *Phys. Rev. E*, 97:012203, 2018.

[14] Lauren M. Childs and Steven H. Strogatz. Stability diagram for the forced Kuramoto model. *Chaos*, 18:043128, 2008.

[15] Tommaso Coletta, Robin Delabays, and Philippe Jacquod. Finite-size scaling in the Kuramoto model. *Phys. Rev. E*, 95:042207, 2017.

[16] John D. Crawford and K.T.R. Davies. Synchronization of globally coupled phase oscillators: singularities and scaling for general couplings. *Physica D*, page 1, 1999.

[17] John David Crawford. Amplitude expansions for instabilities in populations of globally-coupled oscillators. *J. Stat. Phys.*, 74:1047, 1994.

[18] S.M. Crook, G.B. Ermentrout, M.C. Vanier, and J.M. Bower. The role of axonal delay in the synchronization of networks of coupled cortical oscillators. *J. Comput. Neurosci.*, 4:161, 1997.

[19] H. Daido. Scaling behaviour at the onset of mutual entrainment in a population of interacting oscillators. *J. Phys. A*, 20:L629, 1987.

[20] Hiroaki Daido. Discrete-time population dynamics of interacting self-oscillators. *Prog. Theor. Phys.*, 75:1460, 1986.

[21] Hiroaki Daido. Intrinsic fluctuation and its critical scaling in a class of populations of oscillators with distributed frequencies. *Prog. Theor. Phys.*, 81:727, 1989.

[22] Hiroaki Daido. Intrinsic fluctuations and a phase transition in a class of large populations of interacting oscillators. *J. Stat. Phys.*, 60:753, 1990.

[23] Timothy DelSole. A fundamental limitation of Markov models. *J. Atmospheric Sci.*, 57:2158, 2000.

[24] Florian Dörfler and Francesco Bullo. Synchronization and transient stability in power networks and nonuniform Kuramoto oscillators. *SIAM J. Control Optim.*, 50:1616, 2012.

[25] Florian Dörfler and Francesco Bullo. Synchronization in complex networks of phase oscillators: A survey. *Automatica*, 50:1539, 2014.

[26] Jan Fialkowski, Serhiy Yanchuk, Igor M. Sokolov, Eckehard Schöll, Georg A. Gottwald, and Rico Berner. Heterogeneous nucleation in finite-size adaptive dynamical networks. *Phys. Rev. Lett.*, 130:067402, 2023.

[27] G. Filatrella, A. Nielsen, and N. Pedersen. Analysis of a power grid using a Kuramoto-like model. *Eur. Phys. J. B*, 61:485, 2008.

[28] Dror Givon, Raz Kupferman, and Andrew Stuart. Extracting macroscopic dynamics: model problems and algorithms. *Nonlinearity*, 17:R55, 2004.

[29] Georg A. Gottwald. Model reduction for networks of coupled oscillators. *Chaos*, 25:053111, 2015.

[30] Georg A. Gottwald. Finite-size effects in a stochastic Kuramoto model. *Chaos*, 27:101103, 2017.

[31] Edward J. Hancock and Georg A. Gottwald. Model reduction for Kuramoto models with complex topologies. *Phys. Rev. E*, 98:012307, 2018.

[32] Hyunsuk Hong, Hugues Chaté, Lei-Han Tang, and Hyunggyu Park. Finite-size scaling, dynamic fluctuations, and hyperscaling relation in the Kuramoto model. *Phys. Rev. E*, 92:022122, 2015.

[33] JP Kahane. *Random Series of Functions*. Cambridge University Press, Cambridge, 1985.

[34] István Z. Kiss, Yumei Zhai, and John L. Hudson. Emerging coherence in a population of chemical oscillators. *Science*, 296:1676, 2002.

[35] R. Kupferman, A. M. Stuart, J. R. Terry, and P. F. Tupper. Long-term behaviour of large mechanical systems with random initial data. *Stochast. Dynam.*, 02:533, 2002.

[36] Y. Kuramoto. *Chemical Oscillations, Waves, and Turbulence*. Springer, Berlin, 1984.

[37] Y. Kuramoto and D. Battogtokh. Coexistence of coherence and incoherence in nonlocally coupled phase oscillators. *Nonlinear Phenom. Complex Syst.*, 5:380, 2002.

[38] Carlo R. Laing. Chimera states in heterogeneous networks. *Chaos*, 19:013113, 2009.

[39] M.A. Lohe. Synchronization control in networks with uniform and distributed phase lag. *Automatica*, 54:114, 2015.

[40] E. A. Martens, E. Barreto, S. H. Strogatz, E. Ott, P. So, and T. M. Antonsen. Exact results for the Kuramoto model with a bimodal frequency distribution. *Phys. Rev. E*, 79:026204, 2009.

[41] Erik A. Martens, Christian Bick, and Mark J. Panaggio. Chimera states in two populations with heterogeneous phase-lag. *Chaos*, 26:094819, 2016.

[42] Erik A. Martens, Carlo R. Laing, and Steven H. Strogatz. Solvable model of spiral wave chimeras. *Phys. Rev. Lett.*, 104:044101, 2010.

[43] Erik Andreas Martens, Shashi Thutupalli, Antoine Fourrière, and Oskar Hallatschek. Chimera states in mechanical oscillator networks. *Proc. Natl. Acad. Sci.*, 110:10563, 2013.

[44] MATLAB. *version 9.7.0 (R2019b)*. The MathWorks Inc., Natick, Massachusetts, 2019.

[45] Paul C. Matthews, Renato E. Mirollo, and Steven H. Strogatz. Dynamics of a large system of coupled nonlinear oscillators. *Physica D*, 52:293, 1991.

[46] Paul C. Matthews and Steven H. Strogatz. Phase diagram for the collective behavior of limit-cycle oscillators. *Phys. Rev. Lett.*, 65:1701, 1990.

[47] Renato E. Mirollo and Steven H. Strogatz. Amplitude death in an array of limit-cycle oscillators. *J. Stat. Phys.*, 60:245, 1990.

[48] Sung Joon Moon, R. Ghanem, and I. G. Kevrekidis. Coarse graining the dynamics of coupled oscillators. *Phys. Rev. Lett.*, 96:144101, 2006.

[49] Adilson E. Motter, Seth A. Myers, Marian Anghel, and Takashi Nishikawa. Spontaneous synchrony in power-grid networks. *Nat. Phys.*, 9:191, 2013.

[50] Z. Néda, E. Ravasz, T. Vicsek, Y. Brechet, and A. L. Barabási. Physics of the rhythmic applause. *Phys. Rev. E*, 61:6987, 2000.

[51] Takashi Nishikawa and Adilson E Motter. Comparative analysis of existing models for power-grid synchronization. *Mew J. Phys.*, 17:015012, 2015.

[52] Oleh E. Omel'chenko and Matthias Wolfrum. Nonuniversal transitions to synchrony in the Sakaguchi-Kuramoto model. *Phys. Rev. Lett.*, 109:164101, 2012.

[53] Oleh E. Omel'chenko and Matthias Wolfrum. Bifurcations in the Sakaguchi–Kuramoto model. *Physica D*, 263:74, 2013.

[54] Grigory V. Osipov, Jürgen Kurths, and Changsong Zhou. *Synchronization in Oscillatory Networks*. Springer, Berlin, 2007.

[55] Edward Ott and Thomas M. Antonsen. Low dimensional behavior of large systems of globally coupled oscillators. *Chaos*, 18:037113, 2008.

[56] Edward Ott and Thomas M. Antonsen. Long time evolution of phase oscillator systems. *Chaos*, 19:023117, 2009.

[57] Edward Ott, Brian R. Hunt, and Thomas M. Antonsen. Comment on "Long time evolution of phase oscillator systems" [Chaos 19, 023117 (2009)]. *Chaos*, 21:025112, 2011.

[58] Mark J Panaggio and Daniel M Abrams. Chimera states: coexistence of coherence and incoherence in networks of coupled oscillators. *Nonlinearity*, 28:R67, 2015.

[59] James Pantaleone. Synchronization of metronomes. *Am. J. Phys.*, 70:992, 2002.

[60] Grigorios A. Pavliotis and Andrew M. Stuart. *Multiscale Methods: Averaging and Homogenization*. Springer, New York, 2008.

[61] Diego Pazó. Thermodynamic limit of the first-order phase transition in the Kuramoto model. *Phys. Rev. E*, 72:046211, 2005.

[62] Arkady Pikovsky, Rosenblum Michael, and Jürgen Kurths. *Synchronization: A universal concept in nonlinear sciences*. Cambridge University Press, Cambridge, 2001.

[63] Rafael S. Pinto and Alberto Saa. Optimal synchronization of Kuramoto oscillators: A dimensional reduction approach. *Phys. Rev. E*, 92:062801, 2015.

[64] Karthikeyan Rajendran and Ioannis G. Kevrekidis. Coarse graining the dynamics of heterogeneous oscillators in networks with spectral gaps. *Phys. Rev. E*, 84:036708, 2011.

[65] Francisco A. Rodrigues, Thomas K. DM. Peron, Peng Ji, and Jürgen Kurths. The kuramoto model in complex networks. *Phys. Rep.*, 610:1, 2016.

[66] Hidetsugu Sakaguchi and Yoshiki Kuramoto. A soluble active rotater model showing phase transitions via mutual entertainment. *Prog. Theor. Phys.*, 76:576, 1986.

[67] Alwyn Scott. *Nonlinear science: emergence and dynamics of coherent structures*. Oxford applied and engineering mathematics. Oxford University Press, Oxford, 1999.

[68] Lachlan D. Smith and Georg A. Gottwald. Chaos in networks of coupled oscillators with multimodal natural frequency distributions. *Chaos*, 29:093127, 2019.

[69] Lachlan D. Smith and Georg A. Gottwald. Model reduction for the collective dynamics of globally coupled oscillators: From finite networks to the thermodynamic limit. *Chaos*, 30:093107, 2020.

[70] Jordan Snyder, Jared L. Callaham, Steven L. Brunton, and J. Nathan Kutz. Data-driven stochastic modeling of coarse-grained dynamics with finite-size effects using Langevin regression. *Physica D*, 427:133004, 2021.

[71] S. H. Strogatz. *Sync: The Emerging Science of Spontaneous Order*. Hyperion, New York, 2003.

[72] Steven H. Strogatz. From Kuramoto to Crawford: exploring the onset of synchronization in populations of coupled oscillators. *Physica D*, 143:1, 2000.

[73] Steven H. Strogatz and Renato E. Mirollo. Stability of incoherence in a population of coupled oscillators. *J. Stat. Phys.*, 63:613, 1991.

[74] Steven H. Strogatz, Renato E. Mirollo, and Paul C. Matthews. Coupled nonlinear oscillators below the synchronization threshold: Relaxation by generalized Landau damping. *Phys. Rev. Lett.*, 68:2730, 1992.

[75] Shinya Watanabe and Steven H. Strogatz. Integrability of a globally coupled oscillator array. *Phys. Rev. Lett.*, 70:2391, 1993.

[76] Shinya Watanabe and Steven H. Strogatz. Constants of motion for superconducting Josephson arrays. *Physica D*, 74:197, 1994.

[77] Kurt Wiesenfeld, Pere Colet, and Steven H. Strogatz. Frequency locking in Josephson arrays: Connection with the Kuramoto model. *Phys. Rev. E*, 57:1563, 1998.